Indian J Pure & Appl Phys. Vol 21 No. 6, pp 323-382
JUNE 1983
CODEN : IJOPAU ISSN : 0019-5596
21(6) 323-382 (1983)

INDIAN JOURNAL OF PURE & APPLIED PHYSICS

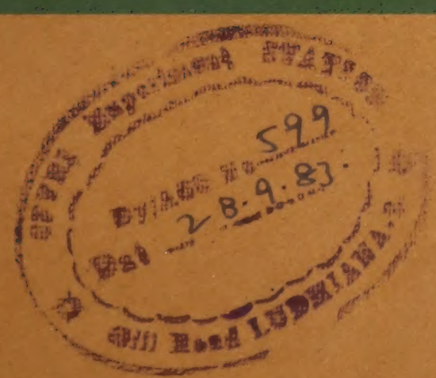

Published by
PUBLICATIONS & INFORMATION DIRECTORATE, CSIR
NEW DELHI
in association with
THE INDIAN NATIONAL SCIENCE ACADEMY, NEW DELHI

CSIR SCIENTIFIC PERIODICALS

JOURNAL OF SCIENTIFJC & INDUSTRIAL RESEARCH (Monthly)

With a fine record of over 45 years service to the scientific community, this journal has grown into India's leading general science periodical. Intended to fulfil the responsibility of helping the research workers to keep themselves abreast of current developments in various fields of science and technology, the journal carries editorial features highlighting important scientific events in India and abroad, articles on science policy and management of science review articles on topics of current research interest, technical reports on international and national conferences: reviews of scientific and technical publications, and notes on major advances in various fields.

Annual subscription	Rs 100.00	£ 17.00	$ 38.00
Single copy	10.00	1.70	3.80

INDIAN JOURNAL OF CHEMISTRY (Monthly)

Section A: In the 20th year of publication, the journal is devoted to papers in Inorganic, Physical, Theoretical and Analytical Chemistry.

Annual subscription	Rs 125.00	£ 21.00	$ 47.00
Single copy	12.50	2.10	4.70

Section B: In the 19th year of publication, the journal is devoted to papers in Organic Chemistry including Medicinal Chemistry.

Annual subscription	Rs 125.00	£ 21.00	$ 47.00
Single copy	12.50	2.10	4.70

INDIAN JOURNAL OF PURE & APPLIED PHYSICS (Monthly)

This journal, which is running 20th year of its publication, is devoted to original research communications (full papers and short communications) in all conventional branches of physics (except radio and space physics).

Annual subscription	Rs 120.00	£ 20.00	$ 45.00
Single copy	12.00	2.00	4.50

INDIAN JOURNAL OF RADIO & SPACE PHYSICS (Bimonthly)

The journal, which is being published beginning from March 1972, is intended to serve as a medium for the publication of the growing research output in various areas of radio and space physics, such as ionospheric propagation, magnetosphere, radio and radar astronomy, physics and chemistry of the ionosphere; neutral atmosphere; airglow, winds and motion in the upper atmosphere; stratosphere-mesosphere coupling, ionosphere-magnetosphere coupling ; solar-terrestrial relationship, etc.

Annual subscription	Rs 90.00	£ 15.00	$ 34.00
Single copy	18.00	3.00	6.80

INDIAN JOURNAL OF TECHNOLOGY (INCLUDING ENGINEERING) (Monthly)

This journal publishes papers reporting results of original research of applied nature pertaining to unit operations, heat and mass transfer, products, processes, instruments and appliances, etc. The journal is of special interest to research workers in the departments of applied sciences in universities, institutes of higher technology, commodity research laboratories, industrial cooperative research institutes, and industrial research laboratories.

Annual subscription	Rs 90.00	£ 15.00	$ 34.00
Single copy	9.00	1.50	3.40

INDIAN JOURNAL OF EXPERIMENTAL BIOLOGY (Monthly)

This journal, devoted to the publication of research communications in the fields of experimental botany, zoology, microbiology, pharmacology, endocrinology, nutrition, etc., is the only one in India with such a wide coverage and scope.

Annual subscription	Rs 180.00	£ 30.00	$ 68.00
Single copy	18.00	3.00	6.80

INDIAN JOURNAL OF BIOCHEMISTRY & BIOPHYSICS (Bimonthly)

This journal, published in association with the Society of Biolog cal Chemists (India), Bangalore, is the only research journal in India devoted exclusively to original research communications in biochemistry and biophysics.

Annual subscription	Rs 60.00	£ 10.00	$ 23.00
Single copy	12.00	2.00	4.60

INDIAN JOURNAL OF MARINE SCIENCES (Quarterly)

Commencing publication from June 1972, this journal is devoted to research communications (full papers and short communications) pertaining to various facets of marine research, viz. biological, physical, geological and chemical oceanography.

Annual subscription	Rs 75.00	£ 13.00	$ 28.00
Single copy	22.00	4.00	8.40

RESEARCH AND INDUSTRY (Quarterly)

Intended to serve as a link between science and industry, this journal is addressed primarily to technologists, engineers, executives and others in industry and trade. It publishes informative original articles containing practical details of processes and products devoted in India, which show promise of ready utilization, and technical digests on new processes, products, instruments and testing methods which are of interest to industry. Developments in Indian industry are regularly reported.

Annual subscription	Rs 45.00	£ 8.00	$ 17.00
Single copy	13.00	2.50	5.00

INDIAN JOURNAL OF TEXTILE RESEARCH (Quarterly)

Commencing publication from March 1976, this journal is devoted to the publication of papers reporting results of fundamental and applied researches in the field of textiles.

Annual subscription	Rs 45.00	£ 8.00	$ 17.00
Single copy	13.00	2.50	5.00

MEDICINAL & AROMATIC PLANTS ABSTRACTS (Bimonthly)

Carries informative abstracts of scientific papers published in important Indian and foreign journals relating to different aspects of medicinal and aromatic plants. Each issue contains about 350 abstracts with a subject index.

Annual subscription	Rs 40.00	£ 7.00	$ 17.00
Single copy	7.50	1.50	3.00

INDUSTRIAL NEWS DIGEST (Monthly)

Provides technical and techno-economic information for industrialists, prospective entrepreneurs and experts in both government and private agencies dealing with the management and planning of industry. Each issue carries at least one profile on a particular industry.

Annual subscription	Rs 20.00	£ 4.00	$ 8.00
Single copy	2.00	0.50	1.00

CURRENT LITERATURE ON SCIENCE OF SCIENCE (Monthly)

Carries abstracts, digests, book reviews, news & notes and R & D statistics with emphasis on problems of S & T in developing countries, it also covers the areas of science policy, R & D planning and management, technology transfer, technology assessment and science and society.

Annual subscription	Rs 100.00	£ 12.00	$ 30.00

Please contact

Manager (Sales & Advertisment)

PUBLICATIONS & INFORMATION DIRECTORATE, CSIR

Hillside Road, New Delhi-110012

Indian Journal of Pure & Applied Physics

Published by the Publications & Information Directorate, CSIR, Hillside Road, New Delhi 110012
Editor-in-Chief : Y R Chadha

The Indian Journal of Pure & Applied Physics is issued monthly. The Directorate assumes no responsibility for the statements and opinions advanced by contributors. The editorial staff in its work of examining papers received for publication is assisted, in an honorary capacity, by a large number of distinguished scientists, working in various parts of India.

Communications regarding contributions for publication in the journal should be addressed to the Editor, Indian Journal of Pure & Applied Physics, Publications & Information Directorate, Hillside Road, New Delhi 110012.

Correspondence regarding subscriptions and advertisements should be addressed to the Sales & Distribution Officer, Publications & Information Directorate, New Delhi 110012.

Annual Subscription
Rs. 120.00 £20.00 $45.00

Single Copy
Rs. 12.00 £2.00 $4.50

50% Discount is admissible to research workers and students and 25% discount to non-research individuals, on annual subscription. Payments in respect of subscriptions and advertisements may be sent by cheque, bank draft, money order or postal order marked payable *only* to **Publications & Information Directorate, New Delhi 110012**. Claims for missing numbers of the journal will be allowed only if received within 3 months of the date of issue of the journal plus the time normally required for postal delivery of the journal and the claim.

Indian Journal of Pure & Applied Physics

VOLUME 21 NUMBER 6 JUNE 1983

CONTENTS

Continued overleaf

---

*The author to whom all correspondence is to be addressed is indicated by the (*) mark.

Indian Journal of Pure & Applied Physics
Vol. 21, June 1983, pp. 323-326

High Field Conduction in Solution-grown Polyvinylidene Fluoride (PVF_2) Films

P C MEHENDRU* & SURESH CHAND
National Physical Laboratory, New Delhi 110012

Received 13 *November* 1982; *revised received* 25 *March* 1983

Current-voltage (I-V) characteristics of PVF_2 films grown from the solution and characterized by having ($\alpha+\beta$) crystalline modification have been studied as a function of temperature and thickness in the M-P-M sandwich configuration. The I-V curves show two distinct regions of conduction, viz. the comparatively low-field ohmic region with a slope ~ 1 and the high field non-ohmic region with a slope ≤ 2. The high field non-ohmic behaviour has been attributed to the tunnelling of charge carriers into or via the traps, the tunnelling process being a thermally activated one.

1 Introduction

The discovery[1] of strong piezo-electricity in uniaxially or biaxially stretched and poled polyvinylidene fluoride (PVF_2) films has drawn considerable interest in recent years particularly with regard to the mechanisms[2] responsible for this effect. PVF_2 films possess many crystalline structures[3-5] such as a polar form (β-form), a non-polar form (α-form), a mixture of polar and non-polar forms ($\beta+\alpha$-form) and a γ-form[6]. However, the β-form has been found to be mainly present in the piezo-electric films of PVF_2. Murayama and Hashizumi[6] have established that in PVF_2 films containing both the β- and the α-forms, the piezo-electricity and the pyro-electricity increase with the increase of β-form. Keeping in view the polymorphology of PVF_2 films, it becomes extremely essential to understand the mechanisms of charge storage and electrical conduction in these films. We have already reported[7,8] the mechanism of charge storage in PVF_2 and this paper aims at discussing the mechanism of high field conduction in PVF_2 films.

2 Experimental Procedure

PVF_2, having a glass transition temperature ~ 220 K and melting point 430-463 K, was obtained from Messrs Polysciences Inc, USA. The polymer, for the preparation of the films, was used as such, without any further purification/recrystallization. PVF_2 films of thickness, ranging from 18-80 μm, were prepared by the solution evaporation technique[9]. An M-P-M sandwich structure where M is the electrode metal and P the polymer was used and its method of preparation and the measurement of current at different voltages and temperatures were the same as reported earlier[7,10,11]. The infra-red (IR) absorption spectra were recorded with a standard double beam IR spectrophotometer (Perkin-Elmer, Model 399) with a normal setting and working on the principle of optical null method.

3 Results and Discussion

In order to see the morphology of PVF_2 films grown from the solution, the IR spectra in the frequency range 530-480 cm^{-1} were recorded at room temperature and were compared with the reported[12] Murayama's spectra. Curves 1,2 and 3 in Fig. 1 correspond to Murayama's IR spectra for PVF_2 films whereas curve 4 corresponds to IR spectra of our films. Murayama[12] had found that in PVF_2 films possessing the α-form, two absorption peaks occur at 520 and 485 cm^{-1} (curve 1) and in those having the β-form, the peaks occur at 500 and 485 cm^{-1} (curve 2). However,

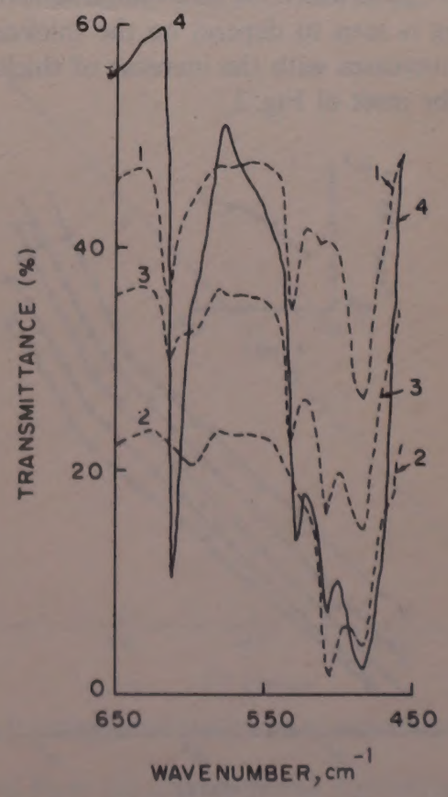

Fig. 1—A comparative IR absorption spectra of pure PVF_2 films in the range 530-480 cm^{-1} [Curves 1, 2 and 3 correspond to Murayama's spectra recorded for α-, β- and ($\alpha+\beta$)-forms, respectively, whereas curve 4 corresponds to the spectra for pure PVF_2 prepared by us and recorded in the same range]

in films possessing the $(\alpha+\beta)$-form, three absorption peaks, namely, at 520, 495 and 485 cm^{-1} (curve 3) are observed. As seen from curve 4 (present study) three absorption peaks at 515, 495 and 485 cm^{-1} have been observed. On comparing curves 3 and 4 (Fig. 1), it is seen that the films studied by us have absorption peaks very close to those reported by Murayama[12] for the $(\alpha+\beta)$-form indicating thereby that our films of PVF_2 consist mainly of the $(\alpha+\beta)$-form. Murayama and coworkers[12,13] have suggested that films having such a crystalline modification would provide trapping sites and their electrical properties will be governed predominantly by the trapping mechanisms. Our TSD studies[7,8] on such PVF_2 films confirm the dominating role of traps for the storage of charge; the charge carriers are trapped either at the microscopic or at the macroscopic level. The conductivity behaviour discussed later in this paper also supports the vital role of the traps in governing the electrical properties of solution-grown PVF_2 films.

Fig. 2 shows the room temperature I-V characteristics in log-log scale for PVF_2 films of different thicknesses. Curves 1 to 5 correspond to thicknesses 18, 27, 35, 57 and 80 μm, respectively. It is seen from these I-V curves that there are distinctly two regions of conduction, viz. the comparatively low-field ohmic region with slope ~ 1 and the high-field non-ohmic region with slope ≤ 2. Further, the transition voltage (V_{tran}) at which the non-ohmic behaviour starts appearing is seen to depend on the thickness of the films; it increases with the increase of thickness as is seen in the inset of Fig. 2.

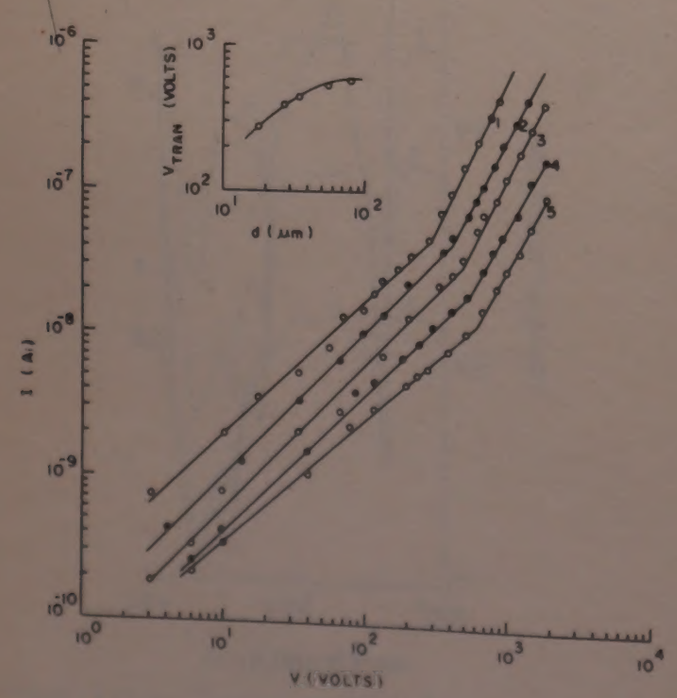

Fig. 2—I-V characteristics of pure PVF_2 films at room temperature (303 K) for different thicknesses [Curves 1 to 5 correspond to thickness of 18, 27, 35, 57 and 80 μm, respectively. In the inset is shown a log-log plot of V_{tran} vs d]

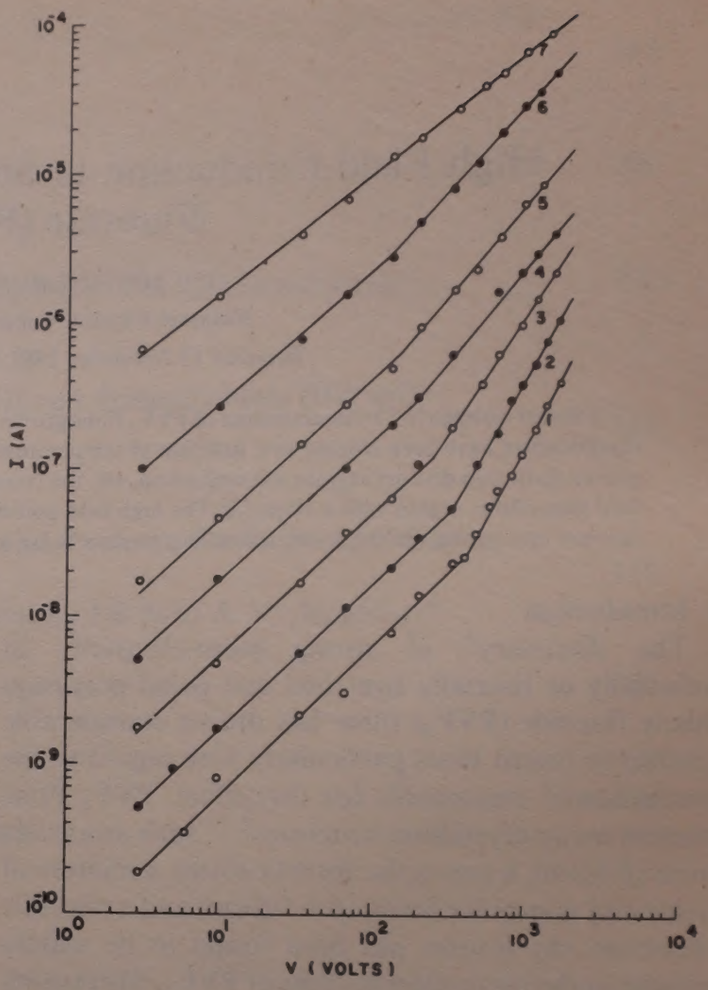

Fig. 3—I-V characteristics of pure PVF_2 films (thickness ~ 35 μm) for different temperatures [Curves 1 to 7 correspond to temperatures of 303, 317, 323, 333, 353, 373 and 393 K, respectively]

Fig. 3 shows the I-V curves in log-log scale for PVF_2 films (thickness ~ 35 μm) at different temperatures. Curves 1 to 7 correspond to the temperatures 303, 317, 323, 333, 353, 373 and 387 K, respectively. It is seen that at low temperatures the same two distinct regions of conduction as stated above are observed whereas at high temperatures, there is practically no break in the I-V curves. Thus with the increase of temperature, i.e. as one goes from curves 1 to 7, the slope of the high-field conduction region decreases.

The high-field electronic conduction mechanisms commonly discussed for various polymer films are space-charge-limited conduction (SCLC), Richardson-Schottky (RS), Poole-Frenkel (PF) emission and tunnelling of carriers into or via traps[14,15]. In order to establish the dominant mode of conduction in a particular material, one has to look into the detailed analysis of I-V data of the material in terms of the theoretical considerations available for different types of processes.

For the currents to be space-charge-limited in the high-field region, the current density I in case of shallow traps should obey[16]

$$I=\frac{9\mu\varepsilon\theta V^2}{8d^3}; \qquad V_{tran}=\frac{8en_0d^2}{9\varepsilon\theta} \qquad \ldots (1)$$

where μ is the drift mobility, ε the high frequency dielectric constant, V the applied voltage, V_{tran} the transition voltage separating the two regions of conduction, d the thickness of the film, e the electronic charge and θ a constant which describes the effect of traps and is the ratio of the free carrier density (n_0) to the trapped carrier density (n_t), i.e. $\theta = n_0/n_t$.

It is seen from Eq. (1) that (i) log-log plot of I vs d in the V^2 region should be a straight line with slope -3, and (ii) log-log plot of V_{tran} vs d should be a straight line with slope 2. Such plots were made and the slopes of -2.2 and 1.2, respectively were obtained which rules out the possibility of space charge limited currents.

If one considers the RS or PF emission as the dominant process of conduction then the current density I follows the relation[14,15]

$$I = I_0 \exp(\beta E^{1/2}/kT) \qquad \ldots (2)$$

where $I_0 = AT^2 \exp(-\varphi/kT)$ for RS

and $I_0 = \sigma_0 V/d$ for PF

and the constant

$$\beta_{RS} = (e^3/4\pi\varepsilon\varepsilon_0)^{1/2} = \tfrac{1}{2}\beta_{PF}$$

where ε_0 is the permittivity of free space, A the Richardson's constant, σ_0 the low field conductivity and E the applied field, i.e. $E = V/d$. Eq. (2) suggests that the plot of $\log I$ vs $V^{1/2}$ should be a linear one having a slope of β/kT. Such a plot was made for PVF_2 and is shown in Fig. 4. The value of β was estimated from the straight portions of the graphs and the value of high frequency dielectric constant was calculated by using Eq. (3). It was found that on substituting the value of β_{RS}, $\varepsilon \geq 13$ and on substituting the value of β_{PF}, $\varepsilon \geq 52$. However, as the reported[17] value of ε for PVF_2 at 10^9 Hz is ~ 2.98; such a large discrepancy in the estimated and the reported values of ε completely eliminates the possibility of RS or PF mechanisms governing the high field currents.

Now, the I-V data on PVF_2 is analysed in terms of the tunnelling of carriers into or via traps, i.e. traps-assisted tunnelling (TAT); the process, however, may be a thermally activated one. The generalized expression for current density I in the case of thermally-assisted tunnelling is given by[18]

$$I_{TAT} = a\exp(-\varphi/kT)\exp\{(b/kT + c)V^{1/2}/d^{1/2}\} \qquad \ldots (4)$$

where a, b and c are the fitting parameters and have the values[18] as 6.80×10^7 A/cm^2, 1.00×10^{-4} eV cm$^{1/2}$/V$^{1/2}$ and 1.20×10^{-3} cm$^{1/2}$/V$^{1/2}$, respectively. Our I-V data on PVF_2 films satisfy Eq. (4) with values of fitting parameters as 7.76×10^6 A/cm^2, 5.86×10^{-4} eV cm$^{1/2}$/V$^{1/2}$ and 1.40×10^{-3} cm$^{1/2}$/V$^{1/2}$, respectively, and these values are in quite good agreement with the theoretical ones as stated above. Further, Eq. (4) suggests that the activation energy (U) for conduction

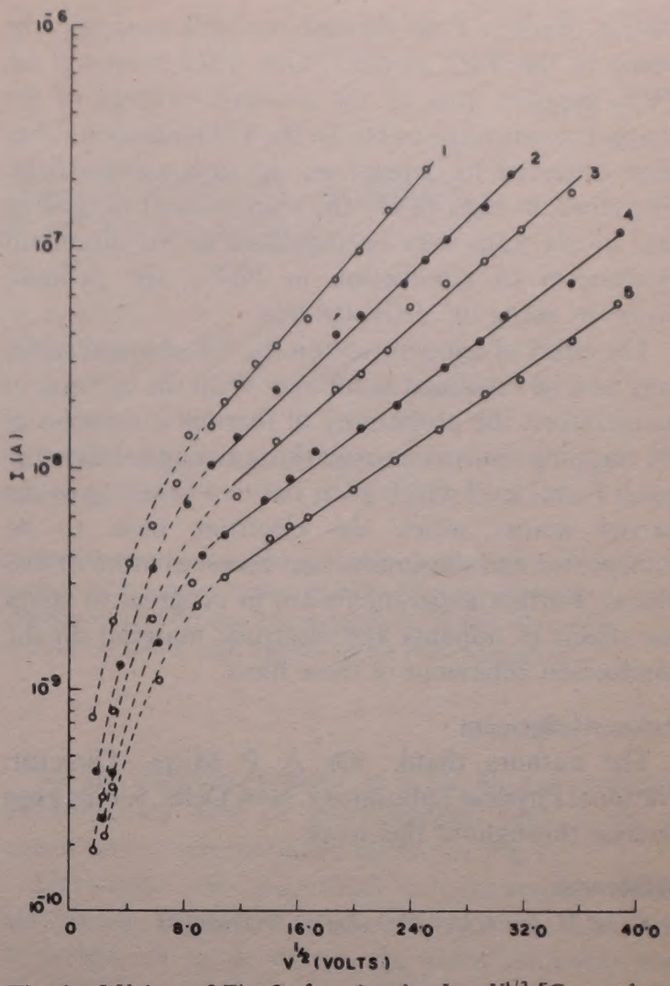

Fig. 4—I-V data of Fig. 2 plotted as $\log I$ vs $V^{1/2}$ [Curves 1 to 5 correspond to thickness of 18, 27, 35, 57 and 80 μm, respectively]

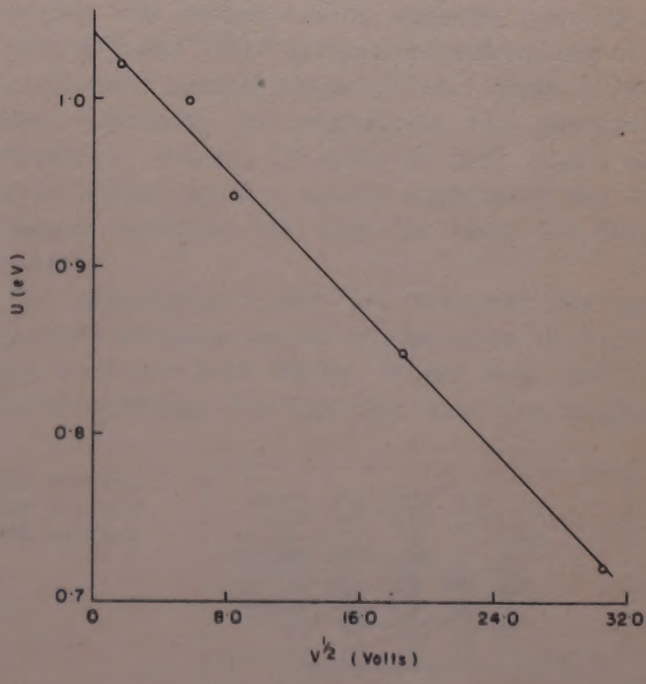

Fig 5—Plot of activation energy (U) vs the sq. root of applied voltage

determined from the conventional Arrhenius plot of $\log I$ vs $1/T$ will be a field-dependent one. This indeed is observed in our case. A plot of activation energy vs sq. root of the applied voltage is shown in Fig. 5. It is seen that U decreases from 1.02 eV at 3 V to 0.72 eV at

1000 V. Such a field dependence will especially be noted in the TSD studies[7]. Our TSD studies[7,8] on PVF_2 support this, as the activation energy of the charge carriers responsible for the TSD relaxations has been observed to depend on the polarization field. Therefore, at high fields, the trap-assisted tunnelling into or via traps may be suggested as the dominant mechanism of conduction in PVF_2; the process, however, being the activated one.

The effect of temperature on the *I-V* characteristics may now be explained as follows. With the increase of temperature, the probability of thermal ionization of the trapping centres increases thus causing a shift in the quasi Fermi level which gives rise to a lowering of the barrier across which the electrons have to be transported and the conduction becomes more or less ohmic. Further experiments are in progress to study the effects of dopants and electrode material on the conduction behaviour of these films.

Acknowledgement

The authors thank Dr A P Mitra, Director, National Physical Laboratory, New Delhi, for his keen interest throughout this work.

References

1 Kawai H, *Jpn J Appl Phys (Japan)*, **8** (1969) 975.
2 Wada Y & Hayakawa R, *Jpn J Appl Phys (Japan)*, **15** (1976) 2041.
3 Lando J B, Olf H G & Peterlin A J, *J Polym Sci (USA)*, Pt A-2, **4** (1966) 941.
4 Doll W W & Lando J B, *J Macromol Sci (USA)*, **B4** (1970) 309.
5 Abkowitz M, Prest W M, Luca D J & Pfister G, *Appl Phys Lett (USA)*, **39** (1979) 19.
6 Murayama N & Hashizumi H, *J Polym Sci Polym Phys Ed (USA)*, **14** (1976) 989.
7 Jain K, Chanq S & Mehendru P C, *Phys Lett A (Netherlands)*, **74** (1979) 288.
8 Mehendru P C, Chand S & Jain K, *Indian J Pure & Appl Phys*, **18** (1980) 183.
9 Pillai P K C, Jain K & Jain V K, *J Electrochem Soc (USA)*, **120** (1975) 435.
10 Goswami A & Radhakrishnan S, *Phys Status Solidi a (Germany)*, **38** (1976) K151.
11 Mehendru P C, Pathak N L, Singh S & Mehendru P, *Phys Status Solidi a (Germany)*, **38** (1976) 355.
12 Murayama N, *J Polym Sci.(USA)*, Pt A-2, **13** (1975) 929.
13 Murayama N, Oikawa T, Katto T & Nakamura K, *J Polym Sci (USA)*, Pt. A-2, **13** (1975) 1033.
14 Lamb D R, *Electronic conduction mechanisms in thin insulating films* (Methuen & Co, London), 1967.
15 Simmons J G, *Handbook of thin film technology* (McGraw Hill, New York), 1970.
16 Lampert M A & Mark P, *Current injection in solids* (Academic Press, New York), 1970, 21.
17 *Encyclopedia of polymer science and technology*, Vol. 14 (Interscience, New York), 1971.
18 Roberts G F & Polanco J I, *Phys Status Solidi a (Germany)* **1** (1970) 409.

Indian Journal of Pure & Applied Physics
Vol. 21, June 1983, pp. 327-331

High Frequency Performance of Thin-Film Capacitor Using Composite Film of SiO and B_2O_3

G C DUBEY & R A SINGH
Solidstate Physics Laboratory, Delhi 110007
and
G C TRIGUNAYAT*
Department of Physics and Astrophysics, Delhi University, Delhi 110007

Received 31 *March* 1982

Thin-film components are useful for miniaturization and high frequency performance of electronic circuitry. The present paper describes the high frequency performance of thin-film capacitors using composite films of SiO + 5% B_2O_3. These films yield thin-film capacitors having low losses and are useful for high frequency applications. The performance of these capacitors is also compared with that of SiO thin-film capacitors. It has been observed that at high frequencies the electrode parameters also contribute towards the losses.

1 Introduction

SiO is commonly used as a dielectric for thin-film capacitors, though the losses of such capacitors increase at high frequency. The dielectric loss of this material depends on the processing parameters[1-3] as well as on doping of the material[4-6]. The addition of impurities like B_2O_3 [Ref. 5,6] to SiO reduces the dielectric losses to a great extent due to increase in non-crystallinity of the film[7]. But it has been observed that the electrode parameters affect the dielectric losses of the films at high frequencies[8,9]. In the present paper, the variation of capacity and dielectric losses of thin-film capacitors of composite film of SiO + 5% B_2O_3 have been compared with the variation of these parameters with thin-film capacitors of SiO film only. The frequency range of interest has been restricted from 1 to 100 MHz. The behaviour at lower frequency is not of much interest as no large difference in dielectric properties of the materials is expected.

2 Experimental Details

The capacitors are fabricated by sandwiching the dielectric films between the two conducting aluminium electrodes. The electrodes are deposited on glass substrates by vacuum evaporation of aluminium (99.999%) through a metal mask. Dielectric material is evaporated in a Drumbeller[10] source heater through another mask. Two types of dielectric materials have been evaporated, i.e. SiO and (SiO + 5% B_2O_3). The substrate temperature has been kept at 250°C. Three masks are required to complete the sandwich of dielectric to delineate the metal-insulator-metal structure: first for lower plate of aluminium, second for dielectric and third again for top plate of aluminium.

All the capacitors made in a set have a common electrode for ease of measurement; such a set of capacitors is schematically shown in Fig. 1.

Electrodes are deposited simultaneously while fabricating capacitors with two types of dielectric materials, so as to ensure the same thickness and conductivity of the electrodes. This makes it possible to compare the behaviour of two types of dielectric materials. The thickness of the dielectric material is kept at 5000 and 7000 Å as measured with the help of a quartz crystal monitor (model DTM-3, Sloan, USA). Other conditions of evaporation like substrate temperature, position of substrate with respect to quartz crystal monitor, source temperature etc. of dielectric materials, are kept the same for both materials.

The capacitance values are measured for the capacitors prepared in the configuration of Fig. 1, using a Wayne-Kerr Bridge, model B-80 (V.H.F. admittance bridge). The capacitors have area ranging

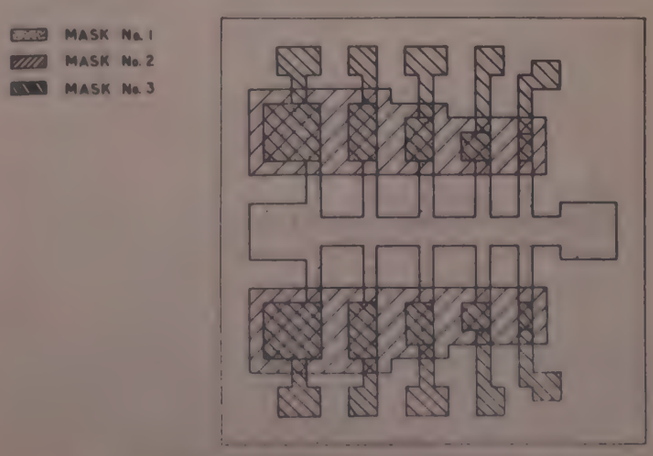

Fig. 1 — Schematic diagram of thin film capacitor

from 0.5 to 4 mm^2. The capacitance of the smallest one is about 50 pF for 5000 Å thickness of the dielectric.

3 Theoretical Model of Capacitor

The theoretical model for the estimation of capacity and dielectric losses is presented first before discussing the experimental observations. The model is based on the analysis done by Prozorvoskii and Negodenko[11] for dielectric losses only.

Consider a thin-film capacitor (Fig. 2) having a dielectric of thickness d. Assuming that there are no free charges between the electrodes, the potential field will satisfy the Laplace equation. Let d be much smaller as compared to the length l and the breadth b of the capacitor. Then the field φ will satisfy the two-dimensional Laplace equation:

$$\frac{\partial^2\varphi}{\partial x^2}+\frac{\partial^2\varphi}{\partial y^2}=0 \qquad \ldots (1)$$

If a potential difference V is applied across the electrodes, having conductivity σ, at points having coordinates $(1, +d/2)$ and $(1, -d/2)$, the solution of the equation is

$$\varphi=\frac{V}{2}\cdot\frac{\sin \alpha y}{\sin(\alpha d/2)}\cdot\frac{\cos h\alpha x}{\cos h\alpha l} \qquad \ldots (2)$$

where α is an arbitrary constant (to be defined later to satisfy the present model). The surface charge density on the metal film (τ) is related to current density by

$$\frac{\partial\sigma}{\partial x}=-j\omega\tau \qquad \ldots (3)$$

where ω is the angular frequency.

The current density in the plate is

$$i=-\sigma\frac{\partial\varphi}{\partial x} \qquad \ldots (4)$$

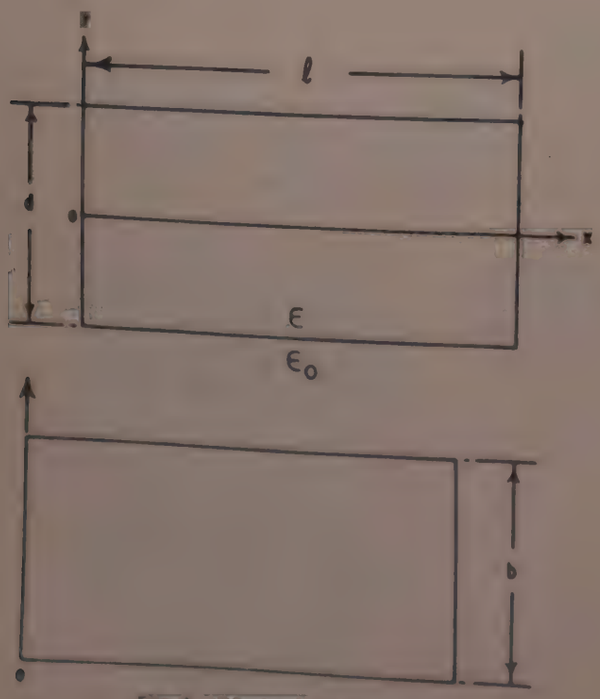

Fig. 2 — Model of a capacitor

The distribution of charge at the boundaries of the dielectric ($y=d/2$) is associated with the normal component of the field density by the expression

$$\tau=\pm\varepsilon\frac{\partial\varphi}{\partial y}, \qquad y=\pm d/2 \qquad \ldots (5)$$

where ε is the dielectric constant of the film. The positive value of charge refers to the upper plate and negative value to the lower plate.

Eqs (3)-(5) yield,

$$\sigma\frac{\partial^2\varphi}{\partial x^2}=\pm i\omega\varepsilon\frac{\partial\varphi}{\partial y} \qquad \ldots (6)$$

From Eqs (2) and (6),

$$\alpha=\pm\frac{i\omega\varepsilon}{\sigma}\cot\alpha\frac{d}{2} \qquad \ldots (7)$$

If $\alpha\frac{d}{2}\ll 1$, $\quad \cot\alpha\frac{d}{2}\simeq 2/\alpha d$

Therefore,

$$\alpha=\frac{i\omega\varepsilon}{\sigma}\cdot\frac{1}{\alpha d/2}$$

or

$$\alpha=\pm\sqrt{\frac{2i\omega\varepsilon}{\sigma d}} \qquad \ldots (8)$$

The presence of free charges in the dielectric is easily taken into account by assuming the dielectric constant to have the complex value

$$\varepsilon=\varepsilon'-jg/\omega-j\varepsilon'' \qquad \ldots (9)$$

where ε' is the real part of the dielectric constant, g the volume conductivity of the dielectric and ε'' the imaginary part of the dielectric constant, which characterizes the losses due to relaxation.

For SiO or a mixture of SiO and B_2O_3, the electron-relaxation and ion-relaxation polarization are characteristics of the material and, in practice, the value of ε'' does not depend on frequency in the rf range[12]. Substituting Eq. (9) into Eq. (8) and taking into account that in the usual frequency range for a capacitor, $\varepsilon''/\varepsilon'\ll 1$ and $g/\omega\varepsilon'\ll 1$, one obtains

$$\alpha=\alpha'+j\alpha''=\sqrt{\frac{\omega\varepsilon'}{\sigma d}}\left[\left(1+\frac{\varepsilon''+\frac{g}{\omega}}{2\varepsilon'}\right)+j\left(1-\frac{\varepsilon''+\frac{g}{\omega}}{2\varepsilon'}\right)\right] \qquad \ldots (10)$$

The current through the capacitor,

$$I=i(l)b=-\frac{V}{2}\alpha\sigma b\tan h\alpha l \qquad \ldots (11)$$

Here $i(l)$ is the current density at a point having coordinates $(l, d/2)$. The negative sign on the right side of Eq. (11) indicates that the current flows in the opposite direction of x-axis. It has been ignored in the subsequent calculations.

The complex admittance of the capacitor is given by

$$Y = \frac{I}{V} = \frac{\alpha\sigma b}{2} \tan h\alpha l \qquad \ldots (12)$$

The dissipation factor, $\tan\delta$, of the capacitor is determined by the ratio of the real part of the admittance to the imaginary part,

$$\tan\delta = \frac{Y_{real}}{Y_{im}} \qquad \ldots (13)$$

By substituting Eq. (10) into Eq. (12), separating the imaginary and real parts, expanding the trigonometric and hyperbolic functions in Maclaurin's series, and neglecting higher order terms, one obtains,

$$\tan\delta = \frac{g}{\omega\varepsilon'} + \frac{\varepsilon''}{\varepsilon'} + \frac{2l^2\omega\varepsilon'}{3\sigma d} \qquad \ldots (14)$$

The first term in this equation is characterized by losses due to conductance. It is large at low frequencies. At high frequencies, the third term, governed by the losses in the plates, predominates.

Consequently, in capacitors having large l values, the losses due to electrode parameters will be dominating, while in the smaller capacitors the losses due to dielectric relaxation will dominate.

The capacitance is given by

$$C = \frac{Y_{im}}{\omega} \qquad \ldots (15)$$

Proceeding in the same way as for the derivation of Eq. (14), one obtains,

$$C = \frac{\varepsilon' lb}{d}\left[1 - \frac{4l^2}{3\sigma d}(\omega\varepsilon'' + g) - \left(\frac{\varepsilon''\omega + g}{2\omega\varepsilon'}\right)^2\right] \qquad \ldots (16)$$

Higher order terms can be neglected, as $g/\omega\varepsilon'$ and $\varepsilon''/\varepsilon' \ll 1$. Therefore,

$$C = \frac{\varepsilon' lb}{d}\left[1 - \frac{4l^2\omega}{3\sigma d}\left(\varepsilon'' + \frac{g}{\omega}\right)\right] \qquad \ldots (17)$$

If the second term is neglected

$$C = \frac{\varepsilon' lb}{d} \qquad \ldots (18)$$

which is the usual expression for a parallel plate capacitor. From Eq. (17) since $g/\omega \ll \varepsilon''$,

$$C = \frac{\varepsilon' lb}{d}\left[1 - \frac{4}{3}\frac{l^2\omega\varepsilon''}{\sigma d}\right] \qquad \ldots (19)$$

It follows that C would decrease with frequency. The extent of decrease will depend upon the thickness and relaxation losses of the dielectric and the length and conductivity of the electrodes as per Eq. (17).

4 Results and Discussion

It has been observed that for a large area capacitor, C values of 350 and 150 pF were measured at 1 kHz and 10 MHz respectively. From Eqs (14) and (19) it is noted that because of the factor l^2 the values of the dielectric losses and capacitance are dominantly influenced by the second term involving l^2.

For large area capacitors the effect of losses due to conductance and relaxation are almost completely obscured by losses due to electrode dimensions. Consequently, the measurements have been restricted to the smallest area capacitors (0.5 mm^2) alone so that the dominance of the term due to electrode parameters in the Eqs. (14) and (19) is avoided (to estimate the conductance and relaxation losses). The effect of thickness of the dielectric (d), which only moderately affects the magnitude of this term has, of course, been ignored. In fact, since it occurs in the denominator of the term, an increase in its value further tends to offset the dominance of l^2, occurring in the numerator.

Fig. 3 shows the variation of capacitance with frequency for SiO of thickness 5000 Å and (SiO + 5 % B_2O_3) for two different thicknesses, viz. 5000 and 7000 Å respectively, while the curve III is the theoretical curve for the same composition and thickness 7000 Å, computed by using Eq. (19). The curve IV is the experimental curve for SiO films of thickness 5000 Å. A comparison of the curves I and IV, which correspond to the same film thickness but different materials, shows that the variation of capacity with frequency for SiO is faster than for (SiO + 5 % B_2O_3). The value of ε'', which represents losses due to relaxation of the dielectric material, is not exactly known, as most of the thin-film materials are dispersive[13].

However, it can be calculated using Eq. (19) and the slope of the curve I, for the film thickness 5000 Å. Then

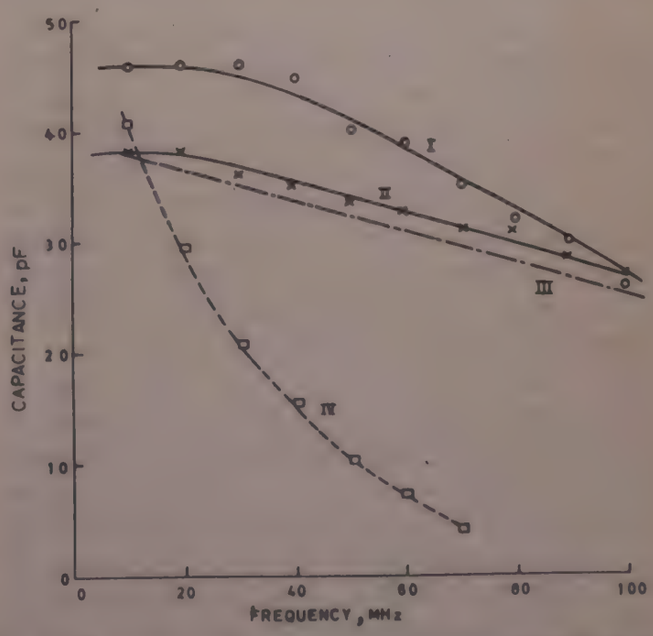

Fig. 3—The variation of capacitances at high frequencies [Curves (I) & (II): Experimental curves for the composition (SiO + 5 % B_2O_3) for thicknesses 5000 and 7000 Å respectively. Curve (III): Theoretical curve for same composition and thickness 7000 Å. Curve (IV): Experimental curve for SiO and thickness 5000 Å]

making use of the same value in Eq. (19), the theoretical curve III has been plotted for a film thickness of 7000 Å. This curve has a close fit with the experimental curve II obtained for the same film thickness. It follows that the value of ε'' computed from curve I represents the correct value. Further, since the slope of curve I is less than that of curve IV, the value of ε'' for the films of ($SiO + 5\%$ B_2O_3) turns out to be smaller than for SiO. It implies that use of the former as dielectric material should improve the performance of the capacitor at high frequencies. At higher frequencies, the inductance offered by the thin-film leads of the electrodes of the capacitor deserves special consideration. The capacitance is measured with an admittance bridge and at high frequencies the impedance offered by the inductance may be large enough of offset the effect of impedance of the capacitor, as follows. The value of inductance[14] per unit length is given by

$$L = 5.08 \times 10^{-3} l \left[\log_e \frac{l}{b+h} + 1.193 + 0.224 \frac{b+h}{l} \right] \quad \ldots (20)$$

where b, h and l denote respectively, the width, the thickness and the length of the electrodes in mils. If $h \ll b$, as is usually the case, the expression becomes

$$L = 5.08 \times 10^{-3} l \left[\log_e \frac{l}{b} + 1.193 + 0.224 \frac{b}{l} \right] \quad \ldots (21)$$

For typical values of l and b, as those employed in the present study, L has values around 1.0 nH/mm; consequently at high frequencies it may offer sufficient impedance to offset the effect of capacitance. The curves in Fig. 3 show that the capacitance decreases with frequency, at high frequencies of 10^6 Hz and above. From Eq. (10), it is seen that this results due to the effect of electrode parameters l and σ. Based on the measurement of capacitance values, Hirose and Wada[13] have observed a decrease in dielectric constant at high frequencies around 1 MHz, which they have attributed to the dispersion. However, it is possible that the observed decrease results from the effect of electrode parameters as in the present work.

Since the capacitance shows a wide range of variation with frequency as in Fig. 3 it is desirable to specify the values of frequency where the capacitance is reduced to approximately 3·4 of the original value. These values lie at 20 and 60 MHz for SiO and SiO + 5% B_2O_3 respectively, for the same thickness (5000 Å) of the dielectric material. Thus the addition of 5% B_2O_3 to SiO has upgraded the performance of the capacitor to much high frequencies.

The variation of tan δ at high frequencies in the range 10-100 MHz has been shown in Fig. 4 for the film of (SiO + 5% B_2O_3) of thickness 5000 and 7000 Å and

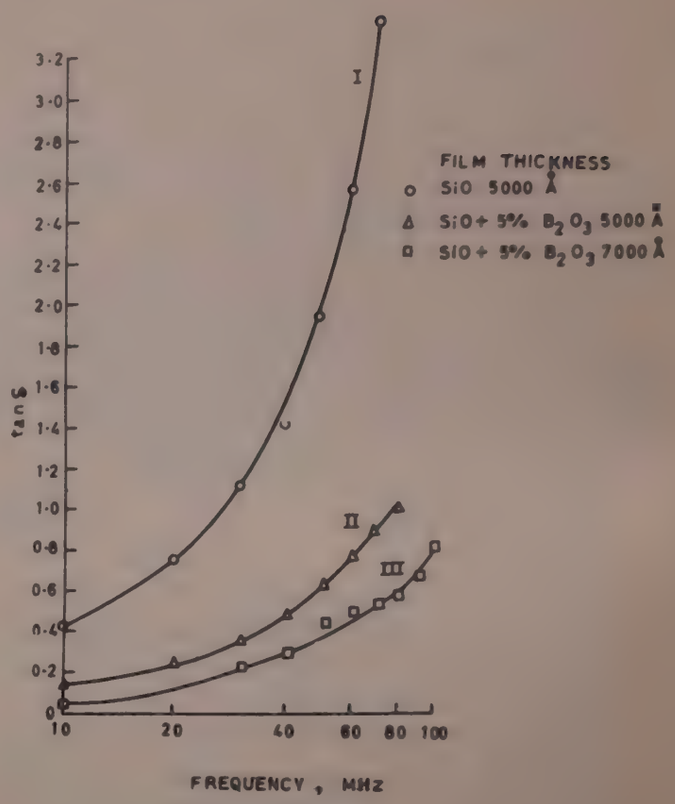

Fig. 4—Variation of dielectric losses with frequency

for SiO films. A comparison of the curves shows that the addition of 5% B_2O_3 to SiO considerably reduces the dielectric losses. The addition of B_2O_3 leads to a suppression of crystallization of SiO and hence to the reduction of dielectric losses. The comparison of curves II and III for ($SiO + 5\%$ B_2O_3) further shows that the dielectric losses decrease when the film thickness is increased. This is in agreement with the observation of Prozorvoskii and Negodenko[10] who have reported a reduction in dielectric losses with thickness for SiO films. Later, Ravez[15] has found that the increase in the film thickness increases the non-crystallinity of the amorphous films of SiO_2. Therefore, it may be concluded that this should lead to a decrease in the dielectric losses as observed in the present work.

Measurement of capacitance over a period of one year is made for a set of capacitors. These capacitors are found to be stable; the variation in the capacitance of a typical capacitor over a period of one year gives almost a straight line parallel to the time axis. This gives a stable value of capacitor.

5 Conclusions

The observed low dielectric losses at high frequencies for the ($SiO + 5\%$ B_2O_3) films suggest that capacitors with higher stability and suitable for high frequency performance can be made using ($SiO + 5\%$ B_2O_3) as the dielectric material.

These losses can be reduced further if the electrode material offers low conduction losses, i.e. it possesses

higher conductivity. At high frequencies, the inductive effect of the electrodes also plays an important role. Therefore, while designing the thin-film capacitors for high frequency applications the electrode leads and plates should be smaller in length.

Acknowledgement

The authors (G.C.D. and R.A.S.) are grateful to the Director, Solidstate Physics Laboratory, Lucknow Road, Delhi-7, for permission to publish this paper.

References

1 Siddall G, *Vacuum (GB)*, **9** (1959) 274.
2 Timson P A & Hogarth C A, *Thin Solid Films (Switzerland)*, **10** (1972) 321.
3 Vantier C, Ranc G & Protin L, *Thin Solid Films (Switzerland)*, **88** (1979) 321.
4 Hanlein W & Gunthu K C, *Advances in vacuum science and technology* (Pergamon Press, London), 1960, 727.
5 Timson P A & Hogarth C A, *Thin Solid Films (Switzerland)*, **8** (1971) R-33.
6 Vardhan H, Dubey G C & Singh R A, *Thin Solid Films (Switzerland)*, **8** (1971) 56.
7 Dubey G C, Mull R P & Chaudhary K L, *Thin Solid Films (Switzerland)*, **24** (1974) 261.
8 Harrop P J, *Dielectrics*: 49 (Butterworths, London), 1972.
9 Wyndrun R W, Stark P D, Pelletier F P & Lee S C, *Electronic Computer Conference* (IEEE, New York, USA), 1969.
10 Drumbeller G E, *Trans 7th Nat Vac Symp* (Pergamon Press, Oxford), 1960, 306.
11 Prozorvoskii V E & Negodenko O M, *Izueztka Yuz Radio Technika*, **9** (1966) 503.
12 Jonscher A K, A many-body universal approach to dielectric relaxation in solids, in *Physics of dielectric solids*, edited by C.H.L. Goodman (Institute of Physics, Bristol, England), 1980, 22.
13 Hirose H & Wada Y, *J Appl Phys (USA)*, **3** (1964) 179.
14 Ganlton M, Heishenov B, Kin S P & Debrechh R E, *IEEE Trans Microwave Theory & Tech (USA)*, **MTT-19** (1971) 588.
15 Ravez A G, *J Non-Cryst Solids (Netherlands)*, **4** (1970) 347.

Indian Journal of Pure & Applied Physics
Vol. 21, June 1983, pp. 332-335

Substituted Benzenes – V: Normal Coordinate Analysis of Out-of-Plane Vibrations of Mono Iodonitrobenzenes

P MURALIDHAR RAO & G RAMANA RAO*
Department of Physics, University College, Kakatiya University, Vidyaranyapuri, Warangal 506 009

Received 15 *October* 1982

Normal coordinate analysis is made for the out-of-plane vibrations of *ortho*, *meta* and *para* iodonitrobenzenes using a 14-parameter modified valence force field. The force constants are refined by the method of least-squares employing the vibrational frequencies of the three molecules. The potential energy distributions are computed and the nature of the absorption bands is discussed.

1 Introduction

The vibrational spectra of mono substituted nitrobenzenes have been reported by Green and Harrison[1] with tentative assignments. Varsanyi[2] has summarized them along with the vibrational spectra of seven hundred benzene derivatives. The normal coordinate analysis of these compounds, which is very essential for a complete understanding of vibrational modes[3], is yet to appear in the literature. In Part IV of this series, we have reported a modified valence force field for the in-plane vibrations of mono iodonitrobenzenes[4]. This paper presents the results of normal coordinate analysis of out-of-plane vibrations of the same compounds.

2 Normal Coordinate Treatment

The computing procedure is the same as that employed in our earlier paper[4]. The structure and definition of out-of-plane internal coordinates of the title compounds are shown in Fig. 1. The structure parameters are those used earlier[4]. The orthonormal set of symmetry coordinates used in the calculations are given in Table 1. The vibrational frequencies of *o*-, *m*- and *p*-iodonitrobenzenes are taken from those reported by Green and Harrison[1]. The initial set of force constants is obtained by transferring the potential constants from those of mono bromonitrobenzenes[5]. In order to avoid large corrections at any time, initial refinements are carried out with a damping factor of 0.10. Only eight of the fourteen force constants are allowed to be refined this way until the calculations converged (Only 30 frequencies of the title compounds could be used for the purpose as the experimental value for C – N torsional modes are not available for these molecules. The corresponding C – N torsional constant is fixed at a very low value of 0.0001 mdyne Å/rad^2 throughout the refinement

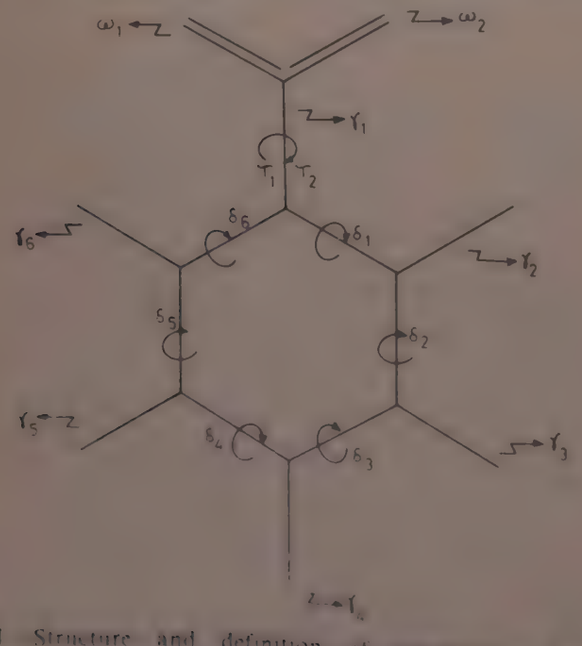

Fig 1 Structure and definition of out-of-plane internal coordinates of *meta* iodonitrobenzenes

Table 1—Symmetry Coordinates for Out-of-Plane Vibrations of Mono Iodonitribenzenes

S_i	C_{2v}	Internal coordinates involved	C_s	Description*
S_1	b_1	$(2\gamma_1+\gamma_2-\gamma_3-2\gamma_4-\gamma_5+\gamma_6)12^{-1/2}$	a''	10b
S_2	b_1	$(\delta_1-\delta_3+\delta_4-\delta_6)2^{-1}$	a''	10b
S_3	b_1	$(2\gamma_1-\gamma_2-\gamma_3+2\gamma_4-\gamma_5-\gamma_6)12^{-1/2}$	a''	17b
S_4	b_1	$(\gamma_1+\gamma_2+\gamma_3+\gamma_4+\gamma_5+\gamma_6)6^{-1/2}$	a''	11
S_5	b_1	$(\delta_1-\delta_2+\delta_3-\delta_4+\delta_5-\delta_6)6^{-1/2}$	a''	4
S_6	b_1	$(\gamma_1-\gamma_2+\gamma_3-\gamma_4+\gamma_5-\gamma_6)6^{-1/2}$	a''	5
S_7	b_1	$(\omega_1-\omega_2)2^{-1/2}$	a''	$\omega(NO_2)$
S_8	a_2	$(-\delta_1+2\delta_2-\delta_3-\delta_4+2\delta_5-\delta_6)12^{-1/2}$	a''	16a
S_9	a_2	$(\gamma_2-\gamma_3+\gamma_5-\gamma_6)2^{-1}$	a''	17a
S_{10}	a_2	$(-\gamma_2-\gamma_3+\gamma_5+\gamma_6)2^{-1}$	a''	10a
S_{11}	a_2	$(\tau_1+\tau_2)2^{-1/2}$	a''	$\tau(NO_2)$
		Redundant coordinates		
S_{12}		$(\delta_1+2\delta_2+\delta_3-\delta_4-2\delta_5-\delta_6)12^{-1/2}$		
S_{13}		$(\delta_1+\delta_2+\delta_3+\delta_4+\delta_5+\delta_6)6^{-1/2}$		
S_{14}		$(\delta_1-\delta_3-\delta_4+\delta_6)2^{-1}$		
S_{15}		$(\omega_1+\omega_2)2^{-1/2}$		
S_{16}		$(\tau_1-\tau_2)2^{-1/2}$		

*Wilson's notation

process). Two more interaction constants are fixed at values calculated with damping. The damping factor is then made zero and further refinement is continued. The calculations converged in two cycles under these conditions with an average error of 9.3 cm^{-1} between the observed and calculated frequencies.

3 Results and Discussion

The initial and final sets of force constants along with their dispersions are presented in Table 2. The observed and calculated frequencies and potential energy distributions (PED) in internal force constants for the three molecules under investigation are given in Table 3. The characteristic feature of PED in internal force constants for out-of-plane vibrations is that there will be large contributions, both positive and negative, from off-diagonal force constants apart from the fact that the contributions from certain diagonal constants exceeds 100% by large amounts[6,7]. As such, it becomes difficult to assess the actual contribution from a diagonal constant. This presents difficulties while interpreting the results. To circumvent these difficulties we have calculated the PED in principal internal coordinates by suitable addition of contributions from off-diagonal constants to the contributions from diagonal constants (A diagonal internal force constant which represents a group of equivalent internal coordinates is known as the principal internal coordinate. For example, ν_R is the principal internal coordinate which stands for the four CH out-of-plane bends). These PEDs are also shown in Table 3. PEDs below 10% are not shown. The same table contains the vibrational assignments in Wilson's notation[8].

Table 2—Out-of-Plane Force Constants (in mdyne Å/rad^2) of Mono Iodonitrobenzenes

Force Constant symbol	Coordinates involved	Common atoms	Initial value	Final value	Dispersion
γ_R	C–H	—	0.4530	0.4531	0.0009
γ_{R1}	C–I	—	0.6242	0.6275	0.0101
δ	C–C	—	0.3955	0.3959	0.0018
γ_M	C–N	—	0.4059	0.3917	0.0068
γ_{M1}	N=O	—	0.2621	0.2629	0.0026
τ	C–N	—	0.0001	0.0001	0.0
γ_R, γ_R	C–H, C–H	C–C	−0.0648	−0.0658	0.0
δ_i, δ_{i+1}	C–C, C–C	$\widehat{CCC}$	0.0103	0.0103	0.0
γ_{R1}, γ_R	C–I, C–H	C–C	−0.1085	−0.1085	0.0
γ_M, γ_R	C–N, C–H	C–C	−0.0311	−0.0311	0.0
γ_{R1}, δ	C–I, C–C	C–C	0.2260	0.2260	0.0
γ_R, δ	C–H, C–C	C–C	0.1741	0.1741	0.0
γ_M, δ	C–N, C–C	C–C	0.1875	0.1878	0.0
γ_M, γ_{R1}	C–N, C–I	C–C	−0.0463	−0.0546	0.0100

3.1 Vibrational Assignments

From Tables 2 and 3 it is clear that:

(i) Observed and calculated frequencies agree well within the limits of experimental error and anharmonicity corrections,

(ii) The final values of the force constants are not much different from the initial values as the corrections have never been very large,

(iii) The dispersions of the force constants are quite small and

(iv) The constants are comparable with those of related molecules.

These observations indicate that the force field obtained in the present case is a physically reasonable set. Therefore, the assignment of various fundamental modes can be done on the basis of this vibrational analysis, rather than from hitherto qualitative considerations[1,2].

C–H out-of-plane bending vibrations—In disubstituted benzenes of the present type, there are four C–H out-of-plane bending modes designated as 5, 11, 17a and 17b in the *ortho* and *meta* compounds and 5, 10a, 17a and 17b in the *para* isomer. The corresponding phase relations in the eigen vector are:

$$+-+-;\ +++\ +;\ ++--\text{ and }+--+$$

As identified from these phase relations and the PED presented in Table 3, the bands at 984, 777, 852 and 952 cm^{-1} in the *ortho* compound are due to the C–H out-of-plane bending modes 5, 11, 17a and 17b respectively. The corresponding vibrations in the *meta* compound are at 980, 798, 925 and 893 cm^{-1} whereas these are identified near 965, 814, 841 and 954 cm^{-1} in the *para* isomer. Thus, mode 5 with the phase relations $+-+-$ is the highest out-of-plane C–H bending vibration in the three molecules studied. This result is against the expectations of Green and Harrison[1] for *para* compounds wherein they infer 17a to be the highest C–H out-of-plane bending mode. The lowest out-of-plane C–H bending mode is that in which the corresponding internal coordinates either increase or decrease simultaneously. It is found that 17b is greater than 17a in *ortho* and *para* compounds whereas the reverse is true in the case of the *meta* isomer. This result agrees with the expectations of Green and Harrison[1]. Further, the present calculations show all the C–H out-of-plane bending modes to be pure as can be seen from Table 3.

Table 3—Potential Energy Distribution (PED) of Out-of-Plane Vibrations of *mono* Iodonitrobenzenes

Obs. freq. (cm^{-1})	Cal. freq. (cm^{-1})	PED in internal force constants	PED in principal internal coordinates	Vibrational assignment
		ortho Iodonitrobenzene (a'' species)		
139	128	$10\gamma_{R1}$, 27δ, $28\gamma_M$, $22\gamma_M$, $^{15}\gamma_{R1}$, δ	$18\gamma_{R1}$, 45δ, $39\gamma_M$	10a + 16b + 10b
194	207	$10\gamma_R$, $25\gamma_{R1}$, 26δ, $62\gamma_M$, $30\gamma_{R1}$, δ	$40\gamma_{R1}$, 21δ, $49\gamma_M$	10a + 16b + 10b
410	416	$29\gamma_R$, $11\gamma_{R1}$, 215δ, $64\gamma_M$	102δ	16a
464	477	$12\gamma_R$, $87\gamma_{R1}$, 149δ	72δ, $34\gamma_{R1}$	16b + 10a
693	662	$25\gamma_R$, $18\gamma_{R1}$, 179δ, $13\gamma_{M1}$	110δ	4
728	734	$10\gamma_{R1}$, 57δ, $29\gamma_M$, $73\gamma_{M1}$	$73\gamma_{M1}$, 18δ	$\omega(NO_2)$ + 4
777	769	$120\gamma_R$	$92\gamma_R$	11
852	863	$121\gamma_R$	$101\gamma_R$	17a
952	950	$123\gamma_R$, 13δ, $11\gamma_R$, γ_R	$109\gamma_R$	17b
984	982	$138\gamma_R$, 30δ, $32\gamma_R$, γ_R	$120\gamma_R$	5
		meta Iodonitrobenzene (a'' species)		
129	143	$26\gamma_{R1}$, $64\gamma_{R1}$, $11\gamma_{R1}$, δ; 10δ	$32\gamma_{R1}$, $64\gamma_M$, 15δ	10a + 16b + 10b
186	199	$13\gamma_R$, $18\gamma_{R1}$, 41δ, $19\gamma_M$, $29\gamma_{R1}$, δ, $10\gamma_{M,\delta}$	$33\gamma_{R1}$, 49δ, $24\gamma_M$	10a + 16b + 10b
414	416	$31\gamma_R$, 216δ, $69\gamma_M$	94δ	16a
466	471	$21\gamma_R$, $66\gamma_{R1}$, 152δ	81δ, $30\gamma_{R1}$	16b + 10a
663	669	$14\gamma_R$, $32\gamma_{R1}$, 179δ	114δ	4
728	728	25δ, $23\gamma_M$, $80\gamma_{M1}$	$80\gamma_{M1}$, 12δ	$\omega(NO_2)$ + 4
798	791	$121\gamma_R$, 17δ	$89\gamma_R$	11
893	886	$126\gamma_R$, 12δ	$107\gamma_R$	17b
925	927	$121\gamma_R$, 22δ, $16\gamma_{R1}$, γ_R	$104\gamma_R$	17a
980	978	$134\gamma_R$, 26δ, $27\gamma_R$, γ_R	$118\gamma_R$	5
		para Iodonitrobenzene (b_1 species)		
96	85	$15\gamma_R$, $14\gamma_{R1}$, 29δ, $29\gamma_M$, $22\gamma_{R1}$, δ, $18\gamma_{M,\delta}$	$25\gamma_{R1}$, 40δ, $38\gamma_M$	10b + 16b + 11
260	242	$27\gamma_{R1}$, 21δ, $78\gamma_M$, $19\gamma_{R1}$, δ	$37\gamma_{R1}$, 10δ, $56\gamma_M$	10b + 16b + 11
458	442	$15\gamma_R$, $67\gamma_{R1}$, 189δ, $52\gamma_M$	79δ, $33\gamma_{R1}$	16b + 10b
673	658	$26\gamma_R$, $29\gamma_{R1}$, 164δ, $14\gamma_{M1}$	99δ, $14\gamma_{M1}$	4
734	734	53δ, $28\gamma_M$, $75\gamma_{M1}$	$75\gamma_{M1}$, 23δ	$\omega(NO_2)$ + 4
954	952	$136\gamma_R$, 40δ, $18\gamma_R$, γ_R $15\gamma_{R1}$, γ_R	$89\gamma_R$	17b
965	970	$127\gamma_R$, 13δ, $18\gamma_R$, γ_R'	$119\gamma_R$	5
		(a_2 species)		
405	440	$33\gamma_R$, 175δ	120δ	16a
814	826	$118\gamma_R$, 14δ, $10\gamma_{R1}$, γ_R	$95\gamma_R$	10a
841	838	$117\gamma_R$	$100\gamma_R$	17a

C – X out-of-plane bending modes—In disubstituted benzenes, as the name implies, there are two out-of-plane bending modes of the substituents. In the present case, these are C – I and C – N out-of-plane bending modes designated as 10a and 10b in the *ortho* and *meta* compounds and 10b and 11 in the *para* isomer respectively. The bands at 139 and 194 cm^{-1} of the *ortho* compounds, absorption bands at 129 and 186 cm^{-1} of the *meta* molecule and 96 and 260 cm^{-1} modes of the *para* isomer could be assigned in combination to these modes. As can be seen from Table 3, the two modes not only mix with each other but one of them has a large contribution from the C – C torsional mode 16b.

C C C out-of-plane bending modes—These are also known as ring torsions. There are three of them designated as 4, 16a and 16b in benzene and substituted benzenes. In mode 4, the alternate CC torsion angles are either increasing or decreasing. In mode 16a, these angle change in the ratio +2, −1, −1, +2, −1, −1 while in 16b they change in the ratio 0, +2, −2, 0, +2, −2 (the +ve and −ve signs indicate increase and decrease respectively). In unsymmetrically disubstituted benzenes of the present type these statements are approximately true.

Thus identified, mode 4 is near 693, 663 and 673 cm^{-1} in *ortho*, *meta* and *para* iodonitrobenzenes. Incidentally, it happens to be the highest ring torsional mode in the three molecules. It is also a pure mode as is evident from Table 3.

Green and Harrison[1] are of the opinion that vibration frequency of 16a should be greater than that

of 16b in *ortho* and *meta* isomers whereas the assignment could be reversed in the *para* compound. The present calculations establish that frequency of 16b is greater than that of 16a in the three isomers considered. Further 16a is a pure mode whereas 16b has a considerable mixing with C−I out-of-plane bending mode in the three molecules.

NO_2 out-of-plane vibrations—Wagging and torsional vibrations of the nitro group fall under this category. According to Green and Harrison[4], $\omega(NO_2)$ is expected near 777, 728 and 734 cm^{-1} in *o*-, *m*- and *p*-compounds respectively. But, as explained earlier, the band at 777 cm^{-1} is a C−H out-of-plane bending mode 11 in the *ortho* compound. According to the present calculations $\omega(NO_2)$ is identified at 728, 728 and 734 cm^{-1} in *ortho*, *meta* and *para* iodonitrobenzenes. It is important to note that this mixes with mode 4 in the three molecules. $\tau(NO_2)$ could not be included in the calculations as the corresponding experimental frequencies are not available. Hence, it is not discussed here.

4 Conclusions

(i) Mode 5, in which the phase relations are + − + −, is the highest C−H out-of-plane bending mode. Similarly, the mode in which the phase relations are + + + + is the lowest C−H out-of-plane bending mode. Further, all the C−H out-of-plane bending modes are pure.

(ii) The out-of-plane bending modes of C−I and C−N mix with each other with additional contributions from the ring torsion 16b.

(iii) The order of the ring torsions is 4 > 16b > 16a. Further, modes 4 and 14a are pure whereas 16b invariably mixes with C−I out-of-plane bending vibration in the three molecules.

(iv) Out-of-plane bending vibration of the nitro group mixes with ring torsional mode 4 to a small extent.

Acknowledgement

The authors are thankful to Prof. K Venkata Ramiah, Member, Union Public Service Commission, New Delhi for helpful suggestions. One of the authors (PMR) is grateful to the University Grants Commission, New Delhi for financial assistance.

References

1 Green J H S & Harrison D J, *Spectrochim Acta Vol A (GB)*, **26** (1970) 1925.

2 Varsanyi G, *Assignments for vibrational spectra of seven hundred benzene derivatives* (Adam Hilger, London) 1974.

3 Fuhrer H, Kartha V B, Krueger P J, Mantsch H H & Jones R N, *Chem Rev (USA)*, **72** (1972) 439.

4 Muralidhar Rao P & Ramana Rao G, *Indian J Pure & Appl Phys*, **20** (1982) 949.

5 Muralidhar Rao P & Ramana Rao G, *Indian J Pure & Appl Phys*, **21** (1983).

6 Patel N D, Kartha V B & Narasimham N A, *J Mol Spectrosc (USA)*, **48** (1973) 202.

7 Kumpawat M P, Osha A & Patel N D, *Can J Spectrosc (Canada)*, **25** (1980) 1.

8 Wilson E B, *Phys Rev (USA)*, **45** (1934) 706.

Indian Journal of Pure & Applied Physics
Vol. 21, June 1983, pp. 336-338

Substituted Benzenes—VI: Vibrational Analysis of Out-of-Plane Vibrations of Mono Bromonitrobenzenes

P MURALIDHAR RAO & G RAMANA RAO*
Department of Physics, University College, Kakatiya University, Vidyaranyapuri, Warangal 506 009

Received 15 *October* 1982

Normal coordinate analysis of *ortho*, *meta* and *para* bromonitrobenzenes is made using a 14-parameter modified valence force field for the out-of-plane vibrations. The force constants are refined by the method of least-squares employing the vibrational frequencies of the three molecules. The potential energy distributions are computed and the nature of the absorption bands is discussed.

1 Introduction

It is well known that, for complete understanding of the vibrational modes of fairly complex molecules, normal coordinate analysis is indispensable[1-3]. For mono bromonitrobenzenes, even though the vibrational spectra are reported with tentative assignments[4,5], their quantitative treatment using normal coordinate analysis is yet to appear in the literature. Hence, we made a rigorous mathematical study of fundamental vibrations of mono bromonitrobenzenes and report the results obtained on their out-of-plane vibrations in this paper.

2 Normal Coordinate Treatment

The computing procedure and the structure parameters are the same as those used in an earlier paper[6] with the C−Br bond length taken as 1.85 Å. The structure, definition of out-of-plane internal coordinates and the symmetry coordinates are the same as those used in part V of this series[7].

The frequencies of the out-of-plane fundamental modes of *o*-, *m*- and *p*-bromonitrobenzenes are taken from those reported by Green and Harrison[4]. The starting set of force constants is transferred from out-of-plane calculations for dihalobenzenes[8] (for the bromobenzene part) and nitrobenzenes[9] (for the C $-NO_2$ group). The C−N torsion constant is taken to be very low (0.0001 mdyne Å/rad^2) and fixed during refinement as the corresponding torsional frequencies are not available for the title compounds. The interaction constants for which no values are available are taken as zero initially. In order to avoid large corrections at any time, initial refinements are carried out with a damping factor of 0.10. Only 8 of the 14 constants are refined in this way using 30 frequencies of the title compounds until the calculations converged. At this stage, two more interaction constants are fixed at their values obtained with damping, damping factor is made zero and the refinement is continued. The calculations converged in two cycles under these

Table 1—Out-of-Plane Force Constants (in mdyne Å/rad^2) of Bromonitrobenzenes

Force constant symbol	Coordinates involved	Common atoms	Initial value	Final value	Dispersion
γ_R	C−H	—	0.4337	0.4530	0.0009
γ_{R1}	C−Br	—	0.5827	0.6242	0.0096
δ	C−C	—	0.3746	0.3955	0.0018
γ_M	C−N	—	0.5408	0.4059	0.0072
γ_{M1}	N=O	—	0.6117	0.2621	0.0027
τ	C−N	—	0.0001	0.0001	0.0
γ_R, γ_R	C−H, C−H	C−C	−0.0733	−0.0648	0.0
δ_i, δ_{i+1}	C−C, C−C	ĈCC	0.0103	0.0103	0.0
γ_{R1}, γ_R	C−Br, C−H	C−C	−0.1085	−0.1085	0.0
γ_M, γ_R	C−N, C−H	C−C	−0.0311	−0.0311	0.0
γ_{R1}, δ	C−Br, C−C	C−C	0.2260	0.2260	0.0
γ_R, δ	C−H, C−C	C−C	0.1741	0.1741	0.0
γ_M, δ	C−N, C−C	C−C	0.0	0.1875	0.0
γ_M, γ_{R1}	C−N, C−Br	C−C	0.0	−0.0463	0.0099

Table 2—Potential Energy Distribution (PED) of Out-of-Plane Vibrations of Mono Bromonitrobenzenes

Obs. freq. cm^{-1}	Calc. freq. cm^{-1}	PED in principal internal coordinates	Vibrational assignment
		ortho Bromonitrobenzene (a'' species)	
132	131	14 γ_{R1}, 45 δ, 40 γ_M	10a + 16b + 10b
199	217	30 γ_{R1}, 44 γ_M	10a + 10b
413	419	105 δ	16a
462	479	71 δ, 37 γ_{R1}	16b + 10a
690	661	111 δ, 13 γ_{M1}	4
730	735	72 γ_{M1}, 17 δ	$\omega(NO_2)$ + 4
775	772	91 γ_R	11
852	864	106 γ_R	17a
953	949	109 γ_R	17b
985	980	120 γ_R	5
		meta Bromonitrobenzene (a'' species)	
147	148	64 γ_M, 21 γ_{R1}	10b + 10a
193	206	34 γ_{R1}, 50 δ, 13 γ_M	10a + 16b + 10b
418	421	101 δ	16a
478	474	77 δ, 34 γ_{R1}	16b + 10a
664	669	112 δ	4
729	731	77 γ_{M1}, 13 δ, 11 γ_M	$\omega(NO_2)$ + 4 + 10b
797	794	99 γ_R	11
891	886	107 γ_R	17b
922	927	103 γ_R	17a
980	976	119 γ_R	5
		para Bromonitrobenzene (b_1 species)	
102	91	23 γ_{R1}, 43 δ, 38 γ_M	10b + 16b + 11
276	251	38 γ_{R1}, 54 γ_M	10b + 11
459	449	75 δ, 33 γ_{R1}	16b + 10b
674	657	97 δ, 16 γ_{M1}	4
737	738	73 γ_{M1}, 26 δ, 10 γ_M	$\omega(NO_2)$ + 4
951	951	102 γ_R	17b
965	968	120 γ_R	5
		(a_2 species)	
405	440	120 δ	16a
820	828	91 γ_R	10a
843	839	100 γ_R	17a

conditions with an average error of 8.7 cm^{-1} between the observed and calculated frequencies.

3 Results and Discussion

The final set of force constants obtained, along with the initial set and dispersions, are presented in Table 1.

The observed and calculated frequencies and the potential energy distributions (PED) in principal internal coordinates obtained as explained in an earlier paper[7] are given in Table 2. Contributions below 10% are not shown and Table 2 contains vibrational assignments also.

3.1 Vibrational Assignments

From Tables 1 and 2 it could be seen that:

(i) The agreement between the observed and calculated frequencies is very good,

(ii) The final values of the force constants are close to their initial values as the corrections have never been very large,

(iii) The dispersions of the force constants are quite small, and

(iv) The potential constants are comparable with their counterparts in related molecules.

As such, all the requirements necessary for an acceptable force field are satisfied by the potential constants obtained for the out-of-plane fundamentals of mono bromonitrobenzenes. Hence, they are physically reasonable. Therefore, the assignment of various frequencies can be made on the basis of this normal coordinate analysis, rather than from qualitative considerations[4,5].

C—H out-of-plane bending vibrations—As identified from the phase relations and the PED presented in Table 2 (please see Ref. 7 for details), the bands at 985, 775, 852 and 953 cm^{-1} are due to the C—H out-of-plane bending modes 5, 11, 17a and 17b respectively in the *ortho* compound. The corresponding vibrations in the *meta* compound are at 980, 797, 922 and 891 cm^{-1} whereas these are identified near 965, 820, 843 and 951 cm^{-1} in the *para* isomer. Thus the mode 5 is the highest out-of-plane C—H bending vibration in the three molecules studied. This result agrees with that of Green and Harrison[4] for *ortho* and *meta* compounds but differs in the case of *para* isomer. The lowest out-of-plane bending mode is found to be that in which the corresponding internal coordinates are either increasing or decreasing simultaneously. It is established that frequency of mode 17b is greater than that of 17a in *ortho* and *para* compounds whereas the reverse is true for the *meta* compound. This is in perfect agreement with the expectations of Green and Harrison[4]. Further, the present computations reveal, all the C—H out-of-plane bending modes to be pure as is evident from Table 2.

C—X out-of-plane bending vibrations—These are C—Br and C—N out-of-plane bending modes in the present set of molecules. It is seen from Table 2 that the bands at 132 and 199 cm^{-1} in the *ortho* compound, the fundamentals near 147 and 193 cm^{-1} in the *meta* compound and the absorptions around 102 and 276 cm^{-1} in the *para* compound exhibit the nature expected of C—Br and C—N out-of-plane bending modes. These two modes mix with each other. It is interesting to note that the lower of the two modes has a large contribution of PED from the ring torsion 16b in the *ortho* and *para* compounds whereas the higher of the two gets such contribution in the *meta* isomer.

Ring torsional vibrations—The three ring torsional modes 4, 16a and 16b are identified at 690, 413 and 462 cm^{-1} respectively in the *ortho* compound (for details please see Ref. 7). The corresponding vibrations

in the *meta* isomer appear near 664, 418 and 478 cm^{-1} whereas in the *para* compound they are around 674, 405 and 459 cm^{-1}. Thus the order of the ring torsions should be 4 > 16b > 16a in these three molecules. This is against the expectations of Green and Harrison[4] for *ortho* and *meta* compounds, viz. the frequency of mode 16a to be greater than that for 16b. Further, the modes 4 and 16a are pure in the three molecules whereas 16b has considerable contribution from C – Br out-of-plane bending mode.

Out-of-plane vibrations of the nitro group—The out-of-plane wagging mode of the nitro group is identified at 730, 729 and 737 cm^{-1} in the *ortho*, *meta* and *para* compounds respectively. Thus, Green and Harrison's[4] assignment for this mode in the *ortho* compound should be corrected from 775 cm^{-1} to 730 cm^{-1}. As mentioned earlier, the band at 775 cm^{-1} is due to mode 11 corresponding to C – H out-of-plane bending vibrations. It is important to note that this mode mixes with the ring torsional vibration 4 in the three molecules under consideration. A discussion of the torsional mode of the nitro group is not given as it could not be included in the calculations for reasons mentioned earlier.

4 Conclusions

(i) Mode 5 is the highest C – H out-of-plane bending mode whereas that in which the corresponding internal coordinates increase or decrease simultaneously is the lowest. Further, all the C – H out-of-plane bending modes are pure.

(ii) The out-of-plane bending modes of C – Br and C – N mix with each other. One of them has strong additional PED contribution from the ring torsion 16b.

(iii) The order of the ring torsions is 4 > 16b > 16a. Modes 4 and 16a are pure whereas 16b has considerable mixing with out-of-plane bending mode of C – Br.

(iv) Out-of-plane wagging vibration of the nitro group mixes with the ring torsional mode 4 to some extent in the three molecules.

Acknowledgement

The authors are grateful to Prof. K Venkata Ramiah, Member, Union Public Service Commission, New Delhi, for useful suggestions. One of the authors (PMR) is thankful to the University Grants Commission, New Delhi, for financial assistance.

References

1 Fuhrer H, Kartha V B, Krueger P J, Mantsch H H & Jones R N, *Chem Rev* (*USA*), **72** (1972) 439.

2 Fuhrer H, Kartha V B, Kidd K G & Mantsch H H, *Natl Res Counc Can Bull* (*Canada*), No. 15, 1976.

3 Patel N D, Kartha V B & Narasimham N A, *J Mol Spectrosc* (*USA*), **48** (1973) 185.

4 Green J H S & Harrison D J, *Spectrochim Acta Vol A* (*GB*), **26** (1970) 1925.

5 Varsanyi G, *Assignments for vibrational spectra of seven hundred benzene derivatives* (Adam Hilger, London) 1974.

6 Muralidhar Rao P & Ramana Rao G, *Indian J Pure & Appl Phys*, **20** (1982) 949.

7 Muralidhar Rao P & Ramana Rao G, *Indian J Pure & Appl Phys*, **21** (1983) 332.

8 Patel N D, Kartha V B & Narasimham N A, *J Mol Spectrosc* (*USA*), **48** (1973) 202.

9 Kuwae A & Machida K, *Spectrochim Acta Vol A* (*GB*), **35** (1979) 27.

Indian Journal of Pure & Applied Physics
Vol. 21, June 1983, pp. 339-343

Dielectric Relaxation Studies in Pure Lutidines at Different Microwave Frequencies

OM VIR SINGH*
Department of Physics, University of Jammu, Jammu 180001

Received 3 *June* 1982; *revised received* 22 *December* 1982

Dielectric constant (ε') and dielectric loss (ε'') have been determined for pure 2, 4-, 2, 6- and 3, 5-lutidines at frequencies 720 kHz, 6.118, 9.8 and 19.22 GHz for four different temperatures. Dielectric relaxation time (τ) and the distribution parameter (α) have been evaluated by Cole-Cole arc plots obtained at temperatures 20, 30, 40 and 50°C. It is observed that α decreases with the increase of temperature for 2, 4- and 2, 6- lutidines. On the contrary it increases for 3, 5-lutidine with temperature. Various thermodynamic parameters have been evaluated by considering the relaxation as a chemical rate process.

1 Introduction

The measurement of relaxation time at different temperatures enables us to calculate various thermodynamic parameters which give very useful information regarding the molecular structure. These investigations give an idea about intramolecular and intermolecular forces. The distribution parameter (α) lies between 0 and 1 and it represents the distribution of the relaxation time. The larger α is, the larger is the extent of distribution of relaxation time.

The various symbols and letters used in this paper signify as follows:

T = temperature in absolute scale
ε' = dielectric constant
ε'' = dielectric loss
τ = macroscopic relaxation time
τ_0 = microscopic relaxation time
h = Planck's constant
k = Boltzmann constant
R = gas constant
η = viscosity
α = distribution parameter
N = Avogadro number
ω = frequency
ΔF = molar free energy of activation
ΔH = molar enthalpy of activation
S = molar entropy of activation

When ε and η appear as subscripts, they stand for relaxation and viscosity processes respectively.

2 Experimental Details

The dielectric constant (ε') and dielectric loss (ε'') of the pure lutidine compounds have been measured at 3 microwave frequencies, viz. 6.118, 9.8 and 19.22 GHz at 4 different temperatures, viz. 20, 30, 40 and 50°C. Surber's method[1] was used for the determination of ε' and ε''. The static dielectric constant was measured by a dipole meter at 720 kHz at the above mentioned temperatures. The apparatus works on the principle of heterodyne-beat method described elsewhere[2,3]. The waveguide transmission technique was used at microwave frequencies because this is most convenient and a fairly accurate method for measuring dielectric constant and loss in the liquid samples.

High-purity lutidine compounds, viz. 2, 4-, 2, 6- and 3, 5-lutidines were imported from Koch-Light (England), BDH Chemicals (England) and E. Merck (West Germany) respectively and were used as such.

3 Results and Discussion

The measured values of ε' and ε'' are represented by Cole-Cole[4] arc plots which are shown in Fig. 1[(A)-(C)] for 2, 4-, 2, 6- and 3, 5- lutidines respectively. Here ε_∞ is taken as the square of refractive index. The τ and the values of α evaluated from these plots are presented in Table 1 for all the 3 compounds. Besides this, the relaxation time for lutidine solutions using carbon tetrachloride as solvent (as a typical example) was also evaluated by Gopala Krishna's method[5] at 9.8 GHz. The relaxation time in solution (τ_{sol}) has also been compared with (τ) in Table 1.

The values of τ_0 calculated using Debye's, Powles and Fatuzzo and Mason's[8] relations are compared with the τ values at 20°C (Table 2). The explicit relations for the τ_0 are given as follows[6-8]

$$\text{Debye relation } \tau_0 = \frac{\varepsilon_\infty + 2}{\varepsilon_0 + 2}\tau \qquad \ldots (1)$$

$$\text{Powles relation } \tau_0 = \frac{2\varepsilon_0 + \varepsilon_\infty}{3\varepsilon_0}\tau \qquad \ldots (2)$$

$$\text{Fatuzzo and Mason relation } \tau_0 = \frac{\varepsilon_0 + 2\varepsilon_\infty}{2\varepsilon_0 + \varepsilon_\infty}\tau \qquad \ldots (3)$$

Viscosity (η) values for all the 3 compounds have also been measured at different temperatures with the help of Ostwald viscometer. These η values and the

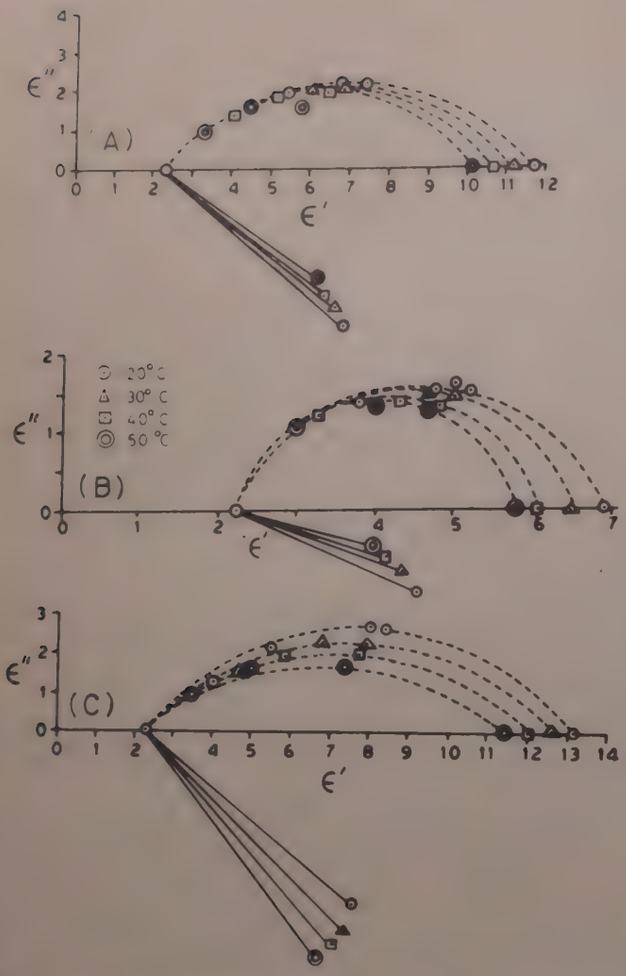

Fig. 1—Cole-Cole arc plots for: (A), 2, 4-; (B), 2, 6- and (C), 3, 5-lutidine

interpolated values of densities are presented in Table 3.

Various thermodynamic parameters for the dielectric relaxation and viscosity processes have been evaluated using Eyring's equation[9]. In this case the dielectric relaxation is considered as a rate process defined by the equation:

$$\tau=(h/kT)\exp(\Delta F_\varepsilon/RT) \quad \ldots (4)$$

where $\Delta F_\varepsilon=\Delta H_\varepsilon-T\Delta S_\varepsilon$

$$\text{Thus } \tau=\left(\frac{h}{kT}\right)\exp\left(\frac{\Delta H_\varepsilon}{RT}\right)\exp\left(\frac{-\Delta S_\varepsilon}{R}\right) \quad \ldots (5)$$

the ΔF_ε, ΔH_ε and ΔS_ε being the same as defined in Section 1.

Our observations support the theory of rate process for a dielectric. For all these compounds, the plots of $\log\eta$ versus $1/T$ and $\log(\tau T)$ versus $1/T$ gave straight lines as demanded by the rate theory equations [Fig. 2].

The ΔH_ε has been evaluated by using the slope of the plot of $\log(\tau T)$ versus $1/T$, and ΔF_ε has been calculated from the relation

$$\Delta F_\varepsilon=2.303RT\log\left(\frac{\tau kT}{h}\right) \quad \ldots (6)$$

The values of ΔF_ε, ΔH_ε and ΔS_ε so evaluated are also presented in Table 1 for the lutidines. The molar volume $V(=M/d)$ calculated from molecular weight and density has been compared in Table 3 with the hypothetical volume (V_D) given by Debye's equation

$$V_D=\tau RT/3\eta \quad \ldots (7)$$

The ΔH_η has been calculated using the slope of the plot of $\log\eta$ versus $1/T$ and the ΔF_η from the relation:

$$\Delta F_\eta=2.303\ RT\log(\eta V/Nh) \quad \ldots (8)$$

The ΔS_η has been calculated from the following relation

$$\Delta F_\eta=\Delta H_\eta-T\Delta S_\eta \quad \ldots (9)$$

The various molar activation energy parameters so evaluated are given in Table 1 for the 3 lutidine compounds.

The factor V^x which gives the dipole rotation volume[10] i.e. the effective molar volume available for dipole rotation process, has been calculated from the knowledge of molecular weight (M) and density (d). It is given by the relation $V^x=(M/d)^x$ where $x=(\Delta H_\varepsilon)/(\Delta H_\eta)=$ ratio of enthalpies for the two processes and the values so calculated are presented in Table 3. For all the 3 compounds, V is found to be much larger than V_D, calculated from Debye's equation, V_D being only 23-24.4% of V, 25.84-29.3% of V and 22-22.7% of V respectively as shown in Table 3. This is in agreement with the results obtained by other authors[11]. The discrepancy is due to the fact that the Debye's equation does not account for the deviation of molecular shape from the spherical symmetry. Another reason is that the macroscopic viscosity is different from the unknown microscopic viscosity,

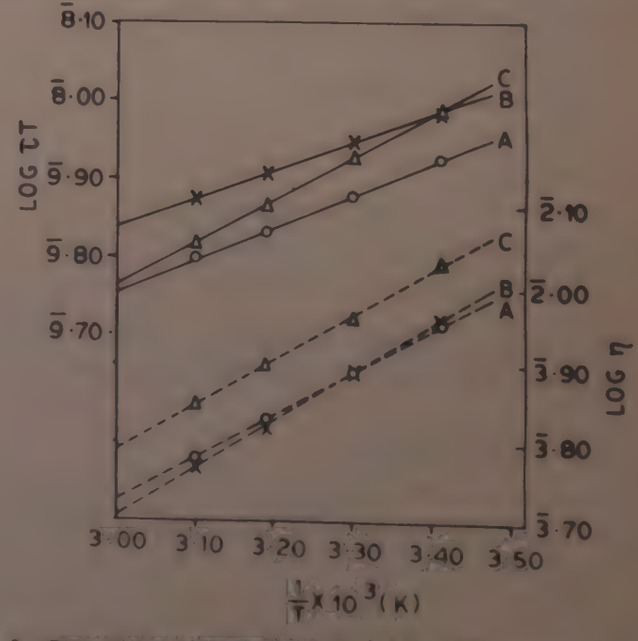

Fig. 2—Plot of $\log\eta$ (dashed lines) and $\log\tau T$ (continuous lines) versus $1/T$ for the 3 lutidine compounds (A), 2, 4-; (B), 2, 6- and (C), 3, 5-lutidine

Table 1—Dielectric Relaxation and Molar Activation Energy Parameters of the 3 Lutidines Studied
[(A), 2, 4-lutidine, (B), 2, 6-lutidine, (C), 3, 5-lutidine]

	20°C			30°C		
	(A)	(B)	(C)	(A)	(B)	(C)
$\alpha_{Cole-Cole}$	0.45	0.27	0.43	0.43	0.23	0.48
$(\tau \times 10^{11})$, sec	2.90	3.35	3.40	2.49	2.95	2.80
$(\tau_{sol} \times 10^{12})$, sec	5.12	7.50	5.30	4.87	5.95	4.55
ΔF_ε, kcal/mol	3.02	3.10	3.11	3.05	3.15	3.12
ΔF_η, kcal/mol	3.23	3.25	3.33	3.27	3.275	3.36
ΔS_ε, cal/mol/K	−3.75	−4.76	−2.12	−3.73	−4.77	−2.08
ΔS_η, cal/mol/K	−2.36	−1.64	−2.22	−2.41	−1.67	−2.24
	40°C			50°C		
$\alpha_{Cole-Cole}$	0.41	0.19	0.53	0.39	0.155	0.58
$(\tau \times 10^{11})$, sec	2.23	2.60	2.37	1.96	2.32	2.05
$(\tau_{sol} \times 10^{12})$, sec	4.49	5.55	3.93	—	—	—
ΔF_ε, kcal/mol	3.08	3.19	3.14	3.13	3.24	3.16
ΔF_η, kcal/mol	3.30	3.29	3.39	3.34	3.32	3.42
ΔS_ε, cal/mol/K	−3.71	−4.74	−2.08	−3.75	−4.75	−2.07
ΔS_η, cal/mol/K	−2.43	−1.66	−2.27	−2.48	−1.70	−2.29

	(A)	(B)	(C)
ΔH_ε, kcal/mol	1.92	1.705	2.49
ΔH_η, kcal/mol	2.54	2.77	2.68
$x = \Delta H_\varepsilon / \Delta H_\eta$	0.76	0.62	0.93
μ_D(static), D	1.67	1.50	1.70
μ_D(microwaves), D	1.65	1.45	1.67
μ_0(static), D	2.52	1.84	2.67

which is the real measure of the internal friction, used in Debye's equation, viz. Eq. (7). The ratio of η_{micro} to η_{macro} is the same as the ratio V_D/V.

It can be observed from Table 1 that for all the 3 compounds the relaxation time for pure liquid is appreciably greater than that for their dilute solutions. This is expected because dipole-dipole interactions present in pure liquid hinder the molecular rotation. Such interactions are largely absent in solutions. In the present case, the relaxation time in pure lutidines has been compared with that in their solutions in carbon tetrachloride as a typical example, though these results are also true for other solvents as reported earlier[1,2]. It is further observed from Table 1 that for all the 3 compounds the relaxation time decreases with the increase of temperature. This can be explained as follows:

When the temperature increases, the energy required for bringing dipoles to activated state increases because of thermal agitation; but when the field is switched off, the time taken by the dipoles for returning to the normal (random distribution) state will decrease because the increased thermal agitation increases the rate of energy loss due to larger number of collisions in this case. Since the time taken by the dipoles to revert to normal state after the removal of the field is a measure of the relaxation time, the relaxation time decreases with the increase of temperature.

Table 2—Macroscopic and Microscopic Relaxation Times in the 3 Lutidines Studied
(All values at 20°C)

Compound	$(\tau \times 10^{11})$ (sec)	$(\tau_0 \times 10^{11})$ sec		
		Debye (Ref. 6)	Powles (Ref. 7)	Fatuzzo & Mason (Ref. 8)
2, 4-Lutidine	2.90	0.9	2.12	1.83
2, 6-Lutidine	3.35	1.60	2.60	2.38
3, 5-Lutidine	3.40	0.96	2.46	2.10

Table 2 compares macroscopic and microscopic relaxation times. It is observed that τ_0s, calculated from the Eqs (1)-(3) are lower than the τs for all the compounds as expected. It is observed that none of these 3 relations [Eqs (1)-(3)] are valid for these compounds. However, the difference between τ_0, calculated from Debye's relation and the observed τ_{sol} is much less.

Table 1 shows that α which is the measure of the asymmetry of molecule, is decreasing with increase in temperature for both 2, 4- and 2, 6-lutidines. This indicates that the potential barrier, hindering the molecular orientation throughout liquid, becomes

Table 3—Comparison of Molar Volumes in the 3 Lutidines Studied

Temp. (T) °C	Viscosity(η) cP	Density(d) g/ml	$V=M/d$	($\tau \times 10^{11}$) sec	V_D	V_D/V,%	Dipole rotation volume(V^x) cc
			2, 4-Lutidine				
20	0.887	0.931	115.10	2.90	26.56	23.10	36.85
30	0.782	0.922	116.23	2.49	26.75	23.01	37.12
40	0.676	0.913	117.40	2.23	28.63	24.40	37.40
50	0.607	0.903	118.63	1.96	28.91	24.40	37.70
			2, 6-Lutidine				
20	0.907	0.923	116.1	3.35	30.00	25.84	19.10
30	0.780	0.910	117.8	2.95	31.80	27.00	19.24
40	0.661	0.900	119.1	2.80	34.13	28.66	19.37
50	0.583	0.880	121.8	2.32	35.63	29.25	19.64
			3, 5-Lutidine				
20	1.073	0.943	113.64	3.40	25.74	22.70	81.60
30	0.912	0.932	115.00	2.80	25.80	22.43	82.50
40	0.795	0.921	116.40	2.37	25.87	22.23	83.43
50	0.700	0.910	117.80	2.05	26.22	22.26	84.40

more uniform at higher temperatures. The increase in the thermal agitation favours predominance of those configurations which have more nearly equal free energies of activation. It may be said that in 2, 4- and 2, 6-lutidines interaction between methyl groups and nitrogen atom is quite significant. Therefore various segments of the molecule relax together. Thus cooperative effect of relaxation occurs in both cases, and the effect increases with temperature. These results are in agreement with those reported in literature[13-15].

It is further observed from Table 1 that in the case of 3, 5-lutidine α is increasing with temperature, contrary to the other two lutidines. In the case of 3, 5-lutidine the cooperative effect of relaxation seems to decrease with increase of temperature. Similar observations have also been reported in literature by other workers[16,18]. This result can be explained in the following manner:

In the case of 3, 5-lutidine two methyl groups are attached in 3, 5 positions with respect to the nitrogen atom, i.e. they are comparatively away from nitrogen atom and there is a weak interaction between them. It is expected that when this compound is excited at higher temperature, thermal fluctuations (vibrations) are more dominant as compared to this weak interaction. Hence two methyl groups and other segments of the molecules are influenced by the thermal vibrations and they relax independently at higher temperature. In other words, as the temperature increases, various segments of the molecule have more thermal energy and they are now capable of relaxing independently.

The molecule of 3, 5-lutidine may be visualized as relaxing due to (1) the rotation of one methyl group (2) the rotation of another methyl group (3) the rotation of H of CH and (4) the overall molecular rotation. Thus at higher temperatures this molecule has four very distinct ways of relaxation which accounts for the increase of α with temperature.

It is evident from Table 3 that V^x available for dipole rotation process increases with temperature in each case viz. 36.85 to 37.70 cc, 19.10 to 19.64 cc and 81.60 to 84.40 cc for2, 4-, 2, 6- and 3, 5-lutidines when the temperature is increased from 20 to 50°C. Evidently, the effective molar volume available for dipole rotation process is largest for 3, 5-lutidine and smallest for 2, 6-lutidine. Consequently, the freedom of dipole rotation is greatest in 3, 5-lutidine which gives rise to the increase of α with temperature.

The process of dielectric relaxation and the process of viscous flow are analogous because in both the cases the molecule requires an activation energy to surmount the hindering potential energy barrier. A comparison of the two energies using Table 1 reveals that for the compounds studied the ΔF_η is greater than ΔF_ε. This is expected because the viscous flow involves the translational and rotational motions of the molecule whereas the relaxation process involves only the rotational motion. Both ΔF_ε and ΔF_η show a gradual increase with temperature. It is observed that for all the 3 compounds the molar enthalpies of activation ΔH are smaller than the corresponding free energies of activation and hence the most probable entropies of activation ΔS are found to be negative. All these results are in agreement with those reported by other workers[13-15]. According to Branin and Smyth[15] a negative entropy of activation indicates that there are fewer configurations possible in the activated state and for these configurations the

activated state is more ordered than the normal state. This may be interpreted as indicating the presence of the cooperative orientations of the molecules resulting from the steric forces or from the dipole-dipole interactions with the dipoles being more nearly aligned with each other in activated state.

It is also found that for 2, 4- and 2, 6-lutidines the change in entropy due to relaxation process is greater than that due to viscosity process. Further, this change in entropy of activation is greater for 2, 6-lutidine than that for 2, 4-lutidine. This suggests that in 2, 6-lutidine an inductive effect may be more significant because of close proximity of two methyl groups to the nitrogen atom. This inductive effect causes more intramolecular polarization, mainly orientational polarization and hence there is greater change in entropy, the latter being a measure of maximum disorder. For 3, 5-lutidine the change in entropy of activation due to viscosity process is found to be greater than that for relaxation process as ΔS_η is more negative than ΔS_ε.

The ratio of enthalpies of activation for the two processes, viz. $(\Delta H_\varepsilon/\Delta H_\eta)$ is found to be 0.76, 0.62 and 0.93 for 2, 4-, 2, 6- and 3, 5-lutidines (Table 1). Therefore, according to the classification rules suggested by Krishnaji and Man Singh[19], it is expected that all of them will belong to class I liquids in which the freedom of dipole rotation is immediately lost on solidification because dipole freezing will occur on solidification. Consequently, there will be a sudden drop of dielectric constant for these compounds at their freezing point.

The values of dipole moments (μ_Ds) have been calculated by Debye's equation at static and microwave frequencies and by Onsager's formula at static frequencies as presented in Table 1. These formulae are as follows:

(Debye) μ_D^2 (Static)

$$= \frac{9kTM}{4\pi Nd}\left[\frac{\varepsilon_0 - 1}{\varepsilon_0 + 2} - \frac{\varepsilon_\infty - 1}{\varepsilon_\infty + 2}\right] \quad \ldots (10)$$

(Onsager) μ_0^2 (Static)

$$= \frac{9kTM}{4\pi Nd}\left[\frac{(\varepsilon_0 - \varepsilon_\infty)(2\varepsilon_0 + \varepsilon_\infty)}{\varepsilon_0(\varepsilon_\infty + 2)^2}\right] \quad \ldots (11)$$

(Debye) μ_D^2 (Microwaves)

$$= \frac{27kTM}{4\pi Nd}\frac{\varepsilon''}{(\varepsilon_0 + 2)(\varepsilon_\infty + 2)}\frac{1 + \omega^2\tau_0^2}{\omega\tau} \quad \ldots (12)$$

where ε_∞ is taken as the square of the refractive index.

As expected, the values of μ_Ds calculated by Debye's equation are found to be lower than those calculated from Onsager's formula. This is because in the Onsager's formula due consideration has been given to the presence of the internal field. The values calculated from Onsager's expression are in good agreement with those obtained for solutions.

Acknowledgement

The author is highly thankful to Prof G P Srivastava, Dr K N Tripathi, Department of Physics and Astrophysics, University of Delhi and to Prof Y Prakash, Head of the Department of Physics, University of Jammu for their guidance and supervision. The valuable discussions with Dr A L Dawar, Defence Science Laboratory, Delhi are gratefully acknowledged.

References

1 Surber (Jr) W H, *J Appl Phys (USA)*, **19** (1948) 514.
2 Krishna B & Srivastava K K, *J Chem Phys (USA)*, **27** (1957) 835.
3 Krishna B & Srivastava K K, *J Chem Phys (USA)*, **32** (1960) 663.
4 Cole K S & Cole R H, *J Chem Phys (USA)*, **9** (1941) 341.
5 Gopalakrishna K V, *Trans Faraday Soc, (GB)*, **53** (1957) 767.
6 Debye P, *Polar molecules*, (Chemical Catalogue Co, New York) 1929.
7 Powles J G, *J Chem Phys (USA)*, **21** (1953) 633.
8 Fatuzzo E & Mason P R, *Proc Phys Soc (GB)*, **90** (1967) 729.
9 Glasstone S, Laider K U & Eyring H, *The theory of rate process* (McGraw-Hill, New York) 1941, 484.
10 Krishnaji & Mansingh A, *Indian J Pure & Appl Phys*, **2** (1964) 176.
11 Krishnaji & Mansingh A, *J Chem Phys (USA)*, **41** (1964) 827.
12 Singh O V, Srivastava G P & Tripathi K N, *Indian J Pure & Appl Phys*, **20** (1982) 66.
13 Krishnaji & Mansingh A, *J Chem Phys (USA)*, **42** (1965) 2503.
14 Nath D, *Dielectric relaxation in liquids*, D Phil thesis, Allahabad University, Allahabad, 1968.
15 Branin F H (Jr) & Smyth C P, *J Chem Phys (USA)*, **20** (1952) 1121.
16 Srivastava S C & Nath D, *Indian J Pure & Appl Phys*, **8** (1970) 191.
17 Krishnaji, Agarwal Vinod K & Kumar P, *Indian J Pure & Appl Phys*, **9** (1971) 171.
18 Garg S K & Smyth C P, *J Chem Phys (USA)*, **42** (1965) 1397.
19 Krishnaji & Mansingh A, *J Chem Phys (USA)*, **44** (1966) 1590.

Indian Journal of Pure & Applied Physics
Vol. 21, June 1983, pp. 344-348

Dielectric Relaxation & Molecular Motion in Highly Viscous Medium

A SINGH, (Miss) A RASTOGI, S K SAXENA†, J P SHUKLA & M C SAXENA*
Department of Physics, Microwave & EPR Research Laboratory, Lucknow University, Lucknow 226 007

Received 11 *February* 1982

Dielectric measurements have been made on some rigid polar molecules in dilute solutions of paraffin oil and benzene mixture at 9.8 GHz microwave frequency and over a temperature range of 298-322 K. The relaxation behaviour has been resolved using the dielectric data by applying the methods of Higasi, and Higasi, Koga and Nakamura. The high value of the distribution parameter obtained for these systems indicates the possibility of hindered motion in highly viscous media. The flexible behaviour of these solutes has been interpreted in terms of recoiling and consequent trapping of the solute molecules between the solvent holes. The hindered motion observed in highly viscous medium in the case of the investigated rigid molecules exhibits good agreement with the earlier study of G A Balogun and C W N Cumper [*J Chem Soc Faraday Trans II (GB)*, **69** (1973) 1172].

1 Introduction

The effect of macroscopic viscosity on the relaxation time of rigid polar molecules has been investigated by several workers[1-3]. Kalman and Smyth[4] observed that the viscous solvents tend to increase the separation between the two relaxation processes and the distribution parameter is considerably increased in highly viscous medium. Balogun and Cumper[5] suggested that the dielectric relaxation in polar molecules occurs by their rotational diffusion and its rate depends upon the magnitude of intermolecular forces present in the viscous solution. They studied methyl iodide, cyanocyclopropane, chlorobenzene, 1-chloronaphthalene, etc. in different mixtures of paraffin oil and benzene of varying viscosity and observed that even rigid solute molecules in a highly viscous medium exhibit a small unsymmetrical distribution of relaxation times and that a Debye treatment based on single relaxation time would no longer be strictly adequate. Keeping this in view, the dielectric measurements on four rigid polar molecules (pyridine, quinoline, bromobenzene and iodobenzene) in six solvents of varying viscosities were made by us at a microwave frequency of 9.8 GHz and at a static frequency in the temperature range 298-322 K. The six solvents were prepared by adding increasing amounts of paraffin oil to benzene.

The distribution parameter α and the most probable relaxation time τ_{0m} were evaluated using the concentration variation method of Higasi[6]. Since all the four rigid molecules show appreciably high values of α in highly viscous media it was considered important to resolve the relaxation mechanism into two separate processes, one pertaining to the hindered rotation $\tau_{(1)}$ and the second representing the molecular rotation $\tau_{(2)}$ using Higasi *et al.* method[7]. The average relaxation time $\tau_{(0)}$ has been calculated using the equation $\tau_{(0)}=[\tau_{(1)}\ \tau_{(2)}]^{1/2}$. The details of evaluating these parameters have already been discussed in our earlier papers[8,9]. The observed results are discussed in the light of Balogun and Cumper's model[5] of hole creation and the subsequent trapping of the rigid solute molecules.

2 Experimental Details

The following six solvents of varying viscosities were taken and the solutions were prepared by changing the amounts of the solute dissolved: (1) 100% benzene; (2) 80% benzene + 20% paraffin oil; (3) 60% benzene + 40% paraffin oil; (4) 40% benzene + 60% paraffin oil; (5) 20% benzene + 80% paraffin oil; (6) 100% paraffin oil. The experimental details of the measurements and evaluation of dielectric parameters have been given in our earlier papers[8-10].

The chemicals pyridine, quinoline, bromobenzene and iodobenzene were obtained from M/s British Drug House, England. The medicinal paraffin oil was obtained from Liberty Pharmaceutical Ltd, Bombay; the other solvent benzene (AR grade), obtained from M/s British Drug House, England, was distilled twice before use.

3 Results and Discussion

The relaxation times, evaluated using the Higasi[6] and Higasi *et al.* method[7], and the distribution parameters of all the four compounds are listed in Table 1 along with the macroscopic viscosities of the corresponding solutions. The dielectric relaxation times $\tau_{(0)}$ and $\tau_{(0m)}$ yield an average value of the relaxation parameters. It has been observed that both these parameters decrease with increasing temperature and increase systematically with increasing solvent

†Permanent address: D B S College, Kanpur

Table 1—Relaxation Times (τ in ps), Distribution Parameter (α) and Macroscopic Viscosity (η_S in mP)

Temperature K	$\tau_{(1)}$	$\tau_{(2)}$	$\tau_{(0)}$	$\tau_{(OH)}$	α	η_S
			I. PYRIDINE			
			100% Benzene			
314	5.4	7.9	6.3	5.1	0.08	4.8
322	4.3	5.7	4.9	4.1	0.06	3.3
			80% Benzene + 20% paraffin oil			
298	8.2	11.7	9.8	8.4	0.11	—
306	7.2	8.4	7.8	7.3	0.05	10.8
314	5.3	7.1	6.1	5.5	0.07	8.8
322	5.2	5.8	5.5	5.3	0.01	6.6
			60% Benzene + 40% paraffin oil			
298	9.9	20.6	14.3	11.3	0.23	—
306	9.6	15.6	12.2	9.0	0.15	16.3
314	8.1	10.2	9.1	8.1	0.07	12.0
322	7.7	8.3	8.0	5.4	0.03	8.9
			40% Benzene + 60% paraffin oil			
298	6.7	31.1	14.4	11.5	0.45	—
306	6.5	27.5	13.4	9.2	0.42	28.7
314	5.2	25.7	11.5	8.3	0.40	20.7
322	5.1	23.1	10.9	5.3	0.39	15.9
			20% Benzene + 80% paraffin oil			
298	6.5	33.4	14.7	11.9	0.47	–
306	6.0	31.8	13.8	9.8	0.46	104.6
314	5.8	28.1	12.8	8.5	0.45	95.1
322	5.3	26.0	11.8	6.2	0.44	78.1
			100% Paraffin oil			
298	7.8	35.2	16.6	16.8	0.45	—
306	7.0	33.8	15.4	14.1	0.46	483.4
314	6.5	30.7	14.1	10.8	0.45	384.6
322	6.5	28.9	13.7	10.0	0.44	240.3
			II. QUINOLINE			
			100% Benzene			
306	12.5	16.0	14.1	13.7	0.09	5.6
314	9.1	13.0	10.9	9.6	0.11	4.8
322	7.8	9.9	8.8	7.8	0.07	3.3
			80% Benzene + 20% paraffin oil			
298	11.5	24.9	16.9	17.6	0.25	–
306	11.1	24.1	16.3	16.4	0.25	10.8
314	10.1	20.9	14.5	10.8	0.31	8.8
322	8.2	9.7	8.9	8.3	0.06	6.6
			60% Benzene + 40% paraffin oil			
298	12.4	30.8	19.5	23.4	0.28	—
306	11.2	29.2	18.1	20.4	0.30	16.3
314	8.6	23.3	14.2	13.2	0.27	12.0
322	10.1	11.2	10.8	10.5	0.03	8.9
			40% Benzene + 60% paraffin oil			
298	11.3	32.8	19.2	23.6	0.33	–
306	9.4	30.0	16.8	21.5	0.43	28.7
314	10.9	25.9	16.8	17.5	0.27	20.7
322	6.7	11.8	8.9	6.7	0.16	15.9

(Contd)

Table 1—Relaxation Times (τ in ps), Distribution Parameter (α) and Macroscopic Viscosity (η_s in mP) *Contd*

Temperature K	$\tau_{(1)}$	$\tau_{(2)}$	$\tau_{(0)}$	$\tau_{(OH)}$	α	η_s
			20% Benzene + 80% paraffin oil			
298	9.3	34.4	17.8	22.8	0.39	—
306	8.8	34.2	17.3	19.4	0.41	104.6
314	7.4	32.5	15.5	18.7	0.43	95.1
322	6.7	21.4	12.0	8.0	0.34	78.1
			100% Paraffin oil			
298	8.1	41.2	18.3	23.7	0.47	—
306	7.8	39.9	17.7	21.3	0.47	483.4
314	6.0	36.5	14.8	16.0	0.51	384.6
322	5.4	31.4	13.0	7.7	0.50	240.3
			III. BROMOBENZENE			
			100% Benzene			
306	9.3	11.6	10.3	9.6	0.07	5.6
314	7.9	10.7	9.2	8.0	0.09	4.7
322	8.0	9.8	8.9	6.8	0.06	3.3
			80% Benzene + 20% paraffin oil			
298	8.2	16.7	11.7	9.7	0.21	—
306	7.5	15.9	10.9	8.2	0.23	10.8
314	7.0	14.6	10.1	7.2	0.22	8.8
322	6.8	13.9	9.7	7.0	0.21	6.6
			60% Benzene + 40% paraffin oil			
298	8.6	20.9	13.4	11.2	0.28	—
306	8.4	17.6	12.2	9.8	0.23	16.3
314	8.3	17.1	11.9	9.5	0.22	12.0
322	6.6	14.1	9.7	6.7	0.22	8.9
			40% Benzene + 60% paraffin oil			
298	7.7	24.3	13.6	11.2	0.35	—
306	7.5	23.1	13.1	10.0	0.34	28.7
314	7.4	19.4	12.0	9.8	0.29	20.7
322	6.8	15.1	10.1	6.9	0.24	15.9
			20% Benzene + 80% paraffin oil			
298	9.6	28.2	16.5	16.6	0.34	—
306	8.9	25.7	15.1	13.8	0.33	104.6
314	7.9	22.4	13.3	10.7	0.32	95.1
322	7.8	16.8	11.4	8.8	0.23	78.1
			100% Paraffin oil			
298	10.6	30.3	17.9	—	—	—
306	9.9	28.1	16.7	17.2	0.32	483.4
314	9.4	27.9	16.2	16.2	0.34	384.6
322	8.4	24.9	14.5	12.6	0.33	240.3
			IV. IODOBENZENE			
			100% Benzene			
306	12.9	13.6	13.2	13.1	0.03	5.6
314	11.9	12.7	12.3	12.1	0.03	4.8
322	10.1	11.9	12.1	10.8	0.11	3.3
			80% Benzene + 20% paraffin oil			
298	11.2	23.5	16.6	16.8	0.22	—
306	9.6	23.4	15.0	13.9	0.28	10.8
314	12.3	16.5	14.2	13.7	0.10	8.8
322	12.0	16.2	13.4	13.9	0.07	6.6

(Contd)

Table 1—Relaxation Times (τ in ps), Distribution Parameter (α) and Macroscopic Viscosity (η_S in mP)—*Contd*

Temperature K	$\tau_{(1)}$	$\tau_{(2)}$	$\tau_{(0)}$	$\tau_{(OH)}$	α	η_S
			60% Benzene + 40% paraffin oil			
298	10.7	28.9	17.6	19.2	0.31	—
306	10.6	27.8	17.2	19.1	0.29	16.3
314	9.6	22.8	14.8	13.5	0.27	12.0
322	8.8	16.7	12.1	12.3	0.15	8.9
			40% Benzene + 60% paraffin oil			
298	11.3	32.8	19.2	21.5	0.32	—
306	11.2	29.2	18.1	20.4	0.30	28.7
314	11.1	26.5	17.2	18.0	0.28	20.7
322	13.8	21.8	17.4	17.9	0.15	15.9
			20% Benzene + 80% paraffin oil			
298	11.7	38.6	21.3	21.7	0.31	—
306	9.4	30.1	16.8	21.5	0.43	104.6
314	9.2	29.0	16.3	16.5	0.35	95.1
322	9.4	26.0	15.6	14.9	0.32	78.1
			100% Paraffin oil			
298	8.2	41.2	18.4	24.2	0.47	—
306	7.9	41.1	18.2	22.8	0.48	483.4
314	7.6	38.4	17.3	19.1	0.47	384.6
322	7.6	36.9	16.7	17.9	0.46	240.3

viscosity. As may be seen from Table 1 for the pyridine molecule, $\tau_{(OH)}$ (at 314 K) varies from 5.1 to 10.8 ps in the range of medium viscosity of 4.78 to 384.6 mP whereas $\tau_{(0)}$ increases from 6.3 to 14.1 ps in the same viscosity range. It is also observed that the two relaxation parameters $\tau_{(0)}$ and $\tau_{(OH)}$ are comparable. A similar behaviour is observed in the case of the other three molecules investigated here.

Since the dielectric data yield substantial values of distribution parameter in the range 0.01-0.47, with increasing viscosity, the process was further resolved into two separate relaxation times $\tau_{(1)}$ and $\tau_{(2)}$ using Higasi *et al.* method[7]. The observed high value of α indicates the possible flexible behaviour of these rigid molecular systems.

A comparison of $\tau_{(1)}$ and $\tau_{(2)}$ for the pyridine system exhibits that the two parameters are nearly equal in the dilute solutions of benzene. With increasing medium viscosity, $\tau_{(2)}$ increases systematically giving a maximum value for the solutions having 100% paraffin oil. A similar behaviour is exhibited by the other three rigid molecules under investigation. On the other hand, the variations observed in the case of $\tau_{(1)}$ values are small and are accompanied by an irregular behaviour with increasing viscosity of the medium. As suggested by Balogun and Cumper, the solvent molecules in a highly viscous system form a type of cage around solute molecules and for the dipolar rotation to occur in the solution, the solute molecules have to pass through various hindrances created due to the solvent cage. The varying degree of freedom experienced by the solute molecules would result in different values of the relaxation times. In the present case of rigid molecules, $\tau_{(1)}$ and $\tau_{(2)}$ are such that $\tau_{(1)}$ would possibly represent the relaxation time of the part of the segment of the solute molecule recoiling around the solvent molecule and $\tau_{(2)}$, the relaxation time of the solute molecule as a whole performing the dipolar rotation. The irregular behaviour of $\tau_{(1)}$, with variation of viscosities, may be ascribed to the small hindrances produced from the segmental motion in the solvent cage. On the other hand, a systematic increase of the $\tau_{(2)}$ values with increase in viscosity would be expected due to the dipolar rotation of the entire molecule as a unit.

Another rigid system, viz. quinoline, exhibits a similar behaviour. It may be seen from Table 1 that the $\tau_{(1)}$ and $\tau_{(2)}$ values for the temperatures investigated are not substantially different in benzene solution. Again, $\tau_{(1)}$ gives an irregular variation with increasing viscosity whereas $\tau_{(2)}$ increases systematically giving values of 16.0-41.2 ps in the viscosity range 5.6-240.3 mP. The other two systems, viz. bromobenzene and iodobenzene, also exhibit a similar behaviour.

These investigations indicate that the distribution in the relaxation times occurs even in the case of rigid systems in highly viscous media. Here the systems taken were both spherical and slightly elongated types and the phenomenon seems to hold true equally in both the systems. As has been mentioned earlier, the behaviour is perhaps governed by the concept of cage formation of the solvent systems and consequent

trapping of the solute molecules. The strength of the hindrance induced depends upon the number of such cages created which varies with solvent viscosity and which would effectively contribute towards the barrier provided for both the molecular motion and the segmental flexibility.

4 Conclusion

All these four rigid polar molecules in the high viscous medium showed sufficient amount of hindered motion. This hindrance is perhaps due to diffusion, recoiling and trapping of solute molecules in the solvent molecules. The observed high values of the distribution parameter (α) would arise from these hindered motions occurring in the system.

References

1 (Miss) Chauhan M, (Miss) Gupta M, Saxena S K & Shukla J P, *Phys & Chem Liq (GB)*, **10** (1981) 335.

2 Smyth C P, *Proc Natl Acad Sci (USA)*, **42** (1956) 234.

3 Grubb E L & Smyth C P, *J Am Chem Soc (USA)*, **83** (1961) 4122.

4 Kalman O F & Smyth C P, *J Am Chem Soc (USA)*, **82** (1960) 183.

5 Balogun G A & Cumper C W N, *J Chem Soc Faraday Trans II (GB)*, **69** (1973) 1172.

6 Higasi K, *Bull Chem Soc Jpn (Japan)*, **39** (1966) 2157.

7 Higasi K, Koga Y & Nakamura M, *Bull Chem Soc Jpn (Japan)*, **44** (1971) 988.

8 Misra C K, Shukla J P & Saxena M C, *Adv Mol Relaxation & Interaction Processes (Netherlands)*, **15** (1979) 181.

9 Saxena S K, Misra C K, Shukla J P & Saxena M C, *Acta Phys Chem Hung (Hungary)*, **25**(1-2) (1979) 47.

10 Saxena S K, Shukla J P & Saxena M C, *Bull Chem Soc Jpn (Japan)*, **53** (1980) 1732.

Indian Journal of Pure & Applied Physics
Vol. 21, June 1983, pp. 349-351

Mutarotation of Glucose Solution under Ultrasonic Irradiation

B V GURUNADHA RAO, V P BHATNAGAR* & S B AGARWAL†
Department of Physics, Delhi College of Engineering, Delhi 110006

Received 2 January 1982; revised received 21 May 1983

Mutarotation of fresh and equilibrium solutions of glucose have been studied under irradiation of ultrasonic waves of 1.5 MHz. The process of mutarotation has been found to be accelerated under ultrasonic exposure. Further, a marked decrease in the optical rotation was noted in case of equilibrium solution. This effect increased with the exposure time to ultrasonic waves and attained a saturation. The time-constant by which the glucose solution attained its new equilibrium value was found to depend on ultrasonic power. The observed effect indicates that the structural state of the glucose can be changed by ultrasonic irradiation.

1 Introduction

It is a well known fact that when glucose is dissolved in water, the optical rotatory power of the solution decreases on standing until finally it reaches a constant value, a phenomenon which came to be known as mutarotation. This change in optical rotation has been attributed to the change in molecular structure of the glucose solution. This explanation received a striking confirmation in the discovery of two forms of this sugar due to asymmetry in the reducing carbon atom number-1 of the cyclic sugar. The alpha and beta modifications of the various ring forms and the open chain modifications are mutually interconvertible and exist in solution in a dynamic equilibrium[1]. The optical rotations of these substances are not alike and consequently when a sugar is dissolved in water, the optical rotation changes as equilibrium is established between various modifications. The equilibrium of glucose solution corresponds to 36% of alpha and 64% of beta form.

Later, the acceleration of the mutarotation rates of the sugars by acids and bases has been the subject of many investigations and the results obtained have been reviewed in the literature[2]. It was found that amphoteric solvents are catalysts for the mutarotation while hydrocarbons, chloroform and carbon tetrachloride do not promote mutarotations. However, according to Hudson, the contribution of the hydroxyl ion (base) to the catalysis is about 40,000 times that of the hydrogen ion (acid) and the residual catalytic effect of the water is nearly 500 times that of the combined catalytic effect of the hydrogen and hydroxyl ions.

Subsequent studies on the equilibrium state of sugars revealed that the equilibrium between the various constituents is altered with further addition of the solvent. In some cases, the solvent combines with sugar and may facilitate the separation of different modifications of the sugar. d-Glucose crystallises from pyridine solution in the form of a pyridine compound which contains the beta pyranose modification. But it crystallises from water solution at ordinary temperatures in the form of a hydrate which contains the alpha pyranose modification. The mutarotational equilibrium thus changes with chemical process.

Sometime back, two of the present authors have reported that the optical rotation of glucose is changed under physical processes like propagation of ultrasonics[3,4]. The experimental data in earlier experiments were obtained by visual polarimetric techniques, without due considerations being given for the age of solution. Since optical rotation of glucose changes with time and attains equilibrium only after a few days, it is essential to use a solution that has attained equilibrium so as to get meaningful results. Also it was of interest to study the time variation of optical rotation of a freshly prepared glucose solution under ultrasonic irradiation in order to understand the mechanism by which ultrasonic irradiation can influence the optical rotation. A need was, therefore, felt to repeat the experiment and to measure the effect more precisely by using better methods. A detailed study was made on the mutarotation of glucose under ultrasonic irradiation by using an electronic polarimeter specially designed for this purpose, the results of which are presented in this paper.

2 Experimental Details

The experimental set-up is shown in Fig. 1. Ultrasonic waves of frequency 1.5 MHz were generated by vibrating a quartz crystal cemented to the bottom of a cubical glass cell ($2'' \times 2'' \times 2''$) containing the experimental solution. The mercury green light was used as the light source. The intensity of the ultrasonic waves was controlled by the rf voltage on the crystal[5]. The polarization of the light beam penetrating

†Department of Physics, MMH College, Ghaziabad 201 001

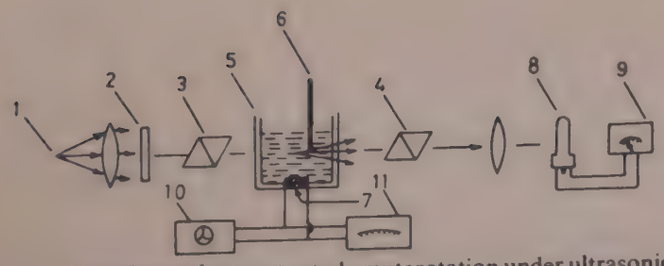

Fig. 1—Experimental set-up to study mutarotation under ultrasonic irradiation [1 Mercury source, 2 Green light filter, 3 Polariser, 4 Analyser, 5 Experimental cell, 6 Thermometer, 7 Transducer, 8 Photomultiplier, 9 Microvoltmeter, 10 CRO and 11 Ultrasonic power generator]

transversely the acoustically disturbed medium was observed using nicols fitted in circular scales. A photomultiplier and a microvoltmeter were used to read the microscopic changes in the optical rotation. For this purpose, a graph between microvoltmeter reading (x) and rotation angle (θ) of the analyser was plotted and a point giving maximum sensitivity, i.e. $(dx/d\theta)_{max}$ was selected as the operating point to study the minute changes in the optical rotation. A sensitive thermometer was kept in the experimental cell to read the temperature variations of the solution during the ultrasonic irradiation. A oscilloscope was also used to check the frequency and to measure the rf voltage across the crystal.

3 Results and Discussion

The experiment was done in two parts. In the first part, the fresh solution of glucose was exposed to ultrasonics and in the second part, the experiment was done on that solution of glucose which after natural process of mutarotation attained the equilibrium. We shall call this solution as 36:64 glucose as it is well known that it contains 36 % of α-glucose and 64 % of β-glucose.

The first reading of optical rotation could not be taken earlier than 3 min with fresh solution. On exposing the solution to ultrasonic waves, the value of optical rotation decreased with a faster rate than otherwise. In this respect the action of ultrasonic waves was similar to that of the catalytic action of adding dilute acids and alkalies. The effect of ultrasonic waves was studied at various intensities and it was found that the acceleration was greater at higher intensities (Fig. 2).

With equilibrium solution, a marked decrease in the value of optical rotation was observed on ultrasonic irradiation. The effect increased with the exposure time and attained a saturation value, which was much lower than the value attained in the natural process of mutarotation. In this connection it is remarked that in the earlier communication no consideration was given to the ageing of solution, with the result that an apparent rise was reported.

The variation in optical rotation of the 36:64 glucose solution with exposure time was studied for different ultrasonic intensities. A family of curves so obtained is presented in Fig. 3.

The curves show that a new equilibrium is reached in an exponential manner according to the following equation:

$$\alpha = A + Be^{-t/\tau}$$

where τ is a time-constant and the normal value α_0 corresponding to $t=0$ is given by

$$\alpha_0 = (A+B)$$

and the new equilibrium value α_∞ corresponding to $t=\infty$ is given by

$$\alpha_\infty = A$$

From the curves in Fig. 3 it is clear that the new equilibrium value attained under different intensities is the same for a particular specimen, however, the half-

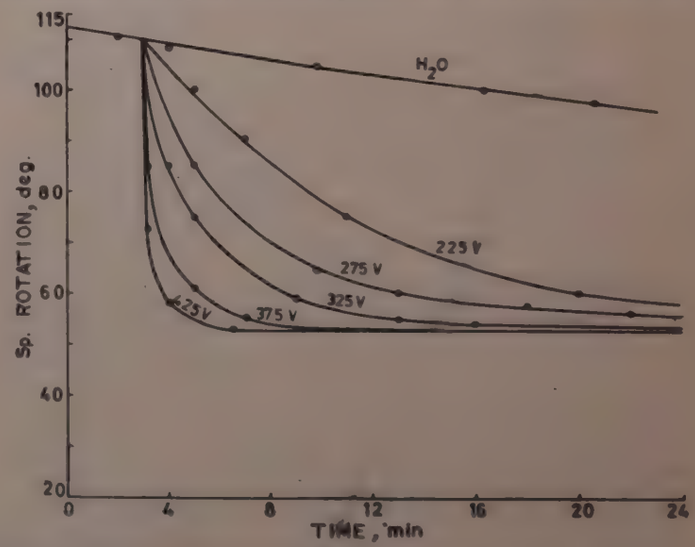

Fig. 2—Optical rotation of fresh glucose as a function of exposure time and ultrasonic power as expressed in terms of crystal rf voltage

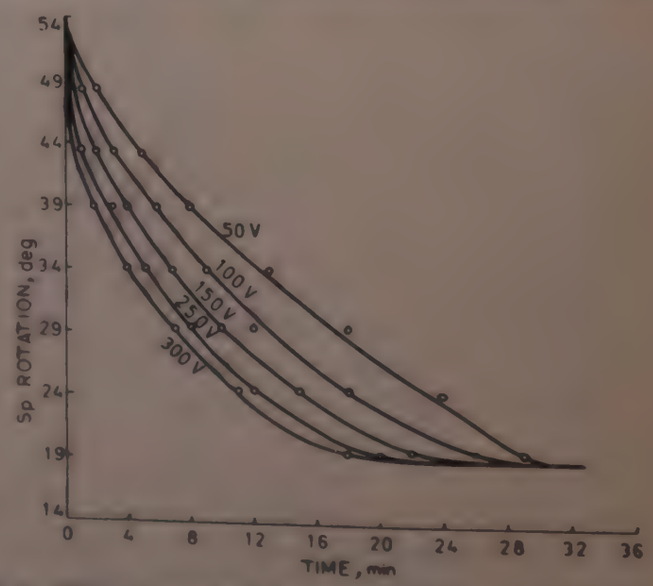

Fig. 3 Optical rotation of 36:64 glucose solution as a function of exposure time and ultrasonic power as expressed in terms of crystal rf voltage

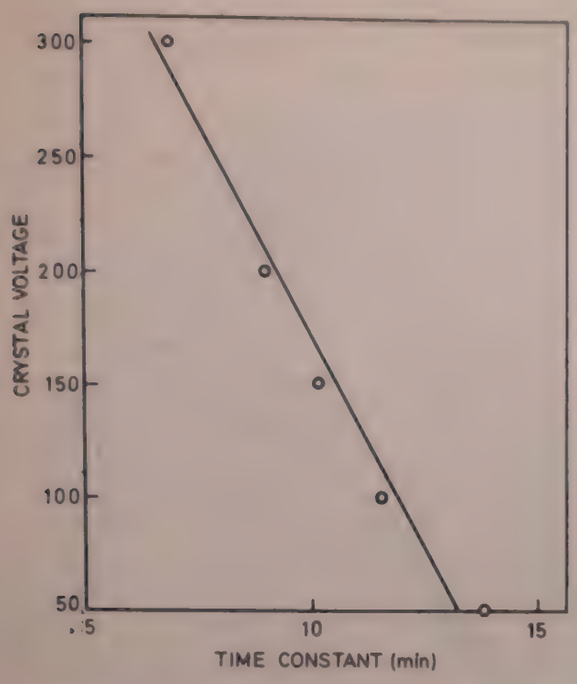

Fig. 4—Variation of time-constant with ultrasonic power as expressed in terms of crystal rf voltage

period time is different for different intensities. The half-period times were determined from the slope of the straight line obtained on plotting $\log(\alpha - A)$ against t. The experimental study also reveals that lower the ultrasonic intensity, higher is the half-period time, i.e. the time taken to reach the value $\frac{1}{2}(\alpha_0 + \alpha_\infty)$ decreases with the increase in the intensity (Fig. 4).

Since the optical rotation is an indication of the composition of the solution, it is apparent to conclude that the composition of original 36:64 glucose changed due to ultrasonic exposure. The fact that the ultrasonic effect showed a saturation indicates that the solution has attained a new equilibrium.

The effect is not due to temperature rise because firstly the increase in temperature is less than 2 C and secondly the effect showed a saturation, indicating a new equilibrium. The fact that even a very long exposure to ultrasonic irradiations causing temperature rise as high as 6 C could not lead to any marked change in the new equilibrium value, shows that the effect is not due to heating of the solution. Moreover, a temperature rise should have caused an increase rather than a decrease in the optical rotation as has been observed.

Petrenko[6] theoretically explained the ultrasonically induced optical rotation as a physical phenomenon, in certain substances. We feel that this explanation is not valid in the case of glucose solution because the effect persists even after the withdrawal of ultrasonic irradiation.

Since the action of ultrasonic waves on freshly prepared solution is similar to the catalytic action of acids and bases which accelerate the process through the addition of H^+ and OH^- ions, it appears that sono-ionization of water of glucose solution is responsible for the ultrasonic action of speeding up the process of conversion of α-glucose into β-glucose to attain the equilibrium condition quicker. Also when equilibrium solution is irradiated by ultrasonic waves, the process of conversion of α-glucose into β-glucose continues further until the whole of the α-form of glucose transforms into the β-form.

Acknowledgement

The authors' grateful thanks are due to University Grants Commission, New Delhi, for the award of a research project under which this work was conducted. We are also thankful to Prof. M L Mandal, Principal, Delhi College of Engineering, Delhi, for providing experimental facilities to conduct the above investigations and to Dr P L Jain of Chemistry Department, for useful discussions.

References

1 Astie M J & Shelton J R, *Organic chemistry* (Oxford Book Co, Calcutta), 1963, 375.

2 Bates F J, *Polarimetry, sacharimetry and the sugars*, Circular of the National Bureau of Standards, C 440 (U S Department of Commerce, United States Govt Printing Office, Washington) 1942.

3 Bhatnagar V P & Agarwal S B, *Lett Al Nuovo Cimento (Italy)*, **15** (1976) 551.

4 Bhatnagar V P & Agarwal S B, *Indian J Pure & Appl Phys*, **14** (1976) 382.

5 Hueter T F & Bolt R H (John Wiley, New York), 1960, 99.

6 Petrenko A D, *Ukr Fiz Zh (USSR)*, **25** (1980) 1021.

NOTES

Indian Journal of Pure & Applied Physics
Vol. 21, June 1983, pp. 352-353

Excess Volumes & Deviations in Isentropic Compressibilities for the Binary Mixtures of Acetonitrile with Alcohols

G DHARMARAJU, P VENKATESWARLU & G K RAMAN*

Department of Chemistry, College of Engineering, Sri Venkateswara University, Tirupati 517 502

Received 5 *June* 1982

Excess volumes (V^E) and deviations in isentropic compressibilities (K_s) have been determined at 30°C for the binary systems of acetonitrile with *n*-pentanol, *n*-hexanol, *n*-heptanol and *n*-octanol. Excess volumes have been measured directly by the dilatometric method and isentropic compressibilities have been computed from experimentally determined densities and velocities of sound. The positive values of V^E and K_s in all the systems are attributed to weak complex formation and predominating dissociation of associated alcohols by acetonitrile. Values of V^E and K_s increase with an increase in chain length of alcohol.

The nature and degree of interactions that are present in the binary mixtures of acetonitrile with *n*-propanol, *i*-propanol, *n*-butanol, *i*-butanol and cyclohexanol have been studied[1] qualitatively in terms of excess volumes and isentropic compressibilities. The present note also reports the same properties but for the mixtures of acetonitrile with *n*-pentanol, *n*-hexanol, *n*-heptanol and *n*-octanol. These alcohols have been chosen to study the effect of chain length on the properties studied.

Actonitrile and alcohols[2] were purified as in our earlier work[1,2] and they were degassed. The purity of the final samples was confirmed by comparing the measured densities with literature[3] values at 30 C. The values agreed within $\pm 5 \times 10^{-5}$ g cm^{-3}.

Excess volumes were measured directly by dilatometric method as in our earlier work[2]. Isentropic compressibilities were computed from experimentally determined densities and velocities of sound at 30 C. Densities were determined by a bi-capillary pyknometer accurate to $\pm 5 \times 10^{-5}$ g cm^{-3}. Ultrasonic velocities of sound were measured with a single crystal interferometer accurate to ± 0.15 ... at a frequency of 2 MHz.

The variation of excess volume with mole fraction of acetonitrile is shown in Fig. 1. The experimental excess volumes may be fitted in to the equation

$$V^E \text{ cm}^3\text{mol}^{-1} = x_A(1-x_A)[a_0 + a_1(2x_A-1) + a_2(2x_A-1)^2] \quad \ldots (1)$$

where x_A is the mole fraction of acetonitrile

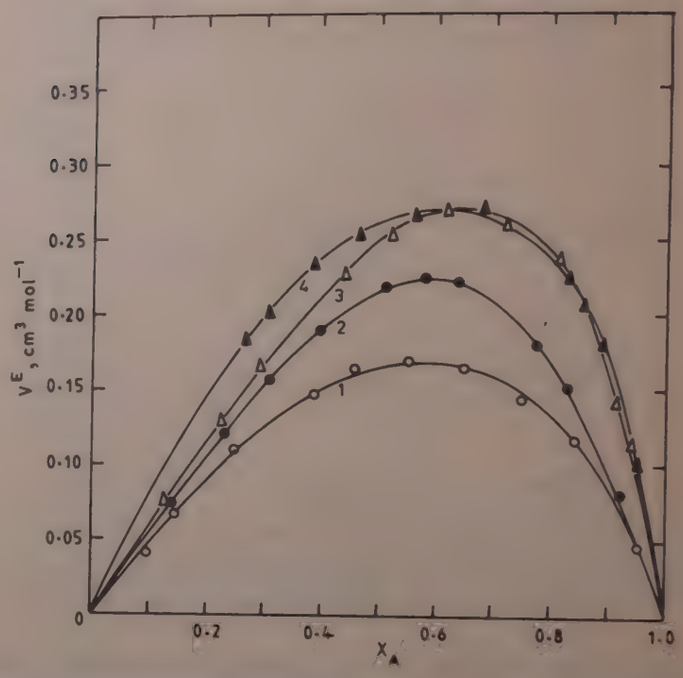

Fig. 1—Excess volumes (V^E) versus mole fraction (X_A) of acetonitrile for the mixtures of acetonitrile with alcohols: 1, *n*-pentanol; 2, *n*-hexanol; 3, *n*-heptanol and 4, *n*-octanol

The isentropic compressibilities (k_s) have been calculated from the equation

$$k_s = u^{-2}\rho^{-1} \quad \ldots (2)$$

where u and ρ denote sound velocity and density respectively. The deviation from linear dependence of isentropic compressibility on volume fraction has been calculated from

$$K_s = k_s - \varphi_A k_{s,A} - \varphi_B k_{s,B} \quad \ldots (3)$$

where k_s, $k_{s,A}$ and $k_{s,B}$ are the isentropic compressibilities for the mixture and pure components and φ_A and φ_B are the volume fractions. The plots of K_s versus volume fraction of acetonitrile are included in Fig. 2. Experimental K_s values against volume fraction may be represented by

$$K_s = \varphi_A\varphi_B[b_0 + b_1(\varphi_A - \varphi_B) + b_2(\varphi_A - \varphi_B)^2] \quad \ldots (4)$$

The values of parameters b_0, b_1 and b_2 obtained by the method of least squares are given in Table 1 along with standard deviation.

Values of V^E and K_s for all the systems studied are positive over the entire range of composition. These results support the contention made in our earlier work that the positive values may be due to weak complex formation and predominating dissociation of self-associated alcohol. They fall in the order *n*-propanol < *n*-butanol < *n*-pentanol < *n*-hexanol < *n*-heptanol < *n*-octanol. This order shows an increase in excess volume with an increase in the chain length of

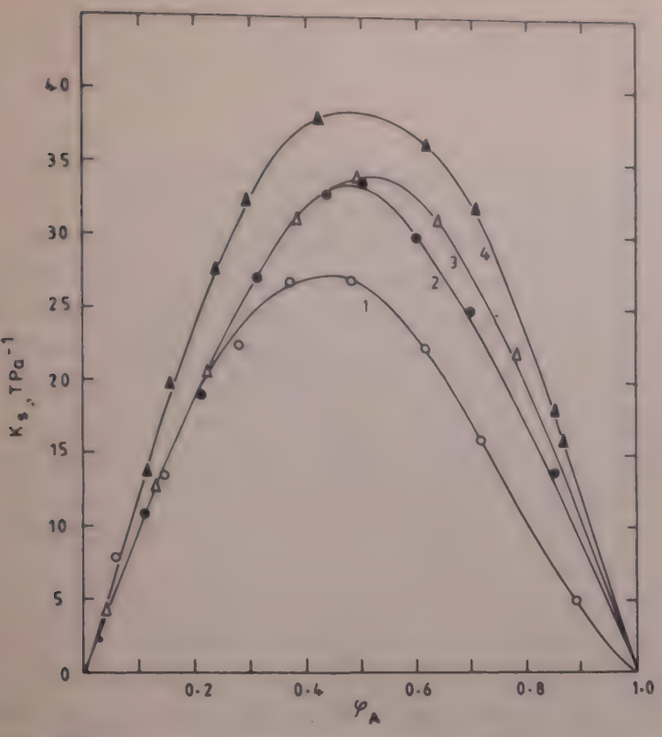

Fig. 2—Variation of isentropic compressibility (K_s) with volume fraction (φ_A) of acetonitrile for the systems of acetonitrile with: 1, *n*-pentanol; 2, *n*-hexanol; 3, *n*-heptanol and 4, *n*-octanol

alcohols. This order may be ascribed to the effect of chain length on the degree of polymerization of alcohols in the pure state and strength of complex formed between unlike molecules. The degree of polymerization of an alcohol increases with decrease in chain length. The strength of hydrogen bond in the aggregates and also the complex formation increases with decrease in chain length. Consequently, when homologous series of alcohols are mixed with a common solvent like acetonitrile the expansion in volume would be minimum in the case of lower alcohol and maximum in respect of higher alcohol. Similarly, the contraction would be maximum in the case of lower alcohol. Hence the observed values are in order. The order for values of K_s may also be attributed to the same factors.

Table 1—Values of Parameters b_0, b_1 and b_2 in Eq. (4)

System	b_0	b_1	b_2
Acetonitrile + *n*-pentanol	109	−39	−71
Acetonitrile + *n*-hexanol	130	−5	−44
Acetonitrile + *n*-heptanol	136	18	−34
Acetonitrile + *n*-octanol	155	−11	1

Standard deviation $\sigma(K_s) = 1$ in each system.

One of the authors (GDR) is grateful to the CSIR, New Delhi, for the award of a research fellowship.

References

1 Narayanaswamy G, Dharmaraju G & Raman G K, *J Chem Thermodyn (GB)*, **13** (1981) 327.

2 Narayanaswamy G, Dharmaraju G & Raman G K, *Can J Chem (Canada)*, **58** (1979) 229.

3 Timmermans J, *Physico-chemical constants of pure organic compounds* (Elsevier, New York), 1950.

Indian Journal of Pure & Applied Physics
Vol. 21, June 1983, pp. 354-356

Surface State Density Determination Based on Conductance Approximation Methods

R J SINGH*

Solid State Electronics Laboratory, Department of Physics, Banaras Hindu University, Varanasi 221 005

Received 11 *March* 1982; *revised received* 16 *August* 1982

Amongst different approximate methods for the determination of interface state density at the Si-SiO_2 interface, the Hill and Coleman method is found to be the most suitable one. Results obtained from various samples having surface state density of varying magnitudes computed by three different methods are compared to support this conclusion.

Amongst different methods proposed in the literature for the analysis of interface state density[1-4] at the Si-SiO_2 interface, MOS parallel conductance technique developed by Nicollian and Goetzberger[5] is the most accurate one. Since the analysis of the parallel conductance data is quite elaborate and difficult, it is unsuitable for quick estimation of surface state density of a system. Several methods for the quick estimation of surface state density at the interface have been suggested by previous workers[6]. These methods are approximate and give results which vary in magnitude by large amounts, say by factors of 2 to 4. Recently Hill and Coleman[7] have proposed a single high-frequency approximation technique which is not only simple and quick in analysis but also provides results within 30% of the most accurate one. In this note, results obtained by three different methods are compared. Various samples having surface state density of varying magnitudes were analyzed. However, representative results of only four samples are given in this work.

Experiments were carried out on Si wafers of *n*-type having different resistivities and crystal orientations. They were chemically polished on one side and treated with hot sulphuric acid and dilute hydrofluoric acid (10 parts water and 1 part HF). Finally they were cleaned with high resistivity deionized water. Diffusion of n^+ was made on the unpolished surface. The polished surface was protected by thick oxide previously grown on it. After cleaning in vapour degreaser the wafers were loaded in oxidation furnace for growing oxide on the polished surface under the appropriate ambient and temperature conditions. Aluminium dots were deposited on the oxide using vacuum vapour-depositing technique. Oxide thickness was determined by ellipsometer and checked from the magnitude of the capacitance of the structure under strong accumulation. A summary of the oxidation and annealing conditions is given in Table 1.

Capacitance and equivalent parallel conductance of the MOS capacitors were measured with the help of H.P. multifrequency LCR meter model 4274A at several frequencies from 100 Hz to 100 kHz. The ac signal amplitude was not allowed to exceed 25 mV so that the non-linear effects were negligible. Fast surface state density (N_{ss}) at the Si/SiO_2 interface was obtained using Hill and Coleman[7] single-frequency approximation formula

$$N_{ss}=\frac{2}{q.A}\cdot\frac{G_{m,max}/\omega}{(G_{m,max}/\omega C_{ox})^2+(1-C_m/C_{ox})^2}$$

where $G_{m,max}$ is the measured conductance maximum

Table 1—Particulars of Si Oxidation and Annealing Conditions for Various Samples

Sample No.	Doping density (cm^{-3})	Crystal orientation	Oxide thickness (Å)	Field plate area, A (cm^2)	Annealing and oxidation processes used
MOS_1	3.5×10^{15}	⟨111⟩	1000	5.1×10^{-3}	Dry oxidation at 1000°C
MOS_2	1.8×10^{16}	⟨111⟩	500	4.91×10^{-3}	Dry oxidation at 1000°C + annealing for 20 min in N_2 ambient at same temperature
MOS_3	2.0×10^{16}	⟨111⟩	1100	3.02×10^{-3}	$O_2+5\%$ gaseous HCl at 1000°C followed by annealing in N_2 ambient for 30 min at 1000°C and PSG** deposition
MOS_4	1.5×10^{15}	⟨100⟩	800	6.36×10^{-3}	$O_2+5\%$ gaseous HCl at 1150°C followed by annealing in N_2 ambient for 40 min at 1000°C + PSG deposition

**For PSG (phospho-silicate glass) deposition, a mixture of N_2 (1.5×10^3 cc per min) + O_2 (30 cc per min) + $POCl_3$ (30 cc per min) was passed for 5 min. This was followed by N_2 treatment at 1000°C for 30 min.

in G-V plot, C_m the corresponding capacitance value on the C-V plot, A the metal plate area, ω the angular frequency used, q the electronic charge and C_{ox} the capacitance of the structure under strong accumulation.

Traditional Nicollian and Goetzberger[5] analysis corresponding to any desired value of surface potential Ψ_s was used for determining the surface state density at the Si-SiO_2 interface. For this, one usually determines C-V and G-V plots at several modulation frequencies. From these C-V and G-V plots and for any desired Ψ_s-value, G_p/ω are calculated for the various signal frequencies used[8]. Next, a plot of G_p/ω versus ω is made. From the peak value of G_p/ω versus ω curve, one finds the interface state density as

$$N_{ss}=\frac{C_{ss}}{q.A}$$

where C_{ss} is the surface state capacitance, given by

$$C_{ss}=2\left(\frac{G_p}{\omega}\right)_{max}$$

The surface state density was also determined using Castagne and Vapaille method[4]. According to this method, N_{ss} is given as

$$N_{ss}=\frac{C_{ox}}{q.A}\left(\frac{C_{LF}/C_{ox}}{(1-C_{LF}/C_{ox})}-\frac{C_{HF}/C_{ox}}{(1-C_{HF}/C_{ox})}\right)$$

where C_{LF} is the low-frequency capacitance and C_{HF} the high-frequency capacitance.

Four different samples having different surface state densities at the Si-SiO_2 interface were analyzed by the three different methods of Castagne-Vapaille, Nicollian-Goetzberger and Hill-Coleman. The results are compared in Table 2. Details of the experimental data for a typical MOS structure (MOS_1) are presented in Fig. 1. High frequency (100 kHz) C-V, G-V (solid curves) and low frequency (100 Hz) C-V (dashed curve) characteristics of the structure are shown in Fig. 1. Flat band capacitance (C_{FB}) calculated on the lines given in Ref. 9 is also indicated on the high frequency C-V curve. It may be pointed out that the peaks in the conductance curves for all the samples pertain to the depletion region. In Fig. 2, $G_p/\omega C_{ox}$ versus f for the structure at the gate bias -2.4 V is plotted. The bias corresponds to the conductance peak in the G_m versus V_G curve (Fig. 1) of the device at 100 kHz signal frequency.

Table 2—Surface State Density (in $cm^{-2}\,eV^{-1}$) for Various Samples as Determined by Different Methods

Sample No.	N_{ss}		
	Nicollian and Goetzberger method	Hill and Coleman method	Castagne and Vapaille method
MOS_1	5.29×10^{11}	3.62×10^{11}	5.60×10^{11}
MOS_2	1.45×10^{11}	1.43×10^{11}	1.70×10^{11}
MOS_3	4.51×10^{10}	4.51×10^{10}	0.75×10^{11}
MOS_4	0.46×10^{10}	0.46×10^{10}	0.58×10^{10}

The single frequency approximation method developed by Hill and Coleman[7] is found to be more suitable than any other approximation method. It may be pointed out that Hill and Coleman approximation method uses single time-constant for the surface states whereas in Nicollian and Goetzberger method provision for spatial fluctuations of surface charge can also be made, leading to the inclusion of time-constant dispersion effects in their framework. Nevertheless, Hill and Coleman's method, being simpler and providing reasonably accurate results, is quite suitable especially for systems having low surface state density. Further, the surface potential dependence of time constant should make only a small contribution to the time constant, especially if one is confined to a small

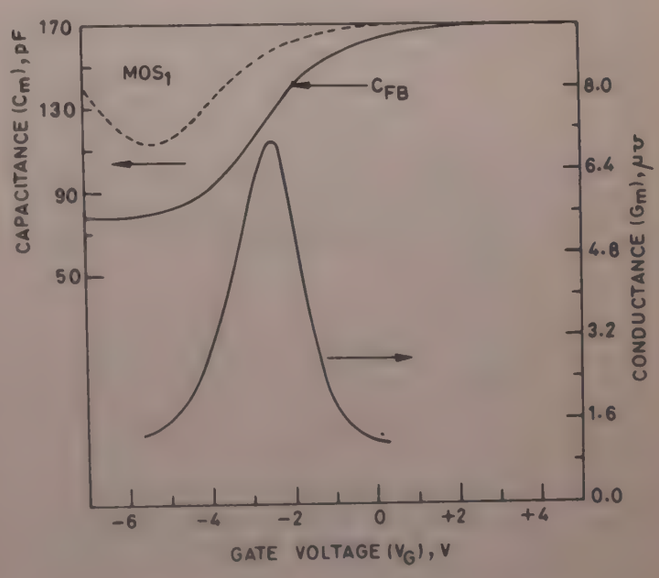

Fig. 1 C-V and corresponding G-V curves

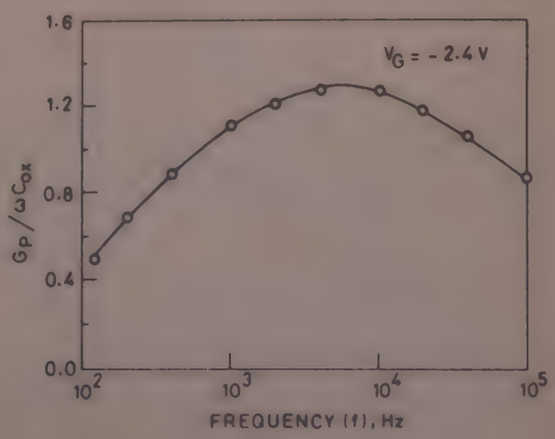

Fig. 2 $G_p/\omega C_{ox}$ versus f for MOS_1 structure

region of the band gap, i.e. near the G-V maximum. The densities of surface states for different samples presented in Table 2 demonstrate that the technique of Hill and Coleman agrees well with the results obtained from Nicollian and Goetzberger's technique for systems having low surface-state densities. This is in conformity with the conclusion drawn by Hill and Coleman[7].

It may be mentioned that in the method of Castagne and Vapaille, both low and high frequencies are employed. In the present study the low frequency employed was 100 Hz which is not indeed very low; yet the author has taken this as low frequency since the C-V curve obtained at this frequency was of low frequency type. Further, by this method all those surface states whose time constants (τ) are $\leq 2\pi/\omega$ would respond to the signal. This, therefore, gives an exaggerated value of N_{ss} than those based on conductance methods.

Acknowledgement

The author expresses his gratefulness to Dr R S Srivastava, Reader, Department of Physics, Banaras Hindu University, for his stimulating supervision and helpful discussions. Financial assistance by CSIR, New Delhi, during the course of the study is also thankfully acknowledged.

References

1 Terman L M, *Solid-State Electron (GB)*, **5** (1962) 285.
2 Lehovec K, *Appl Phys Lett (USA)*, **8** (1966) 48.
3 Berglund C N, *IEEE Trans Electron Devices (USA)*, **13** (1966) 701.
4 Castagne R & Vapaille A, *Surf Sci (Netherlands)*, **28** (1971) 157.
5 Nicollian E H & Goetzberger A, *Bell Syst Tech J (USA)*, **46** (1967) 1055.
6 Gray P V & Brown D M, *Appl Phys Lett (USA)*, **8** (1966) 31.
7 Hill W A & Coleman C C, *Solid-State Electron (GB)*, **23** (1980) 987.
8 Goetzberger A, Klausmann E & Schulz M J, *C R C critical reviews in solid state sciences (USA)*, (January 1976) 15.
9 Sze S M, *Physics of semiconductor devices* (Wiley, New York), Chap. 9, 1969.

Indian Journal of Pure & Applied Physics
Vol. 21, June 1983, pp. 357-358

High Field Single Injection Current in Solid State Diode with Shallow Traps by Exact Method

A S VERMA, Y K SHARMA*, R S AGRAWAL & C S AGRAWAL

Department of Physics, R B S College, Agra 282 003

Received 10 *May* 1982; *revised received* 22 *September* 1982

An exact method is used to evaluate the current-voltage characteristic of a single injection solid state diode with shallow traps operating in a high field regime. A set of curves are drawn for various values of the parameter characterizing the shallow traps.

Injection of current in an insulator has been widely studied in the presence of various physical parameters of interest operating under high field conditions[1-5]. The mobility is field dependent at high fields. The low field region is always present inside the insulator near cathode[5] which is generally neglected by the workers in the field. Here, the low field region is also included to study the current-voltage characteristic of the insulator with shallow traps at high fields.

Let us consider an insulator containing a significant density of shallow traps which generate the concentration of thermally generated free carriers N_0. The general equations characterizing the current flow and Poisson's law at high fields are given by

$$J = e\mu(E)\, n(x)\, E(x) \qquad \ldots (1)$$

$$\frac{\theta\varepsilon}{e}\frac{dE}{dx} = n(x) - N_0 \qquad \ldots (2)$$

where $\mu(E)$ is high field mobility of the current carriers, $n(x)$ the free electron concentration and θ the parameter characterizing the shallow traps. The high field mobility relationship is derived by Gisolf and Zijlstra[1] as follows:

$$\mu(E) = \mu_0\left[\frac{E_c}{E(x)}\right]^{1/2} \qquad \ldots (3)$$

where μ_0 is the low field mobility and E_c the critical field strength at which the high field effect starts. Eqs (1)-(3) are subjected to a boundary condition for ohmic contact:

$$E(0) = 0 \qquad \ldots (4)$$

At low field ($E < E_c$), the insulator is working under low field regime where the mobility (μ_0) is constant throughout the insulator. For medium electric fields ($E > E_c$), the insulator may be divided into two regions by an imaginary transition plane x_c where $E(x_c) = E_c$. The transition plane x_c is shifted towards cathode when the electric field increases. The low field region ($0 \leqslant x \leqslant x_c$) lies adjacent to cathode and the high field region ($x_c \leqslant x \leqslant L$) exists adjacent to anode. At sufficiently high fields, the low field region is negligibly small and the insulator is working under high field conditions.

The exact current-voltage characteristic may be conveniently obtained with the help of the following dimensionless variables:

$$u = \frac{N_0}{n} = \frac{eN_0\mu_0[E_c E(x)]^{1/2}}{J},$$

$$w = \frac{e^2 N_0^2 \mu_0 E_c^{1/2} x}{\theta\varepsilon J[E(x)]^{1/2}},\quad v = \frac{e^3 N_0^3 \mu_0^2 E_c V(x)}{\theta\varepsilon J^2 E(x)} \qquad \ldots (5)$$

The critical dimensionless variables at the transition plane x_c are given from Eq. (5)

$$u_c = \frac{eN_0\mu_0 E_c}{J},\quad w_c = \frac{e^2 N_0^2 \mu_0 x_c}{\theta\varepsilon J},$$

$$v_c = \frac{e^3 N_0^3 \mu_0^2 V(x_c)}{\theta\varepsilon J^2} \qquad \ldots (6)$$

Consider the injection level at which the low field and high field regions are present inside the insulator. From Eqs (1)-(6), the dimensionless variable at anode is derived as

$$w_a = -\frac{2}{u_a}\left[\frac{(u_a^2 - u_c^2)}{2} + (u_a - u_c) + \ln\frac{(1-u_a)}{(1-u_c)}\right] + \frac{u_c w_c}{u_a} \qquad \ldots (7)$$

The dimensionless variable v at anode is given from Eq. (5)

$$v_a = -\frac{2}{u_a^2}\left[\frac{(u_a^4 - u_c^4)}{4} + \frac{(u_a^3 - u_c^3)}{3} + \frac{(u_a^2 - u_c^2)}{2} + (u_a - u_c) + \ln\frac{(1-u_a)}{(1-u_c)}\right] + v_c \qquad \ldots (8)$$

where v_c is given in Eq. (6). From Eq. (5), the current density and applied voltage across the diode are derived in terms of three dimensionless variables

$$J = \left[\frac{e^3 N_0^3 \mu_0^2 E_c L}{\theta\varepsilon}\right]^{1/2}\frac{1}{(u_a w_a)^{1/2}},\quad V = \frac{eN_0 L^2}{\theta\varepsilon}\frac{v_a}{w_a^2} \qquad \ldots (9)$$

where the variables w_a and v_a are given by Eqs (7) and (8) respectively.

The complete current-voltage characteristic of an insulator with shallow traps operating in high field conditions is plotted for three values of θ on a log-log

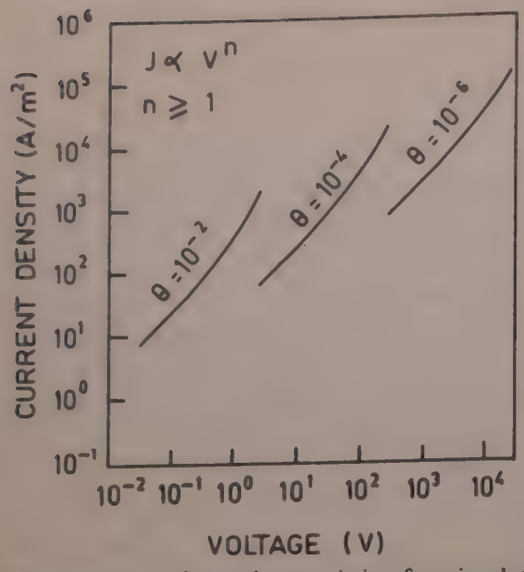

Fig. 1—Exact current-voltage characteristic of an insulator with shallow traps at high fields for $\theta = 10^{-6}$, 10^{-4} and 10^{-2}

scale in Fig. 1 with the help of Eqs. (7)-(9) where the critical dimensionless variables u_c, w_c and v_c are neglected by assuming that the injection level of current is sufficiently high. The dimensionless values $1/(u_a w_a)^{1/2}$ and v_a/w_a^2 are obtained by the numerical tabulation of w_a and v_a against u_a. The range of variable u_a lies between 0 and 1. Other physical parameters are selected for cadmium sulphide at room temperature:

$$N_0 = 10^{16}\,\mathrm{m}^{-3},\ L = 10^{-5}\,\mathrm{m},\ \varepsilon = 10^{-10}\,\mathrm{F/m}$$

$$\mu_0 = 2 \times 10^{-2}\,\mathrm{m^2/V\text{-}s},\ E_c = 10^7\,\mathrm{V/m}$$

and $\theta = 10^{-6}$, 10^{-4} and 10^{-2} ... (10)

The current-voltage characteristics of three samples with different values of θ are drawn in Fig. 1. It is shown that all the curves initially obey Ohm's law ($J \propto V$) and they finally merge into a non-linear current-voltage characteristic. The effect of traps appears on the non-linear portion of the continuous curve, i.e. at a higher injection level. The location of current-voltage characteristic is dependent on θ. The characteristic located on the right side of Fig. 1 is for lower values of θ.

In the present problem, the presence of shallow traps is taken into consideration. The relation between the trapped electron concentration (n_t) and characteristic constant θ is given by[4]

$$(n/n_t) = \theta \qquad \ldots (11)$$

where n is the free electron concentration. In the absence of shallow traps, θ is unity in Eqs (2) and (9). In general, the functional dependence of n_t on n for any trap configuration is given by the simple form[4]:

$$n_t \propto n^p \qquad \ldots (12)$$

which is valid for the limits $0 \leq p \leq 1$. Let us consider a shift in the quasi Fermi level $F \rightarrow F + \delta F$. There will be a maximum change in trap occupancy if traps are shallow, $n_t \propto n$, so that $p = 1$; and the traps are deep for minimum change, i.e. no change at all, in which case n_t = constant, so that $p = 0$.

If there are several sets of shallow trap levels in a given sample, the set with the smallest θ dominates the current flow and this value of θ satisfies Eq. (9). It may be noted that the traps are shallow so long as the quasi Fermi level lies below the energy level of traps. However, the quasi Fermi level keeps rising with injection level, i.e. with applied voltage. The effect of shallow traps on current-voltage characteristic is observed through the parameter θ.

References

1 Gisolf A & Zijlstra R J J, *Solid State Electron (GB)*, **16** (1973) 571.
2 Lampert M A, *J Appl Phys (USA)*, **29** (1958) 1082.
3 Sharma Y K, *J Appl Phys (USA)*, **50** (1979) 5381.
4 Lampert M A & Mark P, *Current injection in solids* (Academic Press, New York) 1970.
5 Sharma Y K, *Electron Lett (GB)*, **16** (1980) 896.

Indian Journal of Pure & Applied Physics
Vol. 21, June 1983, pp. 359-360

Suppression of Noise by a Plasma Shield

A P SAXENA* & N S SURYANARAYANA
Department of Physics, Ravishankar University, Raipur 492010

Received 20 *August* 1982; *revised received* 10 *January* 1983

The transmission of sonics through an ionized medium has been numerically evaluated with the help of a computer. The analysis shows that if a source of noise is surrounded by a plasma barrier it can effectively shield most of the noise spectrum.

The suppression of noise is a subject of great interest because of its technological importance[1-3].

Elastic properties of the medium determine the mode of propagation and the speed of sound through it. In an un-ionized gas, the elastic forces are caused by the gas pressure which results from the collisions between the gas molecules. However, when a sound wave travels in a plasma, the electrical neutrality of a small element of plasma is disturbed owing to the relative displacement of the charged particles and Coulomb forces are called to restore the original state; this exhibits the elastic properties of plasma enabling it to support an acoustic wave.

Two electrostatic-type modes are possible, when an acoustic wave travels through a plasma[4]. One of these modes gives rise to electron acoustic wave, in which the wave is mainly carried by electrons. The other mode gives rise to ion acoustic wave [IAW] which is carried by positive ions and the inertia of the ions determines the wave speed. The applied acoustic wave may choose either of these two modes. The IAW does not travel above a cut-off frequency $(m/M)^{1/2}\,\omega_p$, where m and M are masses of electron and ion respectively and ω_p is the angular plasma frequency. On the other hand, the phase velocity of the electron wave becomes imaginary for $\omega \ll \omega_p$. Therefore the sonic signal travels through plasma as ion acoustic wave.

When an acoustic wave initially travelling in air traverses a plasma slab, it suffers partial reflection at the air-plasma and plasma-air interfaces. Considering normal incidence, transmission of a plane acoustic wave from air (medium 1) into a lossless plasma (medium 2) and into air again (medium 3), the sound power transmission coefficient α is given[1] by the square of the ratio of the pressure amplitudes of the transmitted wave (A_3) to that of the incident wave (A_1) (Fig. 1),

$$\left(\frac{A_3}{A_1}\right)^2 = \frac{4}{4+(x^2-4)\sin^2(2\pi nl/C_2)} \qquad \ldots(1)$$

where n is the frequency of acoustic signal travelling with a speed C_1 in air and C_2 in plasma and l the length of the plasma slab. $x=[r_{12}+(1/r_{12})]$, where $r_{12}(\rho_2 C_2/\rho_1 C_1)$ is the relative acoustic characteristic impedance of medium 2 (plasma) with respect to medium 1 (air) and ρ_1 and ρ_2 are the densities of the media 1 and 2 respectively. If the two mass densities are equal, $r_{12}=C_2/C_1$ and is equal to x provided r_{12} is large. It is, therefore, apparent from Eq. (1) that the ratio A_3/A_1 depends upon n, l, the speed of IAW in the plasma and the speed of sound in air.

If oblique incidence of the acoustic wave is considered and if C_1 is less than C_2 which is usual in the present case[5-7] ($C_2 \simeq 5$-$10\,C_1$), then for some critical angle of incidence θ_c, the refracted ray makes an angle of 90° with the normal to the interface; the critical angle (θ_c) is given by

$$\sin\theta_c = C_1/C_2 \simeq 0.2\text{-}0.1$$

Therefore θ_c is of the order of a few degrees. If the angle of incidence is equal to or greater than a few degrees, no acoustic energy is transmitted to the second medium and it is reflected back entirely in the first medium. Thus, a very narrow cone of acoustic energy is of significance if the transmission from air to plasma is considered.

Numerical evaluation of A_3/A_1 from Eq. (1) was carried out by a computer for various values of l, n and C_2. Some of the results are presented graphically in Figs 2 and 3 for different values of n, C_2 and l. The analysis is quite interesting. A few centimetres ($\simeq$ 7-10 cm) of a plasma slab shall only transmit about 25-30% of the pressure amplitude of the incident acoustic signal and the rest is reflected back in the medium 1.

The loss of amplitude of a sonic signal when it passes through a plasma slab was measured experimentally by us and reported in a number of communications[8-10]. This has yielded an interesting and

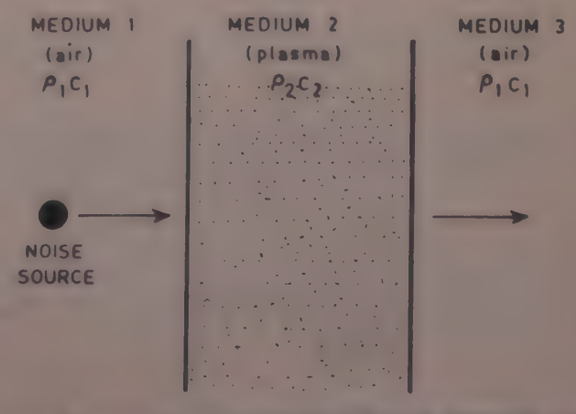

Fig. 1 Transmission of sonic signal through successive media

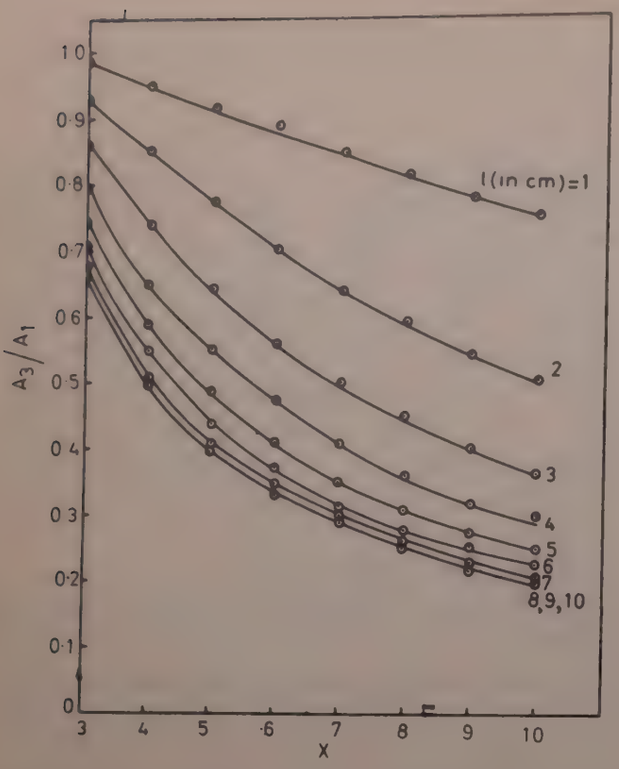

Fig. 2—Square root of sound power transmission coefficient versus relative acoustic characteristic impedance of plasma ($n = 5$ kHz; $l = 1$-10 cm; $C_2 = 5\,C_1$)

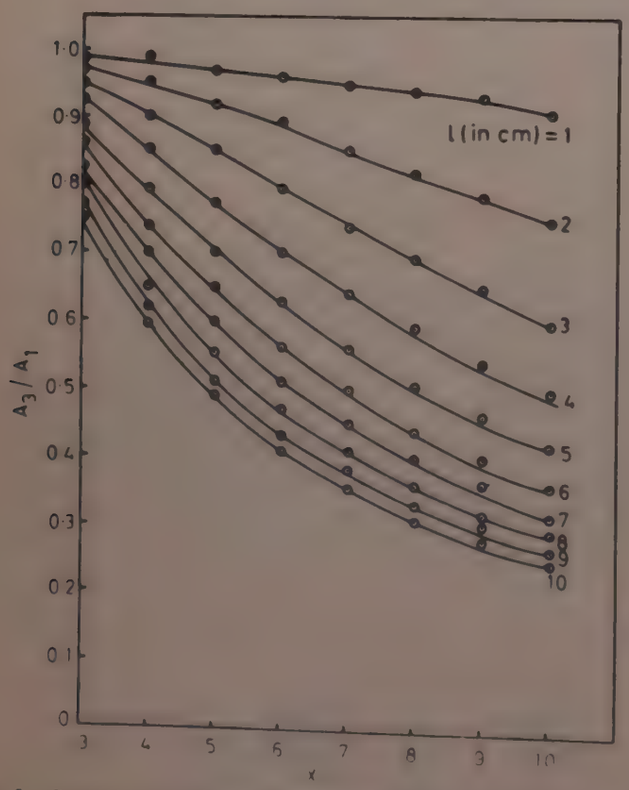

Fig. 3—Square root of sound power transmission coefficient versus relative acoustic characteristic impedance of plasma ($n = 5$ kHz; $l = 1$-10 cm; $C_2 = 10\,C_1$)

potentially powerful addition to the methods for effecting analysis of a plasma and is commonly known as sonic probe technique.

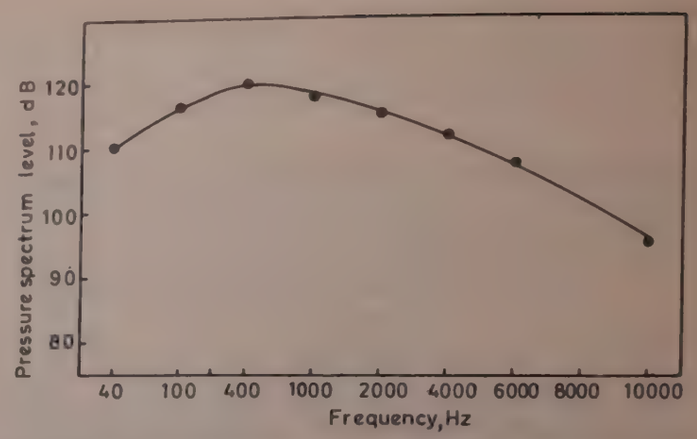

Fig. 4—Noise spectrum of a turbo jet engine: Pressure level versus frequency

Noise has an essentially continuous frequency spectrum. The manner in which the intensity varies with frequency may be represented by a graph showing the sound spectrum of the noise. The abscissas of the graph are the frequencies and the ordinates give the pressure spectrum level of the sound at each frequency. The sound spectrum of a turbo jet engine of 150 dB overall pressure level has been shown in Fig. 4. The spectrum extends from a frequency of 40 Hz to 10 kHz. Thus turbo jet engines are quite rich in high frequency components which need to be suppressed.

The above analysis shows that if such a noise source is surrounded by a plasma barrier of few centimetres thickness, the latter can effectively shield most of the noise spectrum from spreading further.

The authors are grateful to Dr C P Gupta, Scientist In-charge, Computer Section, NGRI, Hyderabad, for carrying out the numerical analysis. They are also thankful to Department of Science and Technology, New Delhi, and to the University Grants Commission, New Delhi, for liberal grants, and to the authorities of Ravishankar University, Raipur, for the facilities provided.

References

1 Kinsler L E & Frey A R, *Fundamentals of acoustics* (John Wiley, New York) 1962.

2 MacDonald D K C, *Noise and fluctuations* (John Wiley, New York), 1962.

3 Harries C M, *Handbook of noise control* (McGraw Hill, New York), 1957.

4 Spitzer L (Jr), *Physics of fully ionized gases* (Interscience, New York), 1956.

5 Wong A Y, Motley R W & D'Angelo N, *Phys Rev A (USA)*, 133 (1964) 436.

6 Alexeff I & Jones W D, *Phys Rev Lett (USA)*, **15** (1965) 286.

7 Jones W D, Lee A, Gleman S M & Doucet H J, *Phys Rev Lett (USA)*, **20** (1975) 1349.

8 Saxena A P & Gaur S C, *Plasma Phys (GB)*, **11** (1969) 611.

9 Saxena A P & Saxena R K, *Indian J Pure & Appl Phys*, **12** (1974) 198.

10 Saxena A P & Gaur S C, *Int J Electron (GB)*, **27** (1969) 13.

Indian Journal of Pure & Applied Physics
Vol. 21, June 1983, pp. 361-362

Electrical Properties of Antimony Oxide Films Formed by Heating Antimony Films in Air

P S NIKAM*† & D L MANKAR‡
M S G College, Malegaon Camp, Dist. Nasik 423 105

Received 13 *September* 1982; *accepted* 17 *February* 1983

A study has been made of resistivity (ρ), activation energy (ΔE), temperature coefficient of resistance (TCR) and mean free-path (l_0) of charge carriers in air-oxidized antimony films in the temperature range 50-240°C. The electrical parameters of these films differ considerably from those of vacuum-evaporated films of antimony oxide.

Dissociation and formation of new species has been observed during vacuum deposition of several oxides and chalcogenides[1-4]. To avoid such dissociation, antimony oxide films were formed by oxidizing flash evaporated antimony films in air. Electrical properties of antimony oxide in bulk have been reported earlier[5-7]. Detailed studies on semiconducting, structural and optical properties of vacuum-deposited antimony oxide films[8-12] have already been made. In the present note, an account is given of our investigation on semiconducting properties of antimony oxide films formed by oxidation of flash evaporated antimony films.

The details of the preparation of antimony oxide films are similar to those for bismuth oxide films[13]. Antimony used was specpure. The deposits of antimony formed in 10^{-6} Torr vacuum were oxidized in air at about 215-220°C for 12 hr. These films were then annealed in vacuum at 110°C for 6 hr. The composition of the films was found to be $Sb_{2\pm x}O_3$ where x varied from 0 to ± 0.2 for thick and thin films respectively.

The plot of log R as a function of reciprocal absolute temperature (T) at reduced pressure (10^{-6} Torr) for different film thicknesses over the temperature range 50-200°C is shown in Fig. 1. The dc dielectric resistance is found to vary as

$$R = R_0 \exp(\Delta E/kT) \quad \ldots (1)$$

In general, values of ΔE for lower film thickness were higher (Table 1). The higher value of ΔE for thinner samples may be explained qualitatively on the basis of island structure theory of Neugebauer and others[14,15]. On the basis of this theory, ΔE in Eq. (1) is given[16] by:

$$\Delta E = \frac{e^2}{Kr} + \frac{\Delta E_g}{2} \quad \ldots (2)$$

where e is the electronic charge, E_g the semiconductor energy gap, r the average linear dimension of the island, and K the dielectric constant of the material. Even though the films studied by us were much thicker and more or less continuous, the variation of ΔE has the same trend as that of very thin films.

Temperature coefficient of resistance (TCR) was negative for thin as well as thick films. For each film, TCR decreased with increase of temperature. Higher value of negative TCR at lower temperature is also explained on the basis of the island structure theory. The expression for TCR is given by:

$$\text{Negative TCR} = -\frac{\mathrm{d}}{\mathrm{d}T}(d)\left[\frac{4\pi\sqrt{2m\varphi}}{h^2} + \frac{1}{d}\right] + \frac{C'}{T^2} \quad \ldots (3)$$

where $C = [2e^2/\varepsilon r + \Delta E_g]/2K$, d is the average distance between islands, m the electronic mass, ε the dielectric constant of the substrate, φ the potential barrier

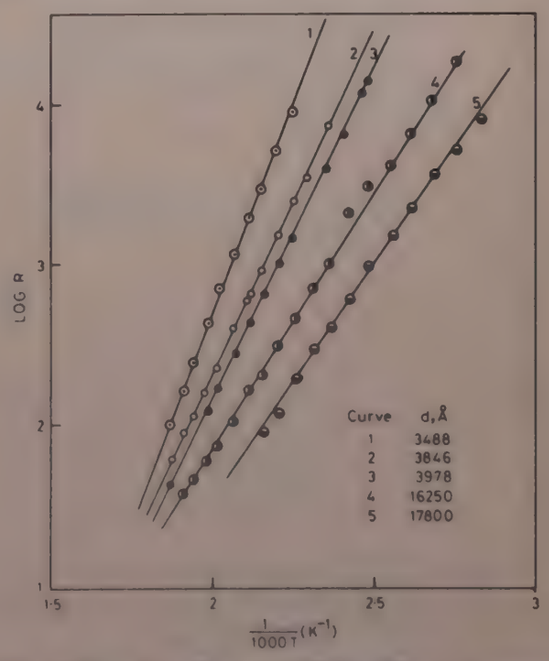

Fig. 1 — Plot of log R versus $1/T$ for different thicknesses

Table 1 — Variation of Activation Energy (ΔE) with Film Thickness

Film thickness Å	ΔE eV
3488	1.59
3846	1.413
3978	1.387
16250	0.9535
17800	0.9217

†Postgraduate Department of Physical Chemistry.
‡Department of Physics.

between islands and h the Planck's constant. In the present investigation, the first term in Eq. (3) predominates.

Mean free-path of charge carriers at different temperatures was obtained graphically for Sb_2O_3 films from ρd versus d curves as done previously by Goswami *et al.*[17] Fig. 2 shows ρd versus d curves for different temperatures and Table 2 shows the variation of mean free-path of charge carriers with temperature for a hypothetical massive material of Sb_2O_3 having the same structure and roughly the same number of lattice defects as those of the films. Thick films exhibit bulk or nearly bulklike properties. In a bulk semiconductor, l_0 increases with decrease of temperature due to lattice (intrinsic) impurities[18]. In our present investigation, l_0 increases with decrease of temperature due to the presence of traces of SbO as intrinsic impurity in thick Sb_2O_3 films which tend to behave like bulk semiconductor.

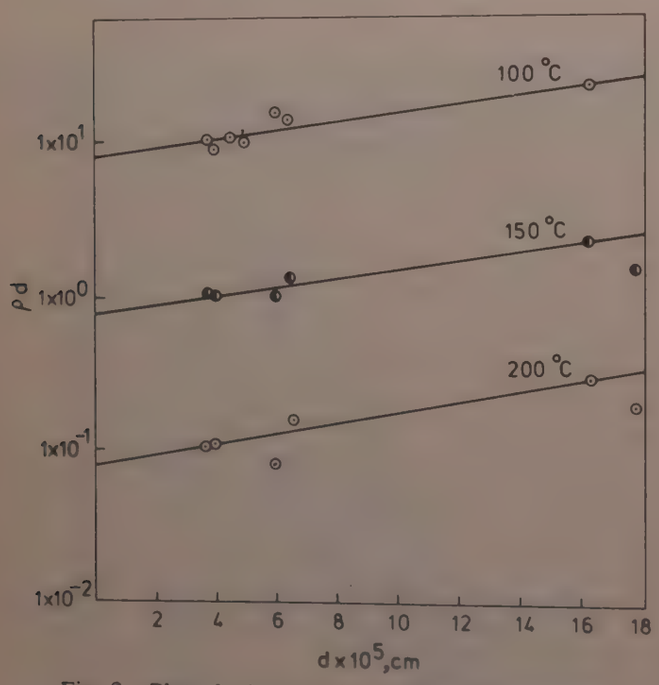

Fig. 2—Plot of ρd versus d for different thicknesses

Table 2—Variation of Mean Free-path (l_0) of Charge Carriers with Temperature

Temperature °C	(l_0) 10^{-4} cm
100	1.224
150	0.7823
200	0.7442

Antimony oxide films are expected to obey an analogue of Mattiessen's rule. Hence the effective mobility of the film (μ_F) is obtainable from the sum of the inverses of the various mobilities, so that

$$\frac{1}{\mu_F} = \frac{1}{\mu_L} + \frac{1}{\mu_I} + \frac{1}{\mu_S} \quad \ldots (4)$$

where μ_L is mobility due to lattice impurities, μ_I that due to imperfections and μ_S that due to surface scattering.

Thus we conclude that films of antimony oxide are semiconducting in nature irrespective of their thickness. This result is only in qualitative agreement with the prediction of Neugebauer's theory since during the gradual oxidation of antimony films, SbO was formed as an intermediate product which acted as lattice impurities in Sb_2O_3 films.

The authors wish to thank Principal R V Khairnar for his constant encouragement and keen interest in this study.

References

1 Goswami A & Treham Y N, *Proc Phys Soc London B (GB)*, **70** (1957) 1006.
2 Goswami A & Nikam P S, *J Cryst Growth (Netherlands)*, **8** (1971) 523.
3 Nikam P S, *Curr Sci (India)*, **41** (1972) 138.
4 Nikam P S, *Indian J Pure & Appl Phys*, **11** (1973) 432.
5 Karzh P D & Gulyaeva G P, *Fiz Tech Polorodikev (USSR)*, **3** (1969) 782.
6 Vincent C A, *J Electrochem Soc (USA)*, **119** (1972) 515.
7 Fedorov I A & Davydev I Ya, *Teplofiz Vys Temp (USSR)*, **16** (1978) 765.
8 Karpovich I A & Feeoseeva N V, *Izv VuZ Fiz (USSR)*, **5** (1969) 52.
9 LeGaillard N, *Thin Solid Films (Switzerland)*, **6** (1970) 289.
10 Wood C, Vanpelt B & Dwight A, *Phys Status Solidi (Germany)*, **54** (1972) 701.
11 Butterfield A W & Medermott I T, *Thin Solid Films (Switzerland)*, **18** (1973) 111.
12 Goswami A & Goswami P, *Thin Solid Films (Switzerland)*, **20** (1974) 533.
13 Aggrwal P S & Goswami A, *Z Naturforsch a (Germany)*, **13** (1958) 885.
14 Neugebauer C A, *Physics of thin films*, Vol 2 (Academic Press, New York), 1964, 25.
15 Neugebauer C A & Webb M B, *J Appl Phys (USA)*, **33** (1962) 74.
16 Barua D C & Barua K, *Indian J Phys*, **48** (1974) 332.
17 Goswami A & Koli S S, *Int Symp on Basic Problems in Thin Films Physics*, September 1965 (Clausthal, Gottingen, West Germany), Abstr p53.
18 Ziman J M, cited in *Thin film phenomena*, edited by K L Chopra (McGraw-Hill, New York) 1969, 444.

Indian Journal of Pure & Applied Physics
Vol. 21, June 1983, pp. 363-364

Effect of Magnetic Field on the Drain Current of JFET BFW-61

N MANOHARA MURTHY*, P MALLIKARJUNA REDDY† & S V SUBRAHMANYAM

Department of Physics, Sri Krishnadevaraya University College, Anantapur 515003

Received 27 *May* 1981; *accepted* 8 *April* 1983

The effect of magnetic field (B) on drain current of FET BFW-61 has been studied. A decrease in drain current on the application of magnetic field has been observed in all the three cases studied, namely B parallel to current flow ($B\|$), B perpendicular to the current flow and along the width of the crystal ($B\perp W$) and B perpendicular to the current flow and along the thickness of the crystal ($B\perp T$). The change in drain current on the application of B has been found to be in the order when $B\perp T > B\| \simeq B\perp W$. The results have been explained as due to the combined effects of Hall effect and magnetoresistance.

The characteristics of p-n junction devices are susceptible to both temperature[1-5] and magnetic field[6-11]. Field effect transistor is being used extensively since it combines the desirable features of the thermionic valves and those of conventional transistors and hence is a superior substitute for both in many circuit applications. In view of this, it is essential to know the degree of susceptibility of the characteristics of these devices to external influences like temperature and magnetic field for proper design of the electronic circuits.

Studies on the effect of temperature on the transfer characteristics of a large number of samples of BFW-10 have been carried out by Jamwal and Peer[4]. Studies on the effect of magnetic field on the drain current and transconductance of JFETs, BFW-10 and BFW-11 have been carried out by Jain and Agarwal[8]. In the present work, studies on the effect of magnetic field on the drain current of a large number of samples of BFW-61 have been carried out with a view to see as to what extent the characteristics of equivalent transistors are susceptible to the influence of magnetic field. The results are presented in this note.

The effect of magnetic field on the drain current of BFW-61 has been studied using the circuit similar to that employed by Jain and Agarwal[8] and by housing the FET between the polepieces of an electromagnet (field strength was determined using Hall probe) and applying the field along the three different directions namely (i) B parallel to current flow ($B\|$), (ii) B perpendicular to the current flow and along the width of the crystal ($B\perp W$) and (iii) B perpendicular to the current flow and along the thickness of the crystal ($B\perp T$). These directions were determined by decapsulating the FET and observing it under a microscope.

The results on the measurement of decrease in drain current (ΔI_D) with magnetic field applied in different directions for various gate-to-source voltages (V_{GS}) are presented in Table 1. Typical results when $V_{DS} = 15$ V and $V_{GS} = 0$ V are shown graphically in Fig. 1.

An examination of the data presented in Table 1 and Fig. 1 clearly shows that the decrease in drain current with field when applied in the $B\perp T$ direction is more than the decrease found when the field is applied along the other two directions, viz. $B\perp W$ and $B\|$. But the magnitude of change in drain current within the limits of experimental error is same in $B\perp W$ and $B\|$ directions. However, Jain and Agarwal[8] observed a greater magnitude of decrease in I_D on the application of magnetic field in $B\perp W$ than in $B\|$ directions for JFETs, BFW-10 and BFW-11 for a field strength of 19.5 kOe. FETs being unipolar devices and since magnetoresistance effect is a majority charge carrier effect, there is every possibility for magnetoresistance to appear in FETs. It is this magnetoresistance effect that is responsible for the decrease in the drain current when

Table 1—Variation of ΔI_D (in μA) with B (in kOe) at Different Gate-to-Source Voltages for BFW-61 [$V_{DS} = 15$ V]

B (KOe)	$V_{GS} = 0$ V			$V_{GS} = -0.5$ V			$V_{GS} = -1.0$ V		
	$B\|$	$B\perp W$	$B\perp T$	$B\|$	$B\perp W$	$B\perp W$	$B\|$	$B\perp W$	$B\perp T$
4.8	0.9	0.8	1.0	0.5	0.5	0.6	0.1	0.1	0.3
10.3	2.6	2.5	4.0	2.0	2.0	2.6	1.4	1.0	1.8
15.4	3.9	3.8	4.9	3.0	2.8	4.5	1.9	1.8	2.6
16.3	4.2	4.1	5.5	3.2	3.1	5.0	2.1	2.1	2.9
17.3	5.0	5.0	7.2	4.0	3.9	6.0	3.0	2.7	3.8

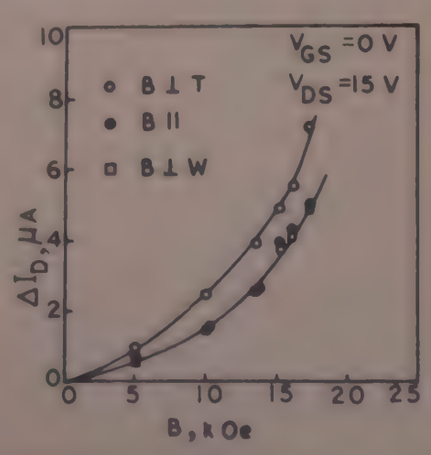

Fig. 1—Variation of change in drain current (ΔI_D) with magnetic field (B) for JFET BFW-61

† Present address: Department of physics, V R College, Nellore

the field is applied parallel to the current flow. In the other two directions, current flows perpendicular to the direction of magnetic field and therefore Hall effect is associated with the device. Hence application of magnetic field leads to the development of Hall voltage which makes the reverse biased gate junction to be more negative. Increased reverse bias increases the channel resistance leading to a decrease in drain current. However, the magnitude of decrease in drain current is found to be different in different directions. This behaviour suggests that the effect of magnetic field on the drain current in the FETs may be considered to be due to the combined effects of Hall effect and magnetoresistance.

The studies carried out on a few other samples of BFW-61 FETs also indicate similar type of behaviour presented in this note. Even though BFW-10, 11 and 61 are considered as equivalent in circuit applications the effects of external influences like temperature and magnetic field are not alike on the characteristics of the FETs. This aspect is to be borne in mind in the application of these devices.

References

1 Sandiford D J, *J Appl Phys (USA)*, **30** (1959) 1981.

2 Bernard M, *J Electron Control*, **2** (1956/57) 579.

3 Millman J & Halkias C C, *Electronic devices and circuits* (McCraw-Hill Kogakusha Ltd, Tokyo) 1967.

4 Jamwal K K S & Peer M A, *Indian J Pure & Appl Phys*, **14** (1976) 674.

5 Nanavathi R P, *Proc IRE (USA)*, **49** (1961) 349.

6 Parshad R & Mehta S C, *Indian J Pure & Appl Phys*, **5** (1967) 165.

7 Misra M, *Indian J Pure & Appl Phys*, **3** (1965) 30.

8 Jain A K & Agarwal V K, *Indian J Pure & Appl Phys*, **13** (1975) 560.

9 Srivastava G P & Misra M, *Z Angew Phys (Germany)*, **14** (1962) 577.

10 Karakushan E & Stafeev V I, *Soviet Phys Solid St (USA)*, **3** (1962), 1476.

11 Mallikarjuna Reddy P, Manohara Murthy N & Subrahmanyam S V, *Indian J Pure & Appl Phys*, **17** (1979) 501.

Indian Journal of Pure & Applied Physics
Vol. 21, June 1983, pp. 365-367

Correlation of Changes in the Electrical Conduction & Dielectric Constant in Naphthalene due to Magneto-Electret Formation

A K BHATNAGAR, M L KHARE & C S BHATNAGAR*

Department of Physics, M A College of Technology, Bhopal 462 007

Received 19 *November* 1981; *revised received* 31 *March* 1982

Electrical conductivity of naphthalene is measured at different voltages before and after its magneto-electret formation. It is observed that electrical conduction decreases by 5-20%, depending on the forming parameters of magneto-electret. The variation of percentage decrease in electrical conduction with forming temperature closely follows the variation of percentage increase in dielectric constant with the forming temperature. An attempt is made to correlate the two phenomena.

The observations on naphthalene samples showed[1] that there is an increase (up to 5%) in its dielectric constant due to magneto-electret formation. On the other hand, measurement of current, which is being reported in this note, shows that electrical conduction in this material decreases (5 to 20%) on magneto-electret formation. The decrease in electrical conduction is an evidence of the loss of charge carriers, whereas an increase in dielectric constant indicates that the charge carriers get associated in such a way that the new configuration (which may be psuedo-dipoles or traps) has a higher polarizability. Since the two phenomena involve charge carriers in the bulk of the material, it is worthwhile to seek a correlation between them. The present note reports the results of measurements on electrical conduction of naphthalene magneto-electret and tries to correlate the observations with those of dielectric constant reported earlier[1].

Magneto-electret samples of naphthalene (diam 1.25 cm and thickness 1.25 mm) were prepared following the usual method[2] at different temperatures (30, 55, 60, 65 and 70°C) using various magnetic field strengths (3.0-17.0 kOe). The total duration of application of the magnetic field was 1.5 hr (1 hr at constant elevated temperature and 0.5 hr during cooling).

The current measurement was done at room temperature with the sample mounted in a holder similar to that described elsewhere[3]. ECIL electrometer (EA 814) was used for the measurement of current at different voltages (in equal steps up to 500 V) applied to the sample before and after magneto-electret formation.

Fig. 1 shows variation of current measured at different voltages for magneto-electret (ME) samples prepared at the forming temperature of 60°C, using different magnetic field strengths. It is seen that current after thermo-magnetic treatment always has a value lower than that for the virgin sample. The decrease in electrical conduction ranges from 5 to 20% in most of the cases depending on the forming temperature and magnetic field strength. The difference between the values of current for the virgin and ME-samples increases systematically with the increase in the measuring voltage, though in some cases, especially in samples formed at low magnetic field, this difference seems to be constant.

A systematic variation is observed on plotting the percentage decrease in current against forming temperature for various forming magnetic fields (Fig. 2a). All the curves exhibit a maximum at the forming temperature of 60°C. Incidentally these curves have a striking resemblance to the variation of the percentage increase in the dielectric constant with forming temperature (Fig. 2b) which also exhibits a maximum at 60°C. However, the resemblance is only qualitative. The increase in dielectric constant ranges from 2 to 5% whereas the decrease in the current is from 5 to 20% and in some cases it is more than 20%. Yet, the qualitative resemblance between the two types of curves prompts one to seek for a correlation between the decrease in current and increase in dielectric constant caused in electret formation.

The I-V characteristic of samples of naphthalene indicates that it perhaps follows the $\log I$-$V^{1/2}$ law. In

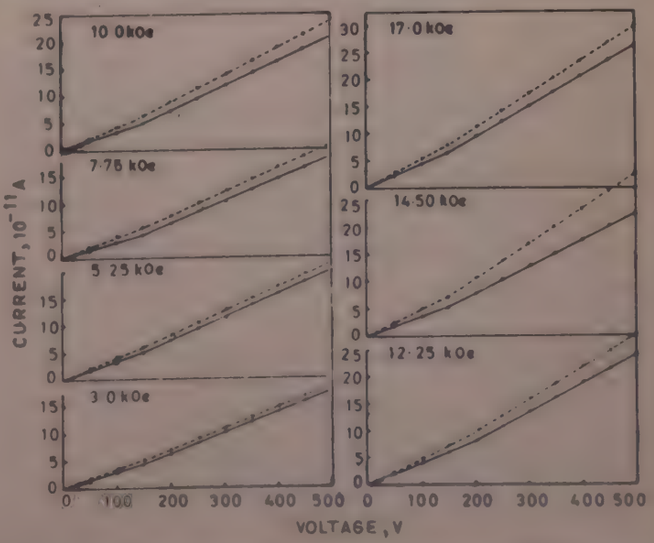

Fig. 1—I-V characteristics of magneto-electret (ME) samples prepared at the forming temperature (T_f) 60 C using different magnetic field strengths [Broken curve: Virgin sample; Continuous curve: ME sample]

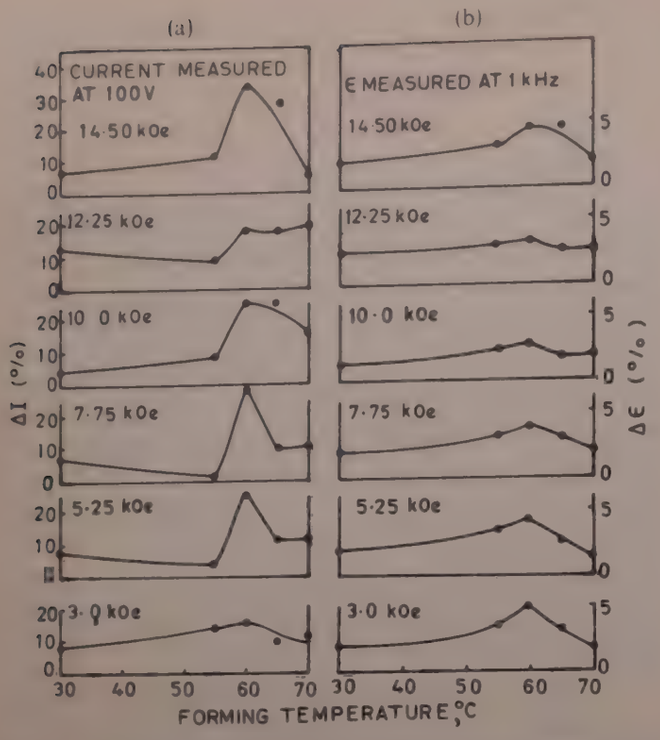

Fig. 2—Comparison of percentage variations of conduction current and dielectric constant due to electret formation of naphthalene samples with forming temperature [(a), conduction current decrease; (b), dielectric constant increase]

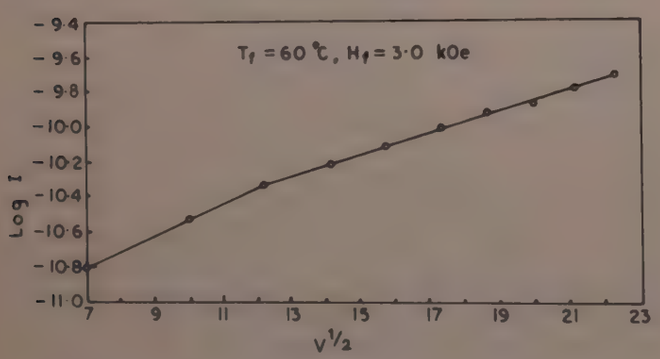

Fig. 3—Plot of log$I$ versus $V^{1/2}$ for magneto-electret sample prepared at forming temperature (T_f) of 60°C using magnetic field strength (H_f) of 3.0 kOe

Fig. 3, log$I$ is plotted against $V^{1/2}$. At lower voltage ranges (up to 150 V), this curve is a straight line, whereas at higher voltages the curve transforms to another straight line of lesser slope. It seems that at lower voltages, the Poole-Frenkel process is responsible for electrical conduction, and this gradually changes to the Schottky process at higher voltages[4].

In the Schottky process, the current is given by[5]

$$I = AT^2 \exp(-\varphi_0/kT)\exp(\beta_s E^{1/2}/kT) \quad \ldots (1)$$

where E is the applied electric field and

$$\beta_s = (e^3/4\pi\varepsilon_0\varepsilon_r)^{1/2} = a/\varepsilon_r^{1/2} \quad \ldots (2)$$

where $a = (e^3/4\pi\varepsilon_0)^{1/2}$ is a constant and other symbols have their usual meaning. Eq (1) shows that at a fixed temperature, log$I \propto E^{1/2}$, as has been observed. Further, if there happens to be any change in the relative dielectric permittivity (ε_r), it will have its effect on the current I.

By differentiating Eq. (1) and using Eq. (2) it is easy to show that

$$-dI/I = (a/2kT)(E/\varepsilon_r)^{1/2}.d\varepsilon_r/\varepsilon_r \quad \ldots (3)$$

For a constant temperature and field, this relation reduces to

$$-dI/I \propto d\varepsilon_r/\varepsilon_r \quad \ldots (4)$$

which shows that a fractional change in current is proportional to a practical change in the dielectric constant. The negative sign shows that as the dielectric constant increases, the current will decrease. This is what has been observed.

It can be seen that Eq. (4) is applicable also for the case where conduction is governed by the Poole-Frenkel process. The Poole-Frenkel current is given by[5]

$$I = \sigma_0\left(\frac{kT}{\beta}\right)^2\left[\left(\frac{\beta E^{1/2}}{kT}\right)-1\right]\exp\left(\frac{\beta E^{1/2}}{kT}\right) \quad \ldots (5)$$

where $\beta = (e^3/\pi\varepsilon_0\varepsilon_r)^{1/2} = b/\varepsilon_r^{1/2}$ ... (6)

where b is a constant.

The measuring field E is of the order of 10^3 V/cm and the value of β/kT at room temperature is of the order of ten[5]. Therefore, 1 in the expression $[(\beta E^{1/2}/kT)-1]$ is neglected in comparison with $\beta E^{1/2}/kT$.

With this approximation, one can get on differentiation of Eq. (5), and using Eq. (6),

$$-dI/I = \tfrac{1}{2}[b/kT)(E/\varepsilon_r)^{1/2}-1]d\varepsilon_r/\varepsilon_r \quad \ldots (7)$$

which at a fixed field and temperature again reduces to Eq. (4).

Naphthalene magneto-electrets develop positive isocharge[2]. This means that in contact with the metal (tin) this material loses some electrons to the metal at elevated temperatures. This loss of conduction electrons reduces its conductivity on subsequent measurement at room temperature. A fraction of electrons, while migrating to the metal at an elevated temperature might get trapped-in at the grain boundaries during cooling in presence of a magnetic field. It seems that a magnetic field somehow induces the electrons to go to the traps[6], the process which is responsible for magneto-electret state.

The localized (trapped) electrons cannot go back to the conduction band at room temperature. They will be loosely bound to the polycrystalline structure giving rise to interfacial polarizability. The samples are, therefore, expected to exhibit an increase in the dielectric constant at low ac fields due to this

additional polarizability acquired by the material. This explains the increase in dielectric constant.

The authors are thankful to the Principal, Maulana Azad College of Technology, Bhopal, for providing necessary facilities. One of the authors (AKB) is thankful to the University Grants Commission, New Delhi, for awarding him a Teacher Research Fellowship. He is also thankful to Government of Madhya Pradesh for sponsoring him to avail of the opportunity.

References

1 Bhatnagar A K, Quamara J K & Bhatnagar C S, *Indian J Pure & Appl Phys*, **21** (1983), in press.

2 Agrawal B M, *Studies of magnetic field polarization on naphthalene*, Ph D thesis, Bhopal University, Bhopal, 1976.

3 Verma D & Bhatnagar C S, *Indian J Pure & Appl Phys*, **14** (1976) 93.

4 Gupta H M & Von Overstraeten R J, *J Appl Phys (USA)*, **47** (1976) 1003.

5 Peter L Young, *J Appl Phys (USA)*, **47** (1976) 235.

6 Agrawal B M & Bhatnagar C S, *Indian J Pure & Appl Phys*, **16** (1978) 50.

Indian Journal of Pure & Applied Physics
Vol. 21, June 1983, pp. 368-369

Electroluminescence in Cu-Phthalocyanine

ANITA DAS & A K TRIPATHI*†

Solid State Physics Laboratories, Department of Physics, Saugar University, Sagar

Received 22 *April* 1982; *revised received* 24 *December* 1982

Voltage and frequency dependence of electroluminescent brightness have been studied for Cu-phthalocyanine at room temperature. The brightness varies according to the relation $B = B_0 \exp(-C/V^{1/2})$ in the low-voltage region and according to $B = B_0 \exp(-C/V)$ in the high-voltage region.

The study of electroluminescence (EL) in organic materials has gained attention only in recent years[1]. Although EL in these materials is similar to those in inorganic materials, the fields necessary are much higher, the mean acceleration paths are much smaller and correspond to molecular size in such materials[2]. Helberger[3] observed the luminescence of magnesium and zinc phthalocyanine in boiling tetraline containing small amounts of benzyl peroxide, hydrogen peroxide or air. The present work is a study of dependence of the EL brightness on the voltage (V) and the frequency of the applied electric field in Cu-phthalocyanine.

Cu-phthalocyanine for the present study was obtained from Schecuardt Munchen Nurfur Laborgeb-rach, Germany. For the preparation of EL cell, the sample in the form of a thick film (200 μm) was fastened to a 100 μm thick mica sheet using araldite as binder. This sheet was sandwiched between a conducting glass plate (resistance 150 ohms/cm) and a tin plate in such a way that the mica sheet was adjacent to the metal electrode[4]. EL excitations were done by sinusoidal voltages from the output of a wide band amplifier (0-1000 V) fed by an audio oscillator (30 Hz-30 kHz). The integrated light emission from the EL cell was measured employing a RCA IP21 photomultiplier tube coupled to a Rubicon galvanometer.

The brightness B versus voltage V curves have essentially the exponential form (Fig. 1). This may be confirmed by curves, representing the logarithm of brightness as an inverse function of $V^{1/2}$ (Fig. 2). The curves were found to be almost linear in the low-voltage region while they show a little deviation from linearity in the high-voltage region. The frequency dependence of EL brightness is shown in Fig. 3.

The brightness is found to be an increasing function of the exciting voltage which can be understood on the basis that initially the number of particles in which EL takes place is small, but on increasing the voltage, more and more active regions are exposed to voltage gradient above the threshold level. It is evident from the linearity of the plot of the mean EL brightness (B) with $1/V^{1/2}$ that the relation between B and V is of the form:

$B = B_0 \exp(-C/V^{1/2})$, where B_0 and C are constants.

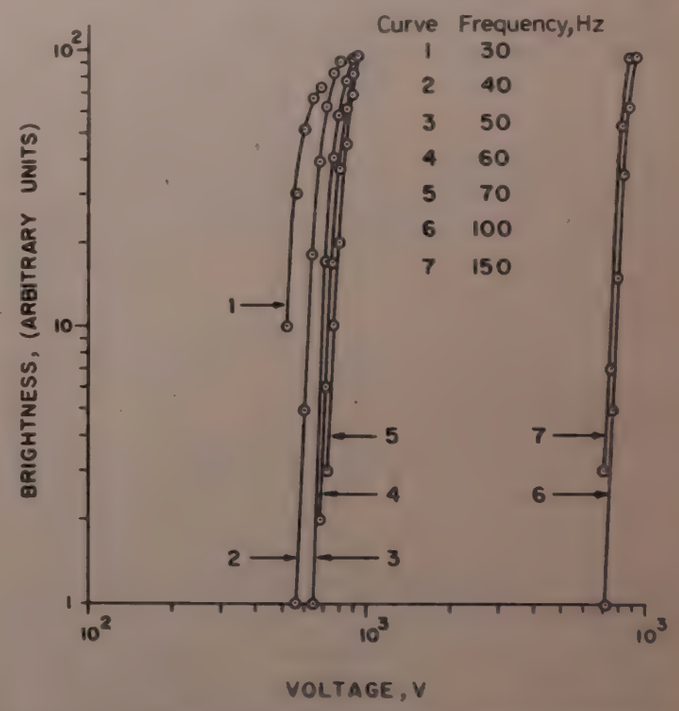

Fig. 1—Log brightness versus log voltage at fixed frequencies (The scale has been shifted for higher frequencies)

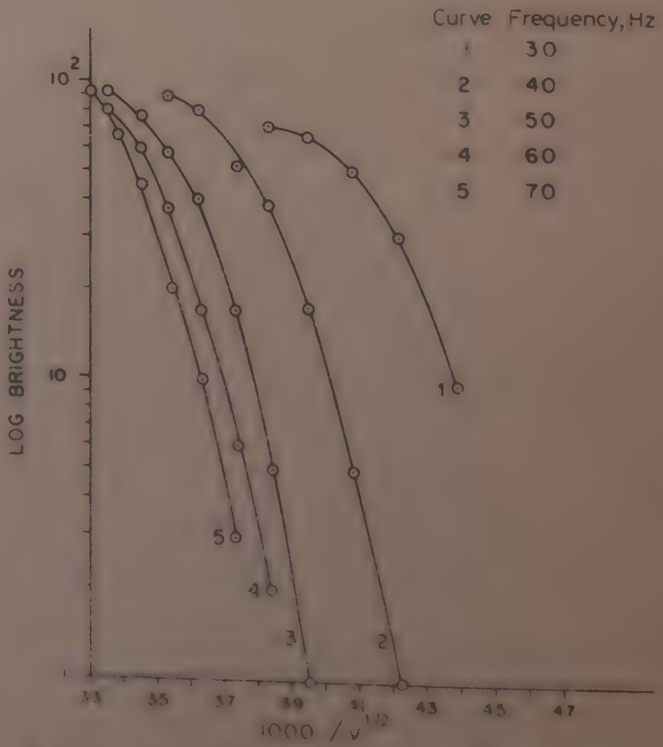

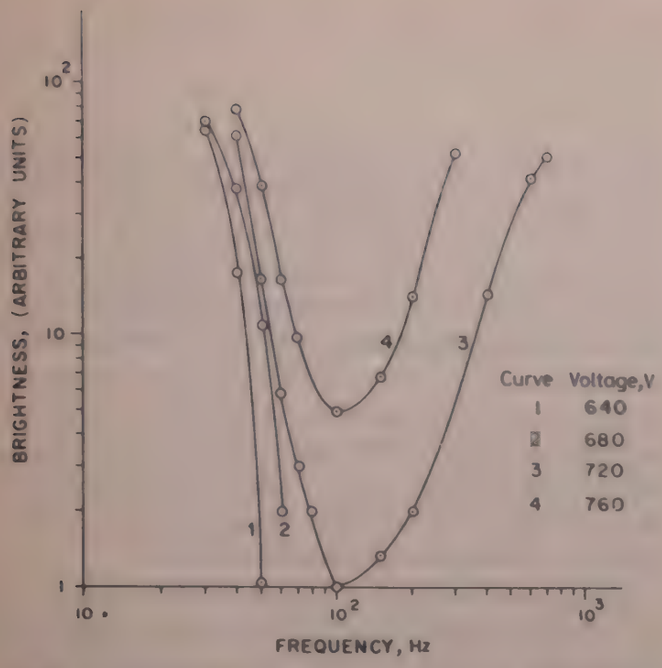

Fig. 3—Log brightness versus log frequency at fixed voltages

This can be considered as a proof for the validity of the exhaustion barrier theory[5] in the present system. It means that for small voltages, the field is not sufficient to produce EL except in the surface barrier, while at high voltages the luminescence emission can occur from the whole of the crystal. According to Thornton[6], for a usual EL cell the relation having the term exp $(-C/V)$ is applicable at high voltages. In the present case also, a slight deviation from linearity is found at higher voltages which may be because of variation of the type exp$(-C/V)$. The increase of EL brightness due to increasing frequency above ~ 100 Hz is obvious because of the more rapid emptying and refilling of luminescent centres[7]. But when the time period of the applied ac field becomes comparable with the lifetime of the excited electron, the electron does not have enough time to emerge out from the traps; hence saturation can be expected in the high frequency range which has been experimentally observed. The decreasing nature of brightness at about 100 Hz can be understood on the basis of carrier injection and polarization effects[8].

References

1 Many A, Burshtein Z, Gonzales Basurto J & Levinson J, in the *conference on Electret and dielectrics* held at Sao Carlos, Brazil, 1975 (Academia Brasileira de Ciencias, Rio de Janeiro, RJ), 1977.

2 Bernanose A, *Br J Appl Phys (GB)*, Suppl. No. 4 (1956) 554.

3 Helberger J G, *Naturwissenschaften (Germany)*, **26** (1938) 316.

4 Curie D, *Luminescence in crystals*, translated by G F J Garlick (Methuen, London), 1963, 238.

5 Piper W W & Williams F E, *Br J Appl Phys (GB)*, Suppl No. 4 (1956) 539.

6 Thornton W A, *Phys Rev (USA)*, **102** (1956) 38.

7 Ivey H F, *J Electrochem Soc (USA)*, **104** (1957) 740.

8 Williams D F & Schadt M, *J Chem Phys (USA)*, **53** (1970) 3480.

Indian Journal of Pure & Applied Physics
Vol. 21, June 1983, pp. 370-373

Efficiency of Binderless Electroluminescence in (ZnS,ZnO): Cu,Cl Electroluminor

SHASHI BHUSHAN*
Department of Physics, Ravishankar University, Raipur 492010

Received 24 *July* 1982; *revised received* 10 *February* 1983

Efficiency of binderless electroluminescence (EL) as a function of voltage of the applied field is investigated. It is found that efficiency first increases, passes through a maximum and then decreases. A new interpretation of binderless EL in terms of Schottky-emission type of transport process is proposed.

Electroluminescence (EL) has been investigated in two ways[1]: (i) by studying the luminescence characteristics, and (ii) by electrical measurements. The first approach has been attempted by many workers and it has served as the basis for the mechanism of EL developed by Georgobiani and Fok[2]. The second approach is concerned with the measurement of absorption of energy of external excitation by the phosphor crystal; the efficiency of the crystal is defined as the ratio of light output to the power absorbed by it.

In intrinsic EL the phosphor is embedded in some dielectric and then pressed between two conducting plates one of which should be transparent. However, Bhushan[3] has shown that if the electroluminor (ZnS,ZnO):Cu,Cl is treated with salt solution of $CuSO_4$ or Na_2SiO_3, EL can be observed just by pressing between two conducting plates (i.e. without the use of a binder or dielectric). Such a process is known as binderless EL. In the present note, efficiency of binderless EL has been investigated as a function of applied voltage for (ZnS,ZnO):Cu,Cl electroluminor, from the ratio of light output to the power absorbed. A new interpretation of binderless EL in terms of Schottky-emission type of transport process has been proposed.

The electroluminor was prepared by firing a mixture of 10 g ZnS (luminescent grade), 2 g ZnO (luminescent grade), 0.093 g $CuSO_4$, 0.058 g NH_4Cl and 0.2 g sulphur (all the three AR grade) at 1000°C for 2.5 hr. An extra amount of sulphur was poured on the upper part of the vessel which was then completely closed. The fired content was washed with 20% acetic acid (to remove excess ZnO) and distilled water, dried and washed again with 4% NaCN (to removeexcess Cu) and dried. The electroluminor thus prepared was treated with salt solution of Na_2SiO_3 or $CuSO_4$ and then dried at about 120°C.

The EL cell was prepared by pressing the treated electroluminor between two conducting glass plates separated by 300 μm thick mica sheet having a circular hole of area 2 sq cm for the electroluminor. For EL, excitation source was a transformer (50 Hz, 3 kV). An RCA IP 21 photomultiplier (PM) tube, operated by a regulated power supply at 1000 V was used to measure the light output. The light output in the form of current was measured by a polyflex galvanometer (10^{-8} A/cm). The current through the EL cell was measured by a Philips GM 6009 VTVM by noting the voltage developed across a resistance of 1 MΩ.

Fig. 1 shows the variation of log of EL brightness (B) as a function of the inverse square root of voltage (V) of the applied ac field at 50 Hz for the electroluminors treated with Na_2SiO_3 and $CuSO_4$. It is seen that except at lower voltages, the nature is well described by the relation $B = B_0 \exp(-b/V^{1/2})$, where B_0 and b are parameters which depend on temperature, frequency of the alternating voltage, the phosphor and the details of construction of the EL cell. Since in the present case the studies have been done at constant frequency and temperature and the same cell has been used for all the studies, these parameters can be taken as constant.

Fig. 2 shows the variation of current (I) through the EL cell measured by the VTVM under the excitation of ac field (50 Hz) as a function of applied voltage. From the straight line nature it is clear that $I \propto \exp(aV^{1/2})$, where a is some constant. The efficiency (ρ) of EL has

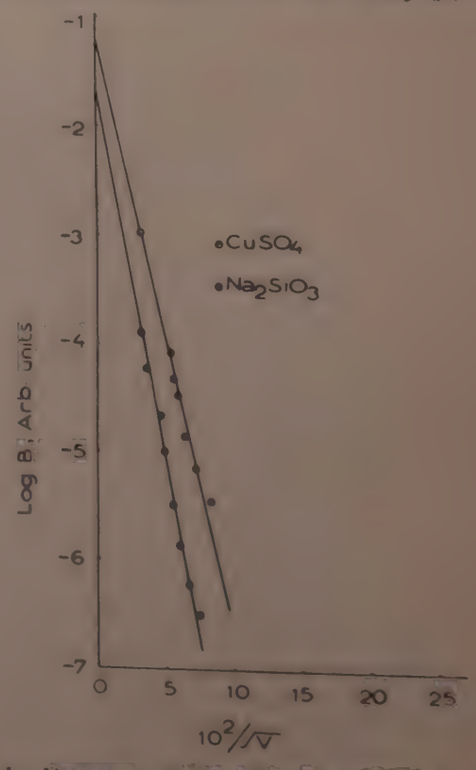

Fig. 1 Variation of log B with applied voltage ($V^{1/2}$)

been determined from the ratio of light output (expressed in arb. units) to the power input (expressed in watts) and plotted as a function of voltage (Fig. 3). With the increase in voltage the efficiency first increases and then, after passing through a maximum, decreases.

The variation of EL brightness according to the relation $B = B_0 \exp(-b/V^{1/2})$ indicates that the mechanism of excitation is of acceleration-collision type, and a barrier of Mott-Schottky type is formed in which the maximum field strength varies as $V^{1/2}$

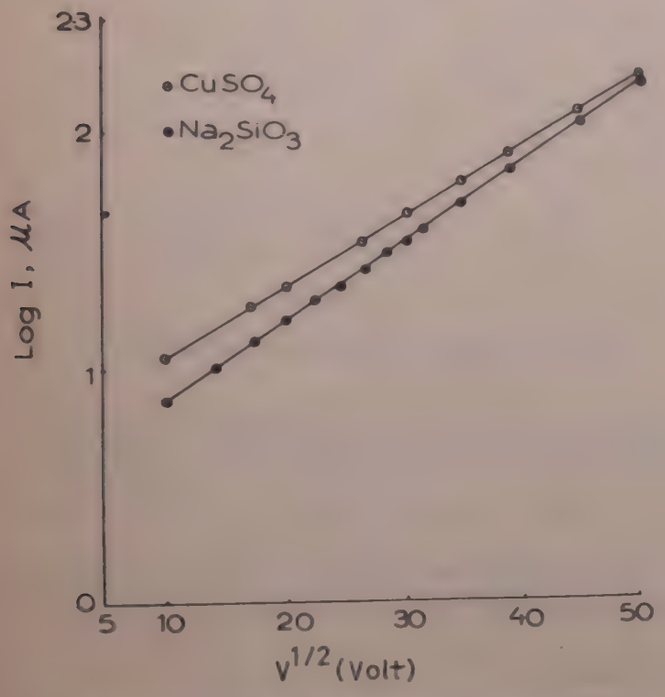

Fig. 2—Variation of log I with applied voltage ($V^{1/2}$)

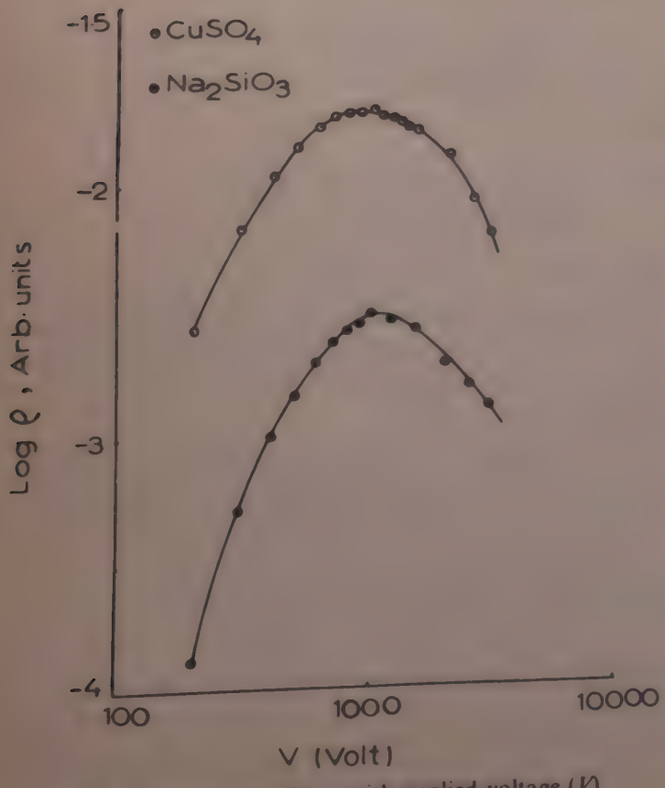

Fig. 3—Variation of log ρ with applied voltage (V)

(Ref. 4). According to this mechanism, electrons from donors or traps are first accelerated in the conduction band which then collide with the electrons in the luminescent centres which get excited and after return to the centres give rise to luminescent emission. The original electrons with their small amount of energy left move in the crystal and again during the next half of the ac cycle get ready for acceleration. Thus the higher the voltage of the applied field the higher is the light output; but for high voltages the power input increases faster than the light output[4] and hence the efficiency is maximum at some intermediate value of voltage.

According to Yu L'vova[1], the value of EL efficiency is governed by the relative roles of (i) number of electrons participating in EL, and (ii) the conditions which exist during their acceleration; factor (i) is the dominant factor. The absorption of energy is governed by the electrons liberated from the luminescent centres and from the deeper traps. Thus by considering a kinetic of EL which consists of transport equations for a crystal phosphor with three levels, namely, luminescent centres, shallow electron traps and deeper donors, Yu L'vova has shown that EL efficiency (ρ) can be represented by the formula:

$$\rho(V) = \frac{\bar{B}}{\bar{W}} = \frac{1}{V^{3/2} \exp(b_1 V + b/V^{1/2})} \qquad \ldots (1)$$

where $\bar{W}$ represents the average power absorbed by a phosphor. In deriving this formula, it has been assumed that liberation of electrons from the local levels occurs by tunnel transitions assisted by thermal vibrations of the lattice; some of the constants which do not depend on V have been left. If the efficiency (ρ) is determined by the ratio $1/\bar{W}$ where the radiant energy 1 is proportional to the brightness $B = [B_0 \exp(-b/V^{1/2})]$, then $\bar{W} = V^{3/2} \exp(b_1 V + b/V^{1/2})$. Constant b is determined from the plot of log B versus $1/V^{1/2}$, and b_1 from the slope of the straight line from the plot of log $W/V^{3/2}$ versus V so as to fit the experimental results. By adopting this procedure, Yu L'vova has found that $\rho - V$ plot of ZnS:Cu is satisfactorily explained.

In the present case the $\log(W/V^{3/2})$ versus V plot (Fig. 4) shows a straight line and from the slope the values of b_1 for the two cases ($CuSO_4$ and Na_2SiO_3) are found to be 2.447×10^{-4} and 3.145×10^{-4} respectively. The constant b (also B_0) has been determined from log B versus $1/V^{1/2}$ plot and listed in Table 1 along with other constants. Substituting these constants in Eq. (1), ρ was evaluated as a function of V and compared with the experimental results, but it did not fit well.

Since the EL cell was prepared by pressing the samples directly between the conducting plates, a Schottky-type barrier can be assumed to be easily formed at the electrode-electroluminor contact. Thus if

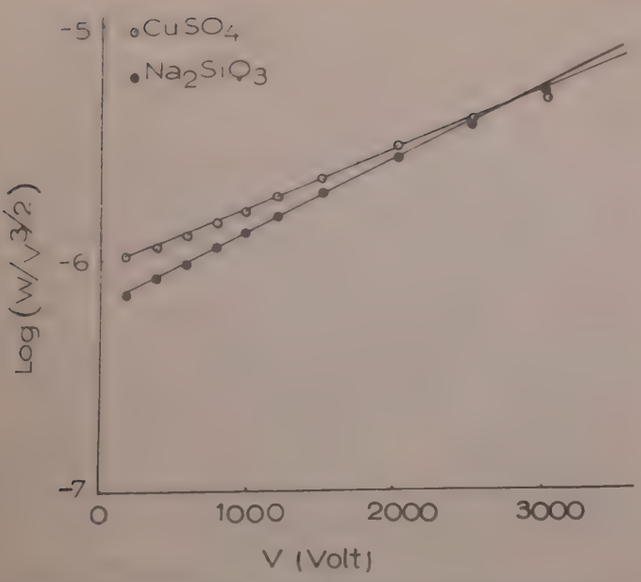

Fig. 4—Variation of $\log(W/V^{3/2})$ with applied voltage (V)

Table 1—Values of Different Constants

Treated with	$B_0 \times 10^2$ Arb. units	b $V^{-1/2}$	A μA	$a \times 10^2$ $A/V^{1/2}$
$CuSO_4$	6.4	124.368	5.4	7.302
Na_2SiO_3	2.0	158.304	3.3	7.992

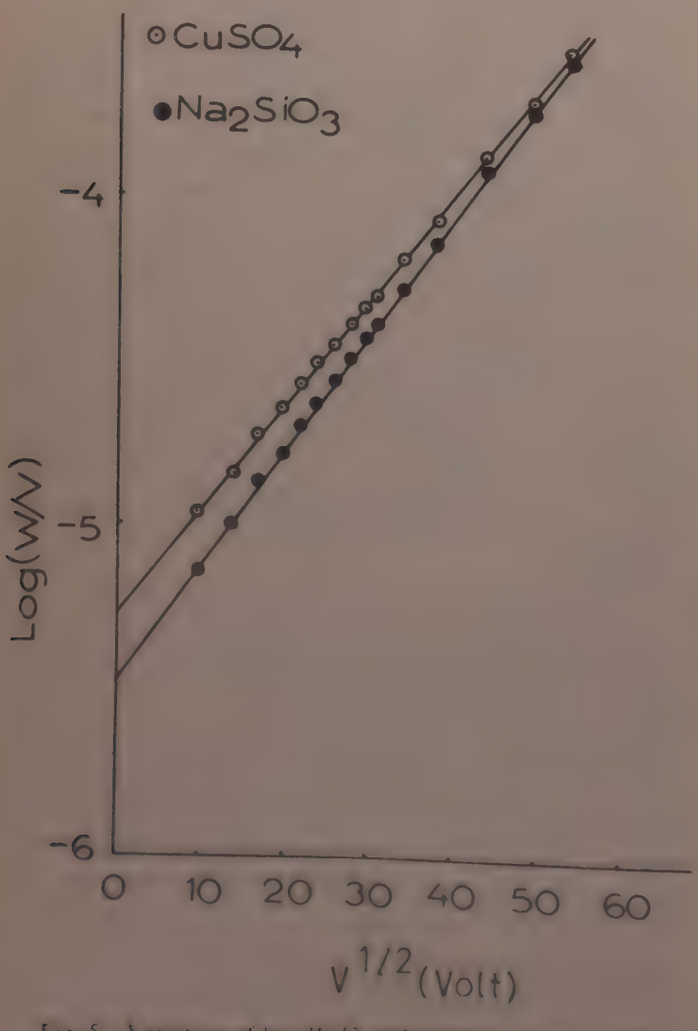

Fig. 5—Variation of $\log(W/V)$ with applied voltage ($V^{1/2}$)

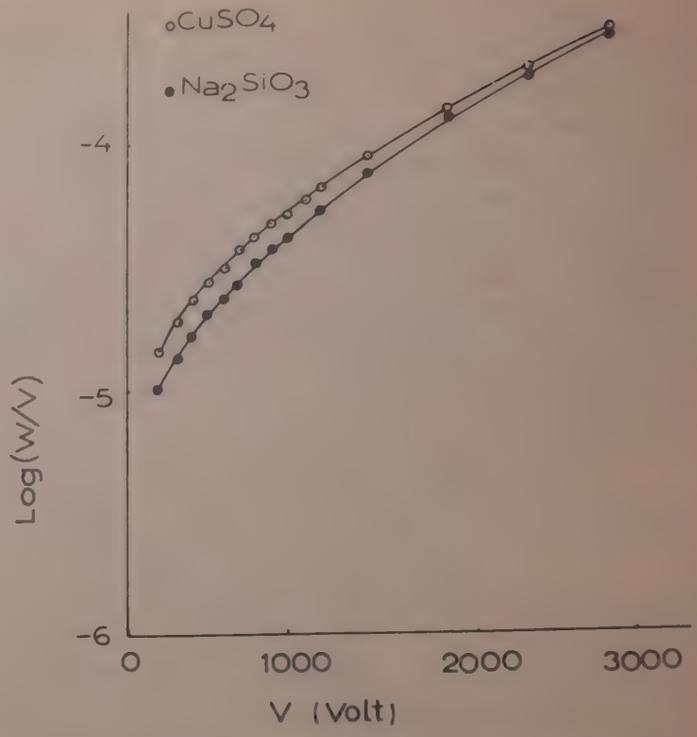

Fig. 6—Variation of $\log(W/V)$ with applied voltage (V)

it is assumed that the conduction process is of Schottky-emission type, the current is given by[5]:

$$I = T^2 [\exp(-C + DV^{1/2})/kT] \quad \ldots (2)$$

where C and D are constants. At a fixed temperature, this expression can be written as:

$$I = A \exp(aV^{1/2}) \quad \ldots (3)$$

where A and a are constants. Thus the efficiency ρ can be written as:

$$\rho = \frac{\overline{B}}{\overline{W}} = \frac{B_0 \exp(-b/V^{1/2})}{AV \exp(aV^{1/2})} \quad \ldots (4)$$

or

$$\log \rho = \log B_0 - \log A - \log V - 0.43 \times [(b/V^{1/2} + aV^{1/2})] \quad \ldots (5)$$

The values of all the constants occurring in this expression are listed in Table 1. The constants A and a are determined from the plot of $\log(W/V)$ versus $V^{1/2}$ (Fig. 5). These values gave quite a good fit to the experimental results.

The insulators have no free carriers to accelerate to produce EL emission. The high field required for EL emission in insulators must first generate the free carriers. The various processes by which they can be produced are: (i) Zener tunneling (electron tunneling from valence band to conduction band), (ii) by excitation from traps (Frenkel-Poole effect), and (iii) over the Schottky barrier at the cathode. Based on the nature of current through the EL cell on the applied voltage (I-V characteristics), it is proposed that the

third process is more effective in the binderless EL of (ZnS,ZnO):Cu,Cl. Eq. (5) has been found to be suitable for CaS system also[6].

Further, the $\log(W/V)$ versus V curve (Fig. 6) deviates from straightness at lower voltages which indicates that, at these voltages, shallow levels in this electroluminor participate in energy absorption[1]. The source of carriers may thus be taken as shallow traps or donors along with process (iii) as mentioned above.

The author is thankful to Prof. R K Thakur for valuable discussions.

References

1 Yu L'vova E, *Kinetics of the Destriau effect in electroluminescence*, edited by D V Skobel'tsyn (Consultants Bureau, New York), 1972, 9, 16, 21.

2 Georgobiani A N & Fok M V, *Opt & Spectrosc (USA)*, **5** (1958) 167; **9** (1960) 775; **10** (1961) 188; **11** (1961) 93.

3 Bhushan S, *Indian J Pure & Appl Phys*, **9** (1971) 1065.

4 Ivey H F, *Electroluminescence and related effects* (Academic Press, New York), 1963, 42, 61.

5 Pankove J I, *Electroluminescence* (Springer-Verlag, Berlin), 1977, 17.

6 Bhushan S & Chandra F S, *dc Electroluminescence in calcium sulphide phosphors*, unpublished work.

Indian Journal of Pure & Applied Physics
Vol. 21, June 1983, pp. 374-375

Electronic Spectra of Complexes of Neodymium (III) and Praseodymium (III) with Amino Acid

M P BHUTRA* & ANUP K GUPTA
Department of Physics, University of Jodhpur, Jodhpur

Received 11 *February* 1982; *accepted* 16 *April* 1983

The electronic spectra of complexes of praseodymium(III) and neodymium(III) with amino glycine, alanine and valine have been recorded in the 360-920 nm region in water. The energies and intensities of various transitions calculated using the Judd-Ofelt relation are in good agreement with those obtained experimentally.

The absorption spectra of complexed rare earth ions in the $f \leftrightarrow f$ transition region have been studied by various workers[1-7]. Other spectroscopic studies have yielded information regarding the structure and composition of the complexes[8-12]. In this note, we report the electronic spectra of neodymium(III) and praseodymium(III) complexes with glycine, alanine and valine.

Various intensity parameters such as the Judd-Ofelt parameter (T_λ), the bonding parameter ($b^{1/2}$), the energy parameters (F_2, F_4, F_6) and the covalency of the complexes have been calculated and discussed.

Experimental Details

The praseodymium(III) and neodymium(III) complexes were prepared by the method reported in literature[13]. The chemicals used were of AR grade and the metals were 99.9% pure (Indian Rare Earths Ltd). The complexes were synthesized with glycine, alanine and valine in molar ratio 1:1 and their formulas are

$[M(H_2NCH_2COO)8H_2O]Cl_2$,
$[M(NH_2CH_2CH_2COO).8H_2O]Cl_2$ and

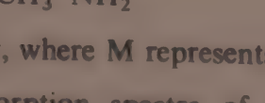

respectively, where M represents the metal.

The absorption spectra of the complexes were recorded on Carl-Zeiss VSU-2 Spectrophotometer in the 360-920 nm region in water solvent. The energies recorded in terms of wavelength were converted into wavenumber.

Results and Discussion

Energy level parameters—The energy levels of various transitions were obtained experimentally as well as theoretically by using the relation[12]

$$E_f(F_k, \xi_{4f}) = E_{0f}(F_k^0 \xi_{4f}^0) + \sum_{K=2,4,6} \left(\frac{\partial E}{\partial F_k}\right)\Delta F_k + \left(\frac{\partial E_j}{\partial \xi_{4f}}\right)\Delta \xi_{4f}$$

The results obtained for different complexes of Nd(III) and Pr(III) are collected in Table 1. The rms deviation found between experimental and theoretical values are small, supporting the validity of the relation used. The red shift of the energy levels from that of free ion in different solvents supports the complexation[14]. The hypersensitive transition in the Nd complexes ($^4I_{9/2} \rightarrow {}^4G_{5/2}$) shows a red shift when the ligands are changed in the order: alanine < glycine ≤ valine.

While in case of the Pr complexes for the associated pseudo-hypersensitive transition ($^3H_4 \rightarrow {}^3P_2$) we have no such trend due to assumption of 4*f*-wavefunctions to be hydrogenic. It is observed that there is not very much shifting in peak position when ligands are changed, which may be attributed to some participation of oxygen atom orbitals only with those of the metal at different distances. Thus, the amino acid coordinates through carboxylic oxygen only while nitrogen remains unaffected.

Table 1—Observed and Calculated Values of Energy (in wavenumbers) of Various Transitions in Nd and Pr Complexes

Complex*	NdG		NdA		NdV	
Levels	Exp.	Calc.	Exp.	Calc.	Exp.	Calc.
$^2P_{1/2}$	23419	23403	23474	23409	23364	23340
$^4G_{11/2}$	21739	21567	21834	21615	21786	21668
$^4G_{9/2}$	21186	21174	21368	21319	21164	21152
$^2G_{9/2}$	19608	19585	19608	19656	19608	19589
$^4G_{7/2}$	19231	19253	19231	19329	19231	19186
$^4G_{5/2}$	17391	17338	17322	17338	17391	17264
$^4F_{9/2}$	14684	14762	14706	14813	14684	14828
$^4F_{7/2}$	13369	13334	13387	13349	13405	13375
$^4F_{5/2}$	12422	12507	12453	12519	12407	12527
$^4F_{3/2}$	11481	11514	11521	11512	11494	11477
rms Dev.	±70.30		±95.33		±83.40	
	PrG		PrA		PrV	
	Exp.	Calc.	Exp.	Calc.	Exp.	Calc.
$^3P_2$	22624	22528	22573	22527	22573	22526
$^3P_1$	21413	21368	21413	21376	21413	21367
$^3P_0$	20790	20838	20790	20864	20790	20840
$^1D_2$	16978	17178	17007	17186	17007	17168
rms Dev.	±115.67		±101.28		±94.60	

* The last letter in the complexes designated as NdG, PrV etc. signifies A, alanine; G, glycine; V, valine.

Table 2—Observed and Calculated Values of Oscillator Strength for Various Transitions in NdA*, NdG* and NdV* Complexes

Complex*	NdA		NdG		NdV	
Levels	Exp.	Calc.	Exp.	Calc.	Exp.	Calc.
	$\times 10^{-6}$		$\times 10^{-6}$		$\times 10^{-6}$	
$^2P_{1/2}$	0.639	0.658	0.177	0.426	0075	0.430
$^4G_{11/2}$	0.876	0.198	0.163	0.179	0.315	0.152
$^4G_{9/2}$	0.765	1.567	0.174	1.287	0.144	1.138
$^2G_{9/2}$	0.744	0.389	0.556	0.336	0.276	0.291
$^4G_{7/2}$	3.387	3.364	2.567	2.749	2.481	2.461
$^4G_{5/2}$	12.731	12.485	11.576	12.011	9.740	10.010
$^4F_{9/2}$	0.450	0.472	0.208	0.476	0.181	0.382
$^4F_{7/2}$	3.932	4.099	4.111	4.344	3.154	3.413
$^4F_{5/2}$	5.471	5.368	4.940	4.941	4.084	4.134
$^4F_{3/2}$	2.163	2.356	1.790	1.710	1.333	1.624
rms Dev.	±0.3742		±0.3730		±0.3680	
	PrA		PrG		PrV	
	Exp.	Calc.	Exp.	Calc.	Exp.	Calc.
$^3P_2$	10.54	10.54	11.046	11.046	8.694	8.694
$^3P_1$	6.718	3.838	6.26	4.549	4.156	2.328
$^3P_0$	0.944	3.772	2.790	4.470	0.498	2.288
$^1D_2$	2.924	2.924	3.362	3.362	2.846	2.846
rms Dev.	±2.018		±1.198		±1.279	

Note regarding abbreviations A, G and V the same as in Table 1.

Intensity parameters—The experimental values of the oscillator strengths for the various transitions have been computed by using the relation:

$$P = 4.6 \times 10^{-9} \times \varepsilon_m \times \Delta\nu_{1/2}$$

where ε_m and $\Delta\nu_{1/2}$ are the molecular extinction coefficient and bandwidth for transition respectively.

Using the Judd-Ofelt relation in terms of T_λ parameters, we have

$$P_{calc.} = [U^{(2)}]^2 \nu_x T_2 + [U^{(4)}]^2 \nu_x T_4 + [U^{(6)}]^2 \nu_x T_6$$

and matrix elements $[U^{(\lambda)}]^2$ represented by Carnall *et al.*[15], we calculate the oscillator strength for the $f \leftrightarrow f$ transition (Table 2). The rms deviation between the observed and calculated values is very small. The parameters T_2, T_4 and T_6 obtained for the complexes are collected in Table 3. The parameter T_2 is sensitive to the environment but its negative value has no physical significance.

It is observed that the ratio of T_4/T_6 is almost constant for the same metal but is more when Nd is replaced by Pr. This supports the fact that the coordinating environment around the metal ions remains unaltered, as mentioned earlier.

Bonding parameter—The parameter $b^{1/2}$ which is a measure of the partial covalency in a metal-ligand bond can be calculated from the relation $b^{1/2} = [(1 - \beta)/2]^{1/2}$ and the results are given in Table 4. In case of Nd, $b^{1/2}$ is negative indicating that the complexes are ionic. The nephelauxetic ratio β together with F_2, F_4, F_6 for the Nd and Pr complexes are also shown in Table 4.

Table 3—Computed Values of Intensity Parameters T_λ (in cm^{-1}) for Nd^{3+} and Pr^{3+} Complexes

Complex	$T_\lambda \times 10^9$			$\frac{T_4}{T_6}$
	T_2	T_4	T_6	
NdA	0.438	0.7355	0.6469	1.137
NdG	0.524	0.4775	0.7163	0.6666
NdV	0.3995	0.4835	0.5505	0.8782
PrA	−4.057	1.05	3.165	0.332
PrG	2.63	1.2445	3.27	0.380
PrV	6.769	0.637	2.671	0.2385

Table 4—Computed Values of Bonding Parameter β (in cm^{-1}) $\beta^{1/2}$ and $b^{1/2}$ for Nd^{3+} and Pr^{3+} Complexes

Complex	F_2	F_4	F_6	β	$b^{1/2}$
Free ion	331.159	50.714	5.154	—	—
NdA	333.58	51.917	5.428	1.0073	—
NdG	336.285	50.717	5.494	1.015	—
NdV	336.927	48.317	5.500	1.0174	—
Free ion	322.09	44.46	4.87	—	—
PrA	311.40	42.98	4.70	0.9668	0.1288
PrG	311.33	42.98	4.70	0.9665	0.1290
PrV	311.40	42.98	4.70	0.9668	0.1288

One of us (AKG) thanks the University Grants Commission (India) for providing a fellowship. We also thank Prof A N Nigam and Dr S P Tandon of the Department for helpful discussions.

References

1 Misumi Siezo, Kida Sigeo, Isobe Toshiyuki & Inazumi Akio, *Bull Chem Soc (Japan)*, **41** (1968) 25.

2 Henrie D F & Choppin G R, *J Chem Phys (USA)*, **49** (1968) 477.

3 Tandon S P & Mehta P C, *J Chem Phys (USA)*, **52** (1970) 4313.

4 Karraker D G, *J Inorg & Nucl Chem (GB)*, **33** (1971) 3713.

5 Peacock R D, *Struct & Bonding (Germany)*, **22** (1975) 83.

6 Henrie D E, *Coord Chem Rev (Netherlands)*, **18** (1976) 199.

7 Yatsimirskii K B & Davidanko N D, *Coord Chem Rev (Netherlands)*, **27** (1979) 223.

8 Mehta P C, Surana S S L, Bhutra M P, *et al.*, *Spectrosc Lett (USA)*, **4** (1971) 181.

9 Vaishnava P P, Tandon S P & Bhutra M P, *Indian J Pure & Appl Phys*, **13** (1975) 494.

10 Vaishnava P P, Bhutra M P & Tandon S P, *Indian J Pure & Appl Phys*, **14** (1976) 329.

11 Judd B R, *Lanthanide and Actinide Chemistry and Spectroscopy*, ACS Symposium Series, Vol 131, edited by N M Edelstein (American Chemical Society, Washington), 1980, 267.

12 Joshi G K, Bhutra M P & Misra S N, *J Inorg & Nucl Chem (GB)*, **43** (1981) 527.

13 Misra S N, Joshi G K & Bhutra M P, *Indian J Chem Soc*, **21** (1982) 275.

14 Bhutra M P & Gupta A K, *Indian J Phys A*, **57** (1983) 58.

15 Carnall W T, Fields P R & Wybourne B G, *J Chem Phys (USA)*, **42** (1965) 3797.

Indian Journal of Pure & Applied Physics
Vol. 21, June 1983, pp. 376-378

Mössbauer Spectroscopic Analysis of Iron in Soils and Rocks in the Eastern Himalayan Foothill Region

S C DAS, S K SENGUPTA, N C PAUL,
N BHATTACHARYA, J B BASU & N CHAUDHURI*
Department of Physics, North Bengal University,
Darjeeling 734 430

Received 16 *August* 1982; *revised received* 13 *November* 1982

As a part of the study of iron-bearing minerals in the eastern Himalayan foothills, the ferrous-ferric ratio for a number of weathered samples in agricultural and forest-covered lands in the altitude range 100-2700 m has been estimated by the Mössbauer method. The results have been compared with similar such results for other countries with a view to indicating the trend of behaviour of iron in bulk and separated samples. The importance of these results in the field of geology and agriculture has been pointed out.

A study has been undertaken to investigate the iron content in rocks and minerals in the eastern Himalayan foothills. As a part of this eco-development programme, soil and rock samples from a number of localities have been analyzed for their iron content using Mössbauer spectroscopic method. The Mössbauer spectroscopic procedure enables the analysis to be made in a non-destructive way and is able to distinguish between the two important oxidation states of iron (Fe^{2+} and Fe^{3+}) that occur in the structure of soil and rock under natural weathering. Accurate estimates of Fe^{2+}/Fe^{3+} ratio are very important in the field of geology and agriculture. In geology, this ratio can be taken as indicative of the temperature and pressure of formation of minerals which constitute the various rocks. In agriculture, this ratio can be taken as a measure of the degree of iron deficiency and hence an index of applicability of fertilizers. The determination of this ratio from chemical analysis is subject to uncertainty due to difficulty in dissolving rock minerals and resulting possible oxidation. Consequently, the estimates from chemical method do not reflect the actual chemical states of iron in the minerals. The Mössbauer method, however, provides a rapid and accurate method for determining this ratio.

The weathered soil samples of A-horizon were collected in autumn of 1979 from localities in the range 22 N, 87 E to 27 N, 89 E at altitude levels in the range 100-2700 m. Each sample under field condition was first disaggregated and the fine fractions of sizes less than 300 μm were separated by sieving. An electromechanical transducer operated in the constant acceleration mode coupled to Nuclear Data 1100 Multichannel Analyzer was used with a 14.4 keV gamma-ray source (^{57}Co in palladium matrix and of 3.8 mCi strength). In all measurements, Mössbauer spectra of samples were taken at room temperature. Fe^{2+} and Fe^{3+} states were assigned to doublet components in the spectra using the procedure of other workers[1]. In the spectrum of CTRI sample (Fig. 1), the doublet AA′ is assigned to Fe^{2+} and the doublet CC′ to Fe^{3+}. Fig. 2 exhibits Mössbauer spectrum of BDTS sample showing only the doublet assigned to Fe^{3+}. The sample CTRI was obtained from a tobacco-field where the annual rainfall is about 400 cm. The sample BDTS was obtained from field under tea plantation where the annual rainfall is about 400 cm.

The Fe^{2+}/Fe^{3+} ratio in a sample has been determined from the area ratio in the following way. If a thin absorber sample contains iron atoms in two different chemical states which give well-resolved Mössbauer spectra of area A_1 and A_2, then $A_1/A_2 = n_1/n_2$, where n_1 and n_2 are the total number of iron atoms of the first and second types respectively. This is true when the full width at half maximum of the Mössbauer lines corresponding to two types of iron and their recoil-free fractions are equal in a very thin

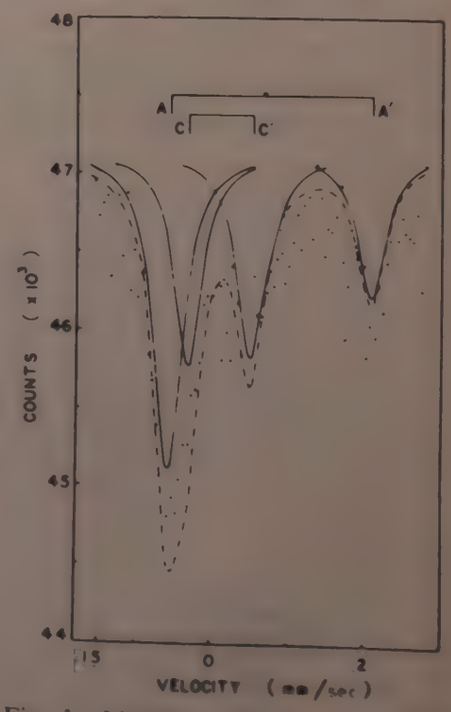

Fig. 1—Mössbauer spectrum of CTRI (Points represent experimental observations, the solid line gives the curve obtained by fitting the experimental points and the dashed curve gives the total envelope of the fitted curves)

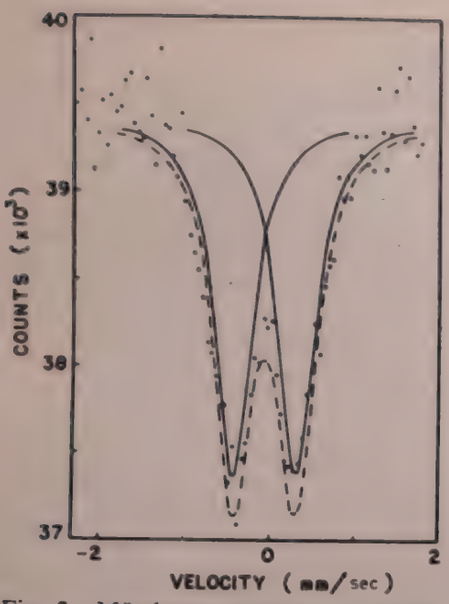

Fig. 2—Mössbauer spectrum of BDTS (Points, solid and dashed curves mean the same as in Fig. 1)

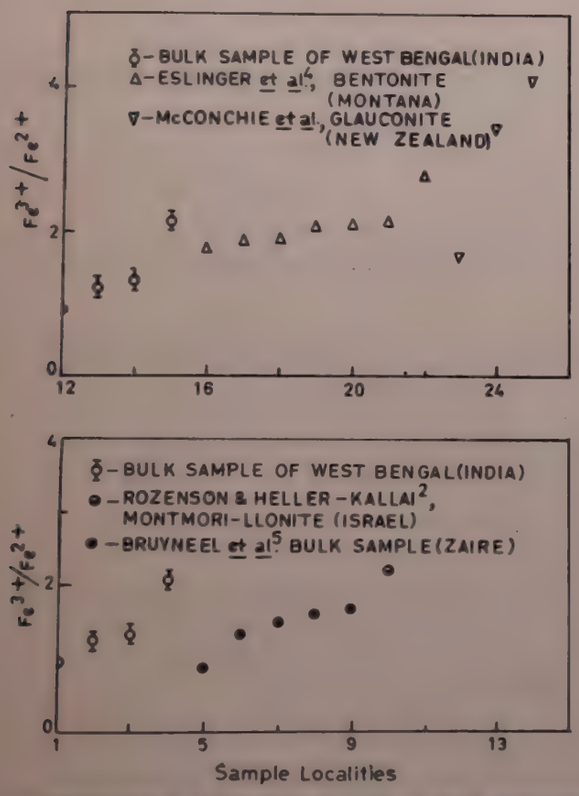

Fig. 3—Comparison of ferric-ferrous ratio of bulk samples and separated rock minerals from different sources [Numbers on the abscissas indicate sample localities)

sample at a given temperature. The results obtained from the present study are presented in Fig. 3. In Table 1, comparison has been made with similar such results of measurements carried out in other countries. The present data have been analyzed along the lines similar to those used by Bancroft[1], Rozenson and Heller-Kallai[2], McConchie *et al.*[3], Eslinger *et al.*[4] The ferric to ferrous ratios for the samples in Zaire, reported by Bruyneel *et al.*[5], are consistent with the results of present measurements, and these

Table 1—Fe^{3+}/Fe^{2+} Ratios for Different Samples

Sample No.	Country	Fe^{3+}/Fe^{2+}	Reference
907	India	0.9345	Present work
908	do	1.3157	do
909	do	1.2610	do
910	do	2.1413	do
911	Zaire	1.6393	Bruyneel *et al.*[5]
1027	do	0.8547	do
2220	do	1.3333	do
2320	do	1.6666	do
2514	do	1.4925	do
912	Israel	2.2222	Rozenson and Heller-Kallai[2]

Table 2—Mössbauer Data for Different Samples

(Mössbauer spectra did not show ferrous doublets)

Sample No.	Country	Fe^{3+}		Fe^{2+}/Fe^{3+}	Reference
		IS*	QS†		
S_5	India	0.57	0.71	0.0	Present work
S_1	do	0.52	0.79	0.0	do
B_5	do	0.53	0.72	0.0	do
BDTS	do	0.40	0.73	0.0	do
C_1	do	0.57	0.65	0.0	do
M_1	do	0.64	0.56	0.0	do
M_2	do	0.61	0.47	0.0	do
T_1	do	0.68	0.71	0.0	do
LT-42	Montana	0.36	0.69	0.0	Eslinger *et al.*[4]
LT-139A	do	0.35	0.59	0.0	do
LTE-1	do	0.37	1.09	0.0	do
Lt-1	do	0.35	0.60	0.0	do

*IS, Isomer shift (in mm/sec) with respect to sodium nitroprusside
†QS, Quadrupole splitting (in mm/sec)

together with the results in respect of montmorillonite samples from Israel indicate a trend of behaviour of ferric-ferrous ratio in earth-surface samples in these localities under natural weathering processes. Such a trend of this ratio may be taken as showing the degree of natural weathering of rocks and minerals in these areas. The results are also useful as an index of availability of ferrous iron as micronutrient for plant growth and productivity. This factor is important because many of the samples analyzed and shown in Table 2 contain iron in the ferric state only. It is known that the iron in the ferric form in agricultural soil does not serve as micronutrient for plants. The present results for samples with iron in ferric form are also consistent with those of Eslinger *et al.*[4] and can be taken as an indication of the degree of necessity of suitable fertilizers in agricultural and forest soils.

The authors wish to thank the University of North Bengal for providing a Junior Research Fellowship to

one of us (SCD) and UGC Teacher Fellowships to four of us (SKS, NCP, NB and JBB). They are also thankful to the Bhabha Atomic Research Centre, Trombay, Bombay, for assistance.

References

1 Bancroft G M, *Mössbauer spectroscopy—An introduction for inorganic chemists and geochemists* (McGraw-Hill, New York), 1973.

2 Rozenson I & Heller-Kallai L, *Clays Clay Miner (GB)*, **26**(2) (1978) 88.

3 McConchie D M, Ward J B, McCann V H & Lewis D W, *Clays Clay Miner (GB)*, **27**(5) (1979) 339.

4 Eslinger E, Highsmith P, Albers D & De Mayo B, *Clays Clay Miner (GB)*, **27**(5) (1979) 327.

5 Bruyneel W, Pollak H & Tack L, *Int J Appl Radiat & Isot (GB)*, **31**(10) (1980) 639.

Indian Journal of Pure & Applied Physics
Vol. 21, June 1983, pp. 379-380

A Data Processor Interface to Multichannel Analyzer

J N JOSHI, REKHA GOVIL*† & S K KATARIA
Nuclear Physics Division, Bhabha Atomic Research Centre, Trombay, Bombay 400 085

Received 2 *September* 1982

A data processor interface for the indigenous hardwired 4 K MCA has been developed. The system consists of Micro-2200 programmable calculator with its peripherals, micro data interface and a floppy disk drive. The data interface is designed for the transfer of data from MCA to Micro and reverse transfer. The hardware of the GET DATA and INV GET DATA functions is briefly described in the present work. The necessary software for programmed transfer of data and for algorithms on statistical analysis of spectra has been developed for the system. The system can be conveniently used to analyze standard nuclear γ-ray and X-ray spectra.

Multichannel analyzers (MCA) have been extensively used in experimental investigations since early sixties. With the semiconductor technology, their memory capacity has increased to 4K-8K channels. The use of microprocessors in the MCA has made such features of data acquisition and on-line data processing possible, which would be impractical to implement in hardwired MCA.

In this note, we briefly describe a data processing extension to the hardwired 4K channel MCA designed by the Computer Section, Bhabha Atomic Research Centre. The data processor consists of a programmable calculator‡ Micro-2200, its peripherals; micro data interface (MDI), floppy disk attachment, magnetic card reader (MCR) and X-Y recorder‡ and a data interface specially designed for the transfer of data from MCA to Micro-2200 and the reverse transfer. For the usual nuclear or X-ray spectroscopy experiments, useful data processing can be accomplished while other spectra are accumulating. Spectrum analysis algorithms-integration, peak search, net area and FWHM calculation, energy calibration, transfer of spectra, etc. can be easily carried out on the system. With floppy disk attachment the mass storage of spectra is also possible.

HARDWARE

A block diagram of the complete system is shown in Fig. 1. Micro-2200 communicates with external devices through MDI. A maximum of four devices can be simultaneously interfaced to MDI, with interrupt facility. The hardware of the data interface connecting MCA to Micro consists of two parts (i) GET DATA, to read the region of interest from MCA to Micro (ii) INV GET DATA, to send data from Micro to MCA sequentially.

GET DATA interface—Fig. 2 shows the block diagram of the interface. The transfer is done by pressing the DATA key on the keyboard of Micro. On the execution of this key function, Micro reads data up to a maximum of 9 digits in steps of two digits at a time. The five lower significant digits are used for the channel contents and the next three digits for the channel address.

When the DATA key is pressed, Micro generates SEND, DEVICE STROBE and ACKNOWLEDGE signals. Region of interest (ROI) signal from MCA is also used in Data Interface. A complete description of the signals available from MDI and their waveforms is given in the HCL manual on MDI and the circuit diagram shows the link of MDI and data interface.

Since Micro accepts 2 BCD digits, i.e. 8 bits at a time, and the data to be fed from MCA to Micro is 32 bits (8 digits), multiplexer chips of type 74153 are used for this purpose (Fig. 2). By pressing DATA key, transfer of one channel number and its content is done. Micro can be programmed to give the transfer of a number of ROIs registered on MCA to Micro.

INV GET DATA Interface—The control logic of the hardware of the interface is similar to the logic used in GET DATA function. To get data on MCA, MDI accepts two digits at a time from Micro and with the signals TAKE, DEVICE STROBE, ACKNOWLEDGE and DEVICE NO, sends them to the interface. The two-digits input from Micro is stored in latches to produce 32 bits output. With the help of latches 7475 and four demultiplexer chips of type

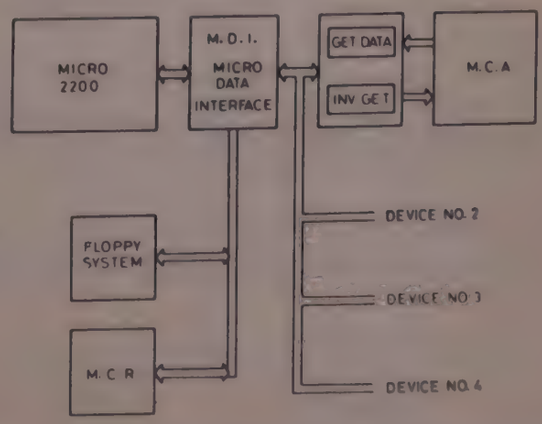

Fig. 1—General block diagram of the data processing system

† Present Address: Atomic Minerals Division, Department of Atomic Energy, West Block No. 7, R K Puram, New Delhi 110066.

‡ Micro-2200 and its peripherals are products of the Hindustan Computers Ltd, New Delhi.

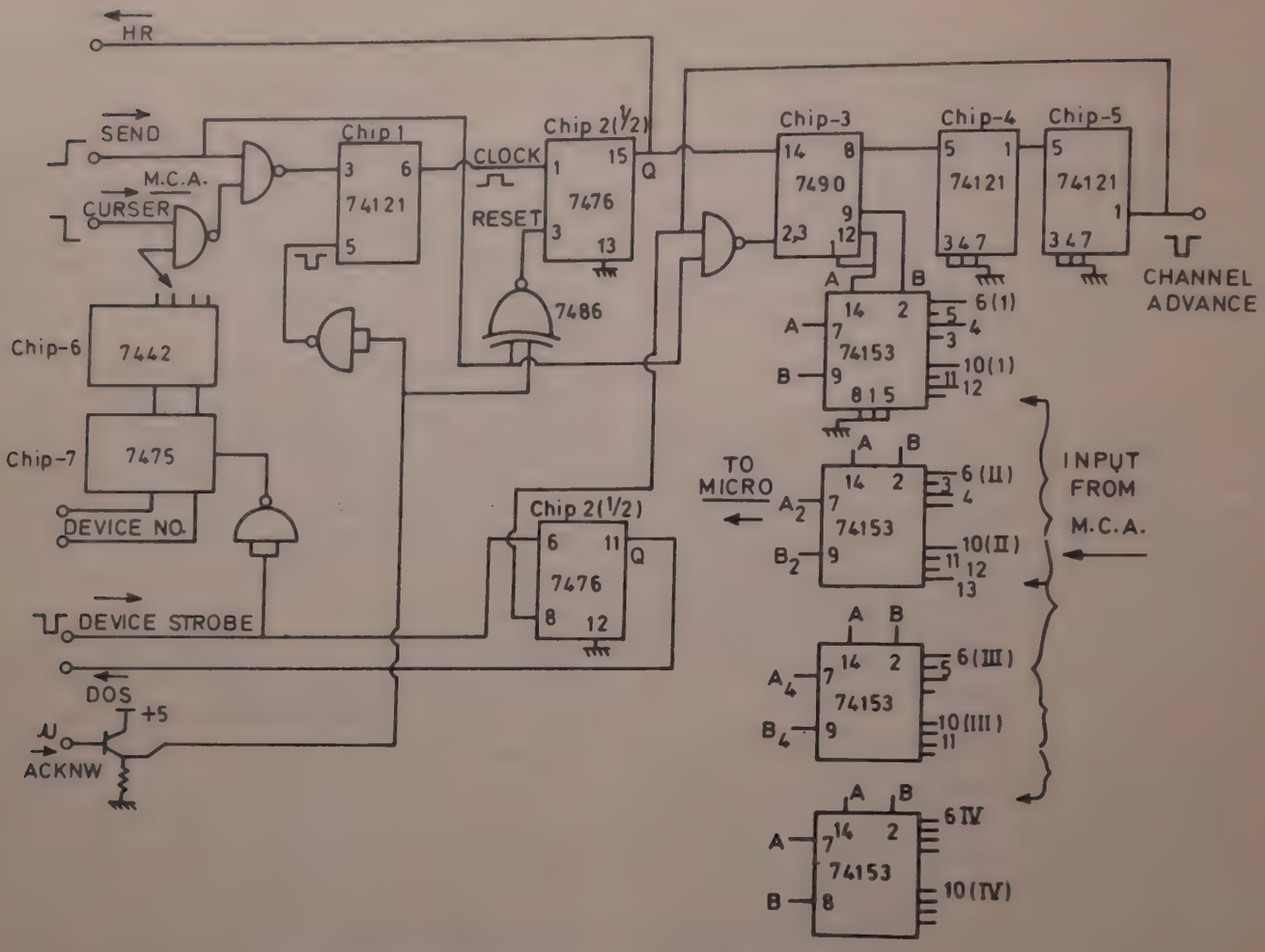

Fig. 2—Block diagram of the GET DATA Interface

74155, a 20 bits output, containing the lower significant 5 digits of Micro register representing the channel contents, is stored on MCA. The channel increment for reverse transfer is sequential.

SOFTWARE

A software package of a number of programmes has been developed on Micro-2200 and is stored on floppy. A brief description of these programmes and subroutines is as follows:

Transfer routines: This is the main programme for the programmed transfer of data from MCA to Micro-2200 and vice versa, with the GET DATA and INV GET DATA keys on the keyboard of Micro. The programme also includes storage of the spectrum on the floppy disk.

Spectrum smoothing: Smoothes the spectrum stored on floppy disk using either three-point or five-point smoothing functions, and stores it back on the disk.

Peak search: Finds the peak start, peak channel and peak stop in a spectrum of MCA or on floppy.

Peak analysis: The peak regions of interest ROI are selected on MCA using the thumbwheel switches on the control panel of MCA.

The programme does peak integration, background calculation by linear interpolation between the extreme channels, peak net area, FWHM and % error in area determination for each ROI and prints the results.

Other programmes are developed for specific use to analyze dispersive X-ray fluorescence spectra.

A complete listing of the programmes and the detailed circuit diagrams for the interfaces are available from the authors on requiest.

We would like to express our thanks to Shri J D Gupta, Sudhir Jain, C G Chatur, B P Dube and G S Lodha for their help in designing the interface. We also thank Dr N S Satya Murthy, Dr S S Kapoor, Dr V S Ramamurthy and Shri Virendra Singh for their guidance and help on various aspects during the development of the system.

Indian Journal of Pure & Applied Physics
Vol. 21, June 1983, pp. 381-382

On Uranium Concentration in Water

B C TALUKDAR†, P K CHOWDHARY‡ & K M PATHAK*†
Gauhati University, Gauhati 781 014

Received 31 *July* 1982; *revised received* 20 *October* 1982

Uranium concentration in water collected from several parts of Assam, India are determined in clear and stirred conditions by the fission track method. In the clear condition U-concentrations are found to vary from $(0.08 \pm .002)$ to $(5.32 \pm .02)$ μg/l. It is observed that the U-concentration increases in the stirred condition. The results are compared with the global background.

Uranium is the heaviest trace element occurring in nature in almost all minerals, rocks, water, etc. It is, therefore desirable to have a knowledge about concentration of uranium in natural samples like water from various sources. Such a study may be useful in throwing new light on the environmental physics of a region and for health physics as well. Uranium concentration which varies from ppb to ppm level can be measured by different methods, the latest being the charged particle track analysis first suggested by Price and Walker in 1963. The advent of the inexpensive and simple solid state track detectors[1] makes possible high sensitivity measurement of mineral concentrations of fissionable impurities or of α-emitters. In our present experiment, uranium in water collected from different parts of the state of Assam, namely Gauhati, Barpeta and Mangaldai sub-division, was measured by using solid state nuclear track detectors.

The water samples from different sources were collected in plastic pots which were first washed with boiling 25% HNO_3 acid. From each sample, subsamples were taken by micro-pipette with and without stirring the original samples. In order to maintain the amount of stirring for various samples at the same level an ultrasonic vibrator was used.

A known volume of water (0.05 ml) using micropipette, rinsed with distilled water and then test water, was placed on a clean circular disc of lexan detector. The water droplet was allowed to evaporate in still air placed inside an oven (at $\sim 70°C$). As shown in Fig. 1, this droplet would leave a thin layer of nonvolatile constituents including uranium. Ordinarily, water droplets would evaporate from the surface of the lexan detector in the manner shown in Fig. 1.

The diameter of the droplet remained same during the time of evaporation. Then the lexan was covered with another piece of lexan detector. The lexan detectors along with a standard glass of known uranium concentration serving as flux dosimeter were exposed to thermal neutrons at the CIRUS reactor, Trombay.

After irradiation, the detectors were separated and washed. The lexan detectors were etched with 6N, NaOH solution at 70°C for 14 min and then were dried up in air. Thereafter the entire surface area of the droplets on the detectors was scanned. In order to find the thermal neutron dose for these samples, the irradiated standard glass was freshly cut and etched in 20% HF at 20°C for 15 sec and then tracks were counted under a high-power optical microscope.

The general formula for uranium concentration (C_w) in units of weight/volume of liquid is given by[2]

$$C_w = \frac{Nm}{VGN_0\sigma E\varphi}$$

where N is the total number of tracks counted on the lexan; V, the volume of the liquid drop; m, the atomic weight of uranium; σ, the reaction cross-section of ^{238}U; φ, the total neutron dose and N_0, the Avogadro number.

G is a geometrical factor that accounts for the number of charged particles produced per neutron capture and the fraction of those that register in the track detecting material. Here the value of G is 1 since 2 fission fragments are produced per reaction and half of these reach each detector plate if the uranium deposit is thin.

The factor $E = 1 - (V_a/V_T)^2$ is the etching efficiency where V_a/V_T is the etching ratio defined as the linear rate of dissolution of the detector divided by the rate of dissolution along the damage track itself. In the present case, as the factor E is close to unity, the dependence of C_w on E may be neglected.

The uranium contents of clear and stirred water samples are given in Table 1. The difference of the uranium content in the clear and the stirred conditions was deemed to have arisen due to the suspended particles which might have settled down under clear

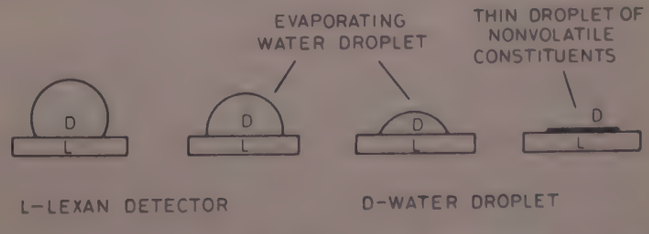

Fig. 1—Diagram showing the stages of evaporation of water droplets from the surface of the lexan detector

† Department of Physics
‡ Department of Geology

Table 1—Suspended and Dissolved Uranium in Water

Sample	Clear sample		Stirred sample		Difference†
	No. of tracks	U-conc. μg/l	No. of tracks	U-conc. μg/l	μg/l
M–I	13315	0.70±.006	15777*	0.83±.007	0.13
–II	3445*	0.18±.003	3873	0.20±.003	0.02
–III	3027*	0.16±.003	3226	0.17±.003	0.01
–IV	3655	0.19±.003	—	—	—
–V	6789	0.36±.004	13330	0.70±.006	0.34
–VI	1562*	0.08±.002	—	—	—
B–VII	101798*	5.32±.02	126999*	6.64±.02	1.32
–VIII	1519*	0.08±.002	1123	0.06±.002	−0.02
–IX	15967	0.84±.007	40690	2.13±.01	1.29
–X	16947	0.89±.007	40133	2.10±.01	1.21
–XI	27785	1.45±.008	78234*	4.09±.02	2.64
–XII	40421	2.11±.01	—	—	—
G–XIII	2977	0.16±.003	—	—	—
–XIV	6668	0.35±.004	—	—	—
–XV	3271	0.17±.003	—	—	—
–XVI	2064	0.11±.002	—	—	—
–XVII	6704	0.35±.004	—	—	—

*Associated with fission stars
†Suspended uranium in particulate matter

condition. The uranium contents are given with one standard deviation derived from the number of tracks counted. In all but one case (B-VIII), the uranium content in stirred condition is found to be higher than that in clear condition. This observation (B-VIII) is perhaps due to the fact that the sample contains fission stars (due to particle in suspension) only in the clear state.

The measurement of uranium content of water by the methods other than this method is (generally) complicated due to the presence of variable mass of suspended uranium-bearing particles in water. But the fission track method described here makes the measurement simple and less expensive.

Applying fission track method, Fleischer and Lovett[2] determined the U-content of city water from the Pasadena, California, water supply and found it to be 9 μg/l, which was roughly three times greater than the U-concentration normally found in sea water[3]. Fleischer and Delany[4] determined U-content in nautral water collected from different sources and found it to vary from (0.08±0.01) to (5.27±0.28) μg/l in the case of clear water samples and from (0.32±0.02) to (7.18±0.14) μg/l in the case of stirred samples. Chakarvarti *et al.*[5] determined the U-concentration of water collected from hot springs, river water, lake water, etc. They found that the U-content of hot spring water samples from Puga valley, Manikaran and Vashist kund varies from 1.4 to 7.4 μg/l; 2.2 to 2.8 μg/l and 2.7 to 4.2 μg/l respectively. In the case of river water and lake water, the U-concentration as obtained by Chakarvarti *et al.*[5] indicated a variation from 4.6 to 6.6 μg/l.

The range of U-content as obtained in this experiment lies within the general range of U-content for background water observed by earlier workers. We observe nothing abnormal in the U-content of various water sources of the region.

The financial assistance from the CSIR, New Delhi for this project is gratefully acknowledged by the authors. The authors wish to thank the Heads of the departments of Physics and Geology, Gauhati University for extending necessary laboratory facilities.

References

1 Fleischer R L, Naeser C W, Price P B, Walker R M & Marvin U B, *Science (USA)*, **148** (1965) 629.
2 Fleischer R L & Lovett D B, *Geochim & Cosmochim Acta (GB)*, **32** (1968) 1126.
3 Rons E, Gilpatrick L O & Jaffrey L M, *Trans Am, Geophys Union (USA)*, **37** (1956) 697.
4 Fleischer R L & Delany A C, *Anal Chem (USA)*, **48** (4) (1976) 642.
5 Chakarvarti S K, Lal N & Nagpaul K K, *The solid state nuclear track detectors* (Pergamon Press, Oxford), 1980, 701.

INSTRUCTIONS TO AUTHORS

SCOPE

The journal welcomes, for publication, full papers and short notes, reporting significant new results of research, in all areas of physics except space physics. The applied fields covered are electronics, electrical engineering, instrumentation and applied mathematics. However, papers in applied mathematics with emphasis on only derivation and proofs and having no direct physical significance, will not be considered. Review articles are not published normally.

SUBMISSION OF MANUSCRIPT

Manuscripts for consideration should be submitted, *in duplicate*, to Editor, Indian Journal of Pure & Applied Physics, Publications & Information Directorate, Hillside Road, New Delhi 110012. They should neither have been already published nor be under consideration elsewhere.

Manuscripts should be in English and typewritten on only one side of good quality paper, in double space, with adequate margin on all four sides. One original and one carbon or photo-copy, each complete in all respects including abstract, illustrations, appendixes, etc. are to be submitted.

PREPARATION OF MANUSCRIPT

Authors may consult recent issues of the Journal to familiarize themselves with the general style and practices adopted in regard to the various elements of a paper.

General

Manuscript should be presented in as concise a form as possible. Good attention should be given to spelling and grammar. In giving names of chemical compounds and structures, abbreviations of units of measurements, symbols and notations, the style and practices recommended by the IUPAP and IUPAC, should be followed.

Frequently repeating combinations of words, e.g. electric field gradient (EFG), junction field effect transistor (JFET), stimulated Raman emission (SRE), should be abbreviated subsequently, indicating the abbreviated form in parenthesis, as shown, at the place of their first occurrence.

Pages should be numbered consecutively and arranged in the following order: Title, authors' names with their institutional affiliations and abstract, along with relevant footnotes whenever necessary (on a separate sheet); introduction; experimental details/theory/method/analysis; results; discussion; conclusion(s); acknowledgement; references and appendixes. Tables, captions for figures (with legends) and appendixes should be typed *on separate sheets* and attached at the end of the manuscript.

Title

The title should be neither too brief/general nor unnecessarily long. It should reflect the content of the paper so as to derive the maximum advantage in indexing. If a paper forms part of a general series, a specific subtitle, indicating the particular aspect of the work covered in the paper, should be provided.

A short running title for the paper, the broad subject heading under which it should be classified in the contents page (authors may consult recent numbers of the journal for this purpose), and the author (indicated by an asterisk on the relevant author's name) and address for correspondence, should also be provided on the title page.

Abstract

The abstract, usually not exceeding 200 words, should indicate the scope and significant content of the paper, highlighting the principal findings and conclusions. It should be in such a form that abstracting periodicals can use it without modification.

Introduction

Long and elaborate introduction should be avoided. It should be brief and state the exact scope of the study in relation to the present status of knowledge in the field. Literature review should be limited strictly to what is necessary to indicate the essential background and the justification for undertaking the study.

Materials, methods, apparatus, etc.

The sources of materials and their purity, methods of preparation, procedure for measurements and their accuracies, etc. should be clearly stated to enable any other worker to repeat the work if necessary. New methods, techniques, theories, etc. should be described in adequate detail; but if they are well known, a mere literature reference to them will do; differences from standard ones, improvements or innovations should, however, be clearly mentioned.

Results

Only such primary data as are essential for understanding the discussion and main conclusions emerging from the study should be included. All secondary data as are of interest to a specific category of readership *should not be included* in the paper. Such data should be retained by the authors for supply, on request, to any interested research worker. A footnote to this effect may be inserted at the relevant place in the paper.

The results must be presented in a coherent sequence in a unified logical structure, avoiding repetition or confusion. Limitations of the results should be clearly stated.

The same data should not be presented in both tabular and graphic forms. Only such tables and figures as are essential should be included. Simple linear plots that can easily be discussed in the text, should not be included. Infrared, ultraviolet, NMR and other spectra, DTA curves, etc. should be included only if they pertain to new compounds and/or are essential to the discussion; otherwise only significant numerical data should be given in the text or in a table.

Discussion

Long rambling discussion should be avoided. The discussion should deal with the interpretation of results without repeating information already presented under results. It should relate new findings to the known and include logical deductions. A separate section on 'conclusions' can be given only when they are well established and of outstanding significance. Mere observation of qualitative trends of results should be distinguished from firm conclusions. Also, limitations, if any, to the conclusions should be clearly pointed out.

Mathematical portions

Special attention should be given to the mathematical portions of the paper. Equations must be well separated from the text and written clearly with good separation between the successive lines. The usual norms of breaking long mathematical expressions should be adhered to. Equations should be numbered consecutively in Arabic numerals with the number in parenthesis near the right hand margin. Superscripts and subscripts should be clearly indicated in pencil by V and Λ sign respectively. Capital and small letters,

particularly of the same letter when both occur, as well as letters or *symbols likely to be confused* one for the other, *should be* clearly *distinguished*. Special characters (e.g. Greek, script, vector, tensor, etc.) required must be indicated by marginal notes. Letters and symbols which should appear in bold face must be clearly indicated. To simplify typesetting: (i) long and complicated mathematical expressions which are frequently repeated should be replaced with single letter/symbol, *without clashing with the others used* in the paper; (ii) the "exp" form of complex exponential functions should be used; and (iii) to simplify fractions, the solidus (/) is to be used and fractional exponents are to be used instead of root signs, e.g.

write $\exp\{-i\omega_0(t_1 - t_2)/2\}$ and *not* $e^{-i\omega_0 (t_1 - t_2)/2}$

write $(4\omega_{pl} K_{3\lambda}^2/\tilde{\omega} K_D^2)^{1/2}$ and *not* $\sqrt{\dfrac{4\omega_{pl} K_{3\lambda}^2}{\tilde{\omega} K_D^2}}$

Tables

Tables should be numbered consecutively in Arabic numerals and *should bear brief titles. Column headings should be brief.* Units of measurement should be abbreviated and placed below the headings. Nil results should be indicated and distinguished clearly from absence of data. Inclusion of structural formulae inside the tables should be avoided as far as possible. Tables should be referred to in the text by numbers and not by terms like 'above', 'below', 'preceding' or 'following'. Results should not be presented to a greater accuracy than that of the method employed.

Illustrations

The number of illustrations should be kept to the minimum. Wherever possible, e.g. a number of individual analogous figures referring to different variables, substances, molecules, etc. may be combined into one composite figure. All illustrations should be numbered consecutively in Arabic numerals. *Captions and legends* to the figures should be *self-explanatory*. Line drawings should be made with Indian ink on white drawing paper/cellophane sheet/tracing cloth, and drawn to approximately twice the printed size.

The lettering should be uniform, preferably in stencil, so as to be *not less than* 1.5 *mm after reduction* widthwise to full page size (165 mm) or column size (80 mm). The size of geometrical shapes (used to distinguish different graphs), dots, lines, etc. should be sufficiently *large to permit* the necessary *reduction without loss of detail*. In the case of photographs, *prints must be on glossy paper and contrasty*. If an illustration is taken from another publication, reference to the source should be given and prior permission secured. Illustrations should be referred to in the text by numbers and not by terms like 'above', 'following' etc.

Acknowledgement

Acknowledgements should not be exuberant and must be made only to real assistance rendered in connection with the work reported in the paper.

References

References cited should be limited to the absolute minimum (particularly in the case of short notes) based on their essential relevance. In the text, references to literature should be *numbered consecutively, in the order of their first occurrence*, and should be indicated by superscript Arabic numbers at the relevant places; as far as possible the placement of references on numerals or other symbols should be avoided; in such cases the reference may be given in parenthesis in running text, e.g. "this yielded for n a value of 2.3 (Ref. 5)". Full bibliographic details for all the references mentioned in the text should be listed in serial order at the end of the paper.

In citing references to research papers, names and initials of authors should be followed, in order, by the title of the periodical in the abbreviated form (underlined), the volume number (two lines underneath), the year within circular brackets and the page number [e.g. Chandra B P & Shrivastava K K, *J Phys & Chem Solids (GB)*, 39 (1978) 939]. For names of periodicals, the abbreviations followed by the *Physics Abstracts* should be used. For periodicals not covered by *Physics Abstracts*, the title abbreviations should be according to the *Bibliographic Guide for Editors and Authors*, 1974, published by the American Chemical Society, Washington DC, USA; additionally the country from which the journal is published should be given in parenthesis immediately after the title abbreviation. If a paper has been accepted for publication, the names of the authors and the journal (with volume number and year, if known) should be given followed by the words "in press" [e.g. Wahi P K & Patel N D, *Can J Spectrosc (Canada)*, in press.].

In references containing *up to four authors*, the *names of all* the *authors* with their respective initials should *be given*. The abbreviations *et al.*, idem and ibid should be avoided. When there are more than four authors, *only* the names of the *first three authors* with their respective initials should *be given*, followed by the words '*et al.*'

Reference to a book should include details in the following order: name and initials of authors, the title of the book (underlined), name of publisher and place of publication within circular brackets and year and page (s) [e.g. Clayton G B, *Operational amplifiers* (Newnes-Butterworths, London), 4th Edn, 1977, 26]. If the reference is to the work of an author published in a book by a different person, the fact that it is cited from the source book should be clearly indicated [e.g. Turnhout Van J, 'Thermally stimulated discharge of electrets' in *Topics in applied physics*: Vol. 33—*Electrets*, edited by C M Sessler (Springer Verlag, Berlin), 1980, 130].

Proceedings of conferences and symposia should be treated in the same manner as books. Reference to a paper presented at a conference, the proceedings of which are not published, should include, in the following order, names and initials of authors, title of the paper (underlined), name of the conference, and where and when it was held (e.g. Herczeg P, *Symmetry-violating kaon decays*, paper presented to the International Conference on High Energy Physics and Nuclear Structure, Vancouver, Canada, 13-17 August 1979).

Reference to a thesis should include the name of the author, title of the thesis (underlined), university or institution to which it was submitted and year of submission (e.g. Mehrotra S N, *Many-body techniques and their applications to interacting bosons*, Ph D thesis, Ranchi University, 1976).

Reference to a patent should include names of patentees, country of origin (underlined) and patent number, the organization to which the patent has been assigned (within circular brackets), date of acceptance of the patent and reference to an abstracting periodical where available [e.g. Labes M M, *US Pat.* 4,066,567 (to Temple University), 3 January 1978; *Chem. Abstr.*, **88** (No. 20) (1978), 138350 n].

PROOFS & REPRINTS

Authors will receive galley proofs and a reprint order form. The galley proofs, indicating the essential corrections, should be returned to the Editor without delay, enclosing the reprint order form. Authors are given 25 *free reprints* for each paper. *Extra* reprints can be had *at cost. If the reprint order is not received with the corrected proofs, it will be presumed that the author needs no extra reprints.* Later requests for *more* reprints cannot be complied with. Covers for reprints cannot be provided.

RN 7092/63

CSIR PUBLICATIONS

WEALTH OF INDIA

An encyclopaedia of the economic products and industrial resources of India issued in two series

RAW MATERIALS SERIES—contains articles on plant, animal and mineral resources

	Rs	$	£
Vol. I (A-B)	80.00	30.00	13.00
Vol. II (C)	95.00	33.00	17.00
Vol. III (D-E)	105.00	32.00	20.00
Vol. IV (F-G)	65.00	27.00	12.00
Supplement (Fish & Fisheries)	40.00	16.00	7.00
Vol. V (H-K)	75.00	28.00	12.50
Vol. VI (L-M)	90.00	34.00	15.00
Supplement (Livestock)	60.00	18.00	6.00
Vol. VII (N-Pe)	30.00	9.00	3.00
Vol. VIII (Ph-Re)	86.00	32.00	14.00
Vol. IX (Rh-So)	104.00	35.00	19.00
Vol. X (Sp-W)	152.00	65.00	23.00
Vol. XI (X-Z)	102.00	42.00	20.00

INDUSTRIAL PRODUCTS SERIES—deals with major, small-scale and cottage industries

Part I (A-B)	54.00	20.00	9.00
Part II (C)	64.00	24.00	11.00
Part III (D-E)	25.00	7.50	2.50
Part IV (F-H)	25.00	7.50	2.50
Part V(I-L)	30.00	9.00	3.00
Part VI (M-Pi)	28.00	8.00	2.80
Part VII (Pl-Sh)	60.00	18.00	6.00
Part VIII (Si-Ti)	66.00	27.00	10.00
Part IX (To-Z)	80.00	34.00	12.00

BHARAT KI SAMPADA (Hindi Edition of Wealth of India, Raw Materials):

Vol. I (अ-औ)	38.00	16.00	6.50
Vol. II (क)	36.00	15.00	6.00
Vol. III (ख-न)	36.00	15.00	6.00
Vol. IV (प)	83.00	34.00	16.00
Vol V (फ-मेरे)	60.00	22.00	10.00
Vol VI (मेल-ह)	80.00	27.00	13.00
Livestock (Kukkut Palan)	34.00	15.00	6.00
Fish & Fisheries (Matsya aur Matsyaki)	49.00	21.00	8.00
A Dictionary of Generic & Specific Names of Plants and Animals Useful to Man with their English and Latin pronunciation in Devanagari.	30.00	11.00	5.00

OTHER PUBLICATIONS

	Rs	$	£
Proceedings:seminar on primary communications in Science & Technology in India by Sh. R.N. Sharma & S. Seetharama	52.00	17.50	9.00
Flora of Delhi by J.K. Maheshwari	28.00	8.00	2.80
Indian Fossil Pteridophytes by K.R. Surange	23.00	8.00	2.30
Indian Thysanoptera by T.N. Ananthakrishnan	26.00	8.00	2.60
The Millipede Thyropygus by G. Krishnan	12.00	3.50	1.20
Drug Addiction with special reference to India by R.N. Chopra & I.C. Chopra	12.00	3.50	1.20
Glossary of Indian Medicinal Plants by R.N. Chopra & I.C. Chopra	35.00	13.00	6.00
Fluidization & Related Processes	12.00	4.00	1.20
Evolution of Life by M.S. Randhawa, A.K. Dey, Jagjit Singh & Vishnu Mitre	22.50	7.00	2.25
Collected Scientific Papers of Meghnad Saha	30.00	9.00	3.00
Proteaceae by C. Venkata Rao	34.00	11.00	3.40
Pinus by P. Maheshwari & R.N. Konar	30.00	11.00	5.00
Cellulose Research I	3.00	0.90	0.30
Cellulose Research II	6.00	1.75	0.60
Chemical Process Design	9.00	2.50	0.90
Low Temperature Carbonization of Non-coking Coals & Lignites & Briquetting Coal Fines:			
Vol. I	17.50	5.50	1.75
Vol. II	17.50	5.50	1.75
Nucleic Acids	10.00	3.00	1.00
IGY Symposium: Vol. I	9.00	2.50	0.90
IGY Symposium: Vol. II	9.00	2.50	0.90
CNS Drugs	16.50	5.00	1.65
Kinetics of Electrode Processes & Null Points of Metals	2.50	0.75	0.25
Indian Sardines by R.V. Nair	22.00	7.00	2.20
Termite Problems in India	9.00	3.00	0.90
Loranthaceae by B.M. Johri & S.P. Bhatnagar	32.00	11.00	3.20
Abies and Picea by K.A. Chowdhury	14.00	6.00	2.10
Gnetum by P. Maheshwari and Vimla Vasil	20.00	6.00	2.00
Aquatic Angiosperms by K. Subramanyam	20.00	6.00	2.00
Supplement to Glossary of Indian Medicinal Plants by R.N. Chopra, I.C. Chopra & B.S. Varma	18.00	7.00	3.00
Herbaceous Flora of Dehra Dun by C.R. Babu	144.00	60.00	22.00
Diosgenin and Other Steroid Drug Precursors by Y.R. Chadha & Miss L.V. Asolkar	36.00	13.00	6.00
Research & Development Management by Inder Dev	25.00	10.00	—
Rural Development and Technology—A Status Report-cum-Bibliography by P.R. Bose & V.N. Vashist	100.00	38.00	17.00

Packing and Postage extra

Please contact:

Manager (Sales & Advertisement)

PUBLICATIONS & INFORMATION DIRECTORATE, CSIR

Hillside Road, New Delhi 110012

Printed & Published by D.S. Sastry, Editor, Publications & Information Directorate (PID) Hillside Road, New Delhi 110012, at PID Photocomposition Unit

D(C)340